NASA/TP—2019-220054

Compass Final Report: Europa Tunnelbot

Steven Oleson and J. Michael Newman
Glenn Research Center, Cleveland, Ohio

Andrew Dombard and D'Arcy Meyer-Dombard
University of Illinois at Chicago, Chicago, Illinois

Kate Craft
Johns Hopkins University, Applied Physics Laboratory, Laurel, Maryland

James Sterbentz
Idaho National Laboratory, Idaho Falls, Idaho

Anthony Colozza
Vantage Partners, LLC, Brook Park, Ohio

Brent Faller
Glenn Research Center, Cleveland, Ohio

James Fittje
Vantage Partners, LLC, Brook Park, Ohio

John Gyekenyesi
ZIN Technologies, Inc., Middleburg Heights, Ohio

Robert Jones, Geoffrey Landis, Nicholas Lantz, Lee Mason, Steven McCarty, and Terri McKay
Glenn Research Center, Cleveland, Ohio

Thomas Packard and Paul Schmitz
Vantage Partners, LLC, Brook Park, Ohio

Elizabeth Turnbull and June Zakrajsek
Glenn Research Center, Cleveland, Ohio

June 2019

NASA STI Program . . . in Profile

Since its founding, NASA has been dedicated to the advancement of aeronautics and space science. The NASA Scientific and Technical Information (STI) Program plays a key part in helping NASA maintain this important role.

The NASA STI Program operates under the auspices of the Agency Chief Information Officer. It collects, organizes, provides for archiving, and disseminates NASA's STI. The NASA STI Program provides access to the NASA Technical Report Server—Registered (NTRS Reg) and NASA Technical Report Server—Public (NTRS) thus providing one of the largest collections of aeronautical and space science STI in the world. Results are published in both non-NASA channels and by NASA in the NASA STI Report Series, which includes the following report types:

- TECHNICAL PUBLICATION. Reports of completed research or a major significant phase of research that present the results of NASA programs and include extensive data or theoretical analysis. Includes compilations of significant scientific and technical data and information deemed to be of continuing reference value. NASA counter-part of peer-reviewed formal professional papers, but has less stringent limitations on manuscript length and extent of graphic presentations.

- TECHNICAL MEMORANDUM. Scientific and technical findings that are preliminary or of specialized interest, e.g., "quick-release" reports, working papers, and bibliographies that contain minimal annotation. Does not contain extensive analysis.

- CONTRACTOR REPORT. Scientific and technical findings by NASA-sponsored contractors and grantees.

- CONFERENCE PUBLICATION. Collected papers from scientific and technical conferences, symposia, seminars, or other meetings sponsored or co-sponsored by NASA.

- SPECIAL PUBLICATION. Scientific, technical, or historical information from NASA programs, projects, and missions, often concerned with subjects having substantial public interest.

- TECHNICAL TRANSLATION. English-language translations of foreign scientific and technical material pertinent to NASA's mission.

For more information about the NASA STI program, see the following:

- Access the NASA STI program home page at http://www.sti.nasa.gov

- E-mail your question to help@sti.nasa.gov

- Fax your question to the NASA STI Information Desk at 757-864-6500

- Telephone the NASA STI Information Desk at 757-864-9658

- Write to:
  NASA STI Program
  Mail Stop 148
  NASA Langley Research Center
  Hampton, VA 23681-2199

NASA/TP—2019-220054

Compass Final Report: Europa Tunnelbot

Steven Oleson and J. Michael Newman
Glenn Research Center, Cleveland, Ohio

Andrew Dombard and D'Arcy Meyer-Dombard
University of Illinois at Chicago, Chicago, Illinois

Kate Craft
Johns Hopkins University, Applied Physics Laboratory, Laurel, Maryland

James Sterbentz
Idaho National Laboratory, Idaho Falls, Idaho

Anthony Colozza
Vantage Partners, LLC, Brook Park, Ohio

Brent Faller
Glenn Research Center, Cleveland, Ohio

James Fittje
Vantage Partners, LLC, Brook Park, Ohio

John Gyekenyesi
ZIN Technologies, Inc., Middleburg Heights, Ohio

Robert Jones, Geoffrey Landis, Nicholas Lantz, Lee Mason, Steven McCarty, and Terri McKay
Glenn Research Center, Cleveland, Ohio

Thomas Packard and Paul Schmitz
Vantage Partners, LLC, Brook Park, Ohio

Elizabeth Turnbull and June Zakrajsek
Glenn Research Center, Cleveland, Ohio

National Aeronautics and
Space Administration

Glenn Research Center
Cleveland, Ohio 44135

June 2019

Acknowledgments

The authors wish to thank the outstanding men and women of the Compass team, including the visiting scientists, for their dedication to performing the many analyses involved in completing the various designs and trade studies presented in this paper. Thank you to Dr. Curt Niebur for his guidance and support in steering the requirements for these concepts. Finally, thank you to the Radioisotope Power Systems (RPS) program for funding these Compass studies.

Available from

NASA STI Program
Mail Stop 148
NASA Langley Research Center
Hampton, VA 23681-2199

National Technical Information Service
5285 Port Royal Road
Springfield, VA 22161
703-605-6000

This report is available in electronic form at http://www.sti.nasa.gov/ and http://ntrs.nasa.gov/

Contents

Compass Final Report: Europa Tunnelbot

Steven Oleson and J. Michael Newman
National Aeronautics and Space Administration
Glenn Research Center
Cleveland, Ohio 44135

Brent Faller
National Aeronautics and Space Administration
Glenn Research Center
Cleveland, Ohio 44135

Andrew Dombard and D'Arcy Meyer-Dombard
University of Illinois at Chicago
Chicago, Illinois 60607

James Fittje
Vantage Partners, LLC
Brook Park, Ohio 44142

Kate Craft
Johns Hopkins University
Applied Physics Laboratory
Laurel, Maryland 20723

John Gyekenyesi
ZIN Technologies, Inc.
Middleburg Heights, Ohio 44130

James Sterbentz
Idaho National Laboratory
Idaho Falls, Idaho 83402

Robert Jones, Geoffrey Landis, Nicholas Lantz, Lee Mason, Steven McCarty, and Terri McKay
National Aeronautics and Space Administration
Glenn Research Center
Cleveland, Ohio 44135

Anthony Colozza
Vantage Partners, LLC
Brook Park, Ohio 44142

Thomas Packard and Paul Schmitz
Vantage Partners, LLC
Brook Park, Ohio 44142

Elizabeth Turnbull and June Zakrajsek
National Aeronautics and Space Administration
Glenn Research Center
Cleveland, Ohio 44135

Summary

A complete design explanation along with science goals is provided in the following sections, but a summary of the results is described here for the three Compass designs: the 43-kW_{th} reactor Tunnelbot, the 54-general purpose heat source (GPHS) Tunnelbot, and the associated radioisotope heater unit (RHU) powered repeaters that are carried by each design (Compass Document (CD) 2018-153). A comparison of the reactor and the GPHS Tunnelbot designs are shown in Table 1.

Reactor Tunnelbot

- Onboard 43-kW_{th} reactor to melt a probe through 20 km of Europa ice and stop at the ocean (or lake if reached first)
- Mass: 1,350 kg (with three repeaters and growth)
- Dimensions: 0.5 m diameter by 5.3 m length
- 2032 launch on Space Launch System (SLS) Block 1B class launcher
- Science: biodetection (broad mass organic compounds using mass analyzer and Raman, or alternative) by gathering and analyzing ice samples (eight locations during descent) and at ocean or lake (also meteorology of ice and water and seismometry)
- Thermal: 43.3-kW_{th} reactor provides heat to melt 50-cm tunnel using glycol pumped loop to tip and body
- Power: reactor heat powers Stirlings to power Tunnelbot and pumps (~300 W_e)
- Radiation protection: Jupiter (1.4-cm-thick pressure vessels should be sufficient), reactor (2.5-m-long in situ filled water shield and spot shielding)
- Mechanical: instrument and reactor pressure vessels, water chambers, and repeater and anchor cable spools
- Command and Data Handling (C&DH): 500-krad controller and data storage
- Communications: three 1-GHz radiofrequency (RF) and laser optic booster repeaters connected by steel-shielded fiber optic cable

TABLE 1.—COMPARISON OF TUNNELBOT DESIGNS

	Reactor Tunnelbot	General purpose heat source (GPHS) Tunnelbot
Science	Biodetection instruments (~30 kg), formatted for 48-cm Tunnelbot inside diameter	Biodetection instruments (~30 kg), formatted for 22-cm Tunnelbot inside diameter
20 km descent	~3 yr	~ 3 yr
Landed mass	~ 1,350 kg (with 30 percent growth)	~750 kg (with 30 percent growth)
Launcher	Space Launch System Block 1B (100 t low Earth orbit (LEO))	Space Launch System Block 1 (70 t LEO)
Size	5.2 m long by 51 cm diameter	5.7 m long by 25 cm diameter
Technology readiness level	3 to 5 (biodetection and sampling, power, thermal, and repeaters and tethers)	3 to 5 (biodetection and sampling, power, thermal, and repeaters and tethers)
Ice melting heat	~ 43 kW_{th} from a reactor (based on Kilopower)	~ 12 kW_{th} (58 GPHS bricks)
Electric power systems	~400-W_e Stirling using reactor heat (most of electric power needed for pump loops)	Batteries and ~50 W_e (thermoelectric or dynamic) using dedicated GPHS heat (much less than reactor version by using valved heat pipes)

- Guidance, Navigation, and Control (GN&C): accelerometer, magnetometer, pressure for attitude and location, and sonar in nose to detect upcoming water and deploy anchor cable (~500 m max.)

GPHS Tunnelbot

- Onboard 54-GPHS ^{238}Pu bricks (12 kW_{th}) to melt a probe through 20 km of Europa ice and stop at the ocean (or lake if reached first)
- Mass: 750 kg (with three repeaters and growth)
- Dimensions: 0.25 m diameter by 5.75 m length
- 2032 launch on SLS Block 1 class launcher
- Science: biodetection (broad mass organic compounds using mass analyzer and Raman) by gathering and analyzing ice samples (eight locations during descent) and at ocean or lake (also meteorology of ice and water and seismometry)
- Thermal: 12 kW_{th} of GPHS bricks provides heat to melt 25-cm tunnel using variable conductance heat pipes to tip and body
- Power: standalone, new thermoelectric (four-GPHS) system to power Tunnelbot and pumps (~50 W_e)
- Radiation protection: Jupiter (1.4-cm-thick pressure vessels should be sufficient), GPHS (not an issue)
- Mechanical: Instrument and GPHS pressure vessel, and repeater and anchor cable spools
- C&DH: 500-krad controller and data storage
- Communications: three 1-GHz RF and laser optic booster repeaters connected by steel-shielded fiber optic cable
- GN&C: accelerometer, magnetometer, pressure for attitude and location, and sonar in nose to detect upcoming water and deploy anchor cable (~500 m max.)

Communication Repeaters

- Mass: 12 kg
- Dimensions: 12-cm diameter by 70-cm length cylinder
- Science: temperature, pressure, and conductivity plus seismometer
- C&DH: small, 500-krad controller for brief operations, hibernation for battery charging using smaller control computer
- Communications: provides both optical signal boost or 1-GHz RF for Tunnelbot communications, 1 kb/s
- Power: eight-RHU Dynamic 1-W_e beginning of life (BOL) system (roughly same mass/volume), rechargeable Li-ion battery for communication sessions
- Thermal: power system plus a few RHUs for >150 K ice operations
- Mechanical: vacuum pressure vessel, handle pressures down 15 km depth (~2,500 psi)n

1.0 Introduction

1.1 Mission Concept

Europa is a distant ocean world that may harbor life. Unfortunately, it is covered by many kilometers of ice that must be penetrated to reach the ocean below. This shifting ice shell is projected to be around 20 km thick, and if traversed by a vehicle, must be communicated through if any secrets found by a Tunnelbot are to be transmitted back to a lander and thence to Earth (Figure 1).

The engineering challenges to gathering in situ subsurface science on Europa are many. Delivery and landing are themselves a great challenge due to both Europa's distance and the extreme radiation levels that are present on its surface. Both the Europa Clipper and Europa Lander designs have addressed these challenges so one may assume that their lessons can be applied to delivering a sub-ice vehicle to the Europan surface. Penetrating the ice down to the ocean while sampling for biomarkers and communicating back to the surface were the focus of three Compass concurrent engineering team designs.

Figure 1.—Tunnelbot reaching ocean after deploying communication repeaters and anchor (artist impression).

These conceptual designs, while providing complete conceptual layouts for these penetrators, or Tunnelbots along with the associated communication repeaters (shown in Figure 1 and magnified in callout), primarily focused on the power and thermal systems needed for these devices. Trades for these systems will provide advantages and challenges for each option. These results will be used to guide power technology development.

Other relevant conceptual designs for penetrating robots were reviewed, including the Philberth Probe (Ref. 1), Ice Diver (Ref. 2), ICEcube (Ref. 3), Cryobot (Ref. 4), Deep Subsurface Ice Probe (Ref. 5), Mars Cryobot (Ref. 6), Mars Ice Cap Explorer (Ref. 7), VALKYRIE (Ref. 8), and the 2017 Keck Study (Ref. 9). Based on both terrestrial experience and past Europa concepts, it was determined that melting through the ice is the quickest and most efficient use of power to penetrate multiple kilometers of ice. An ice thickness of 20 km and a penetration time of 3 yr were set as constraints for the concept trades. Two potential thermal sources were considered: a nuclear reactor and plutonium. Both can provide sufficient heat, and with appropriate power conversion equipment, can provide the hundreds of watts of electrical energy to power the vehicles. The reactor systems were based on the recent Kilopower testing (Ref. 10), which should allow for thermal power levels of approximately 4 to 40 kW_{th}. Plutonium was also considered, which when packaged in a general purpose heat source (GPHS) brick can provide about 250 W_{th}. Both of these systems have a minimum footprint that in turn defines the minimum tunnel diameter that would be bored through the ice sheet. Many trades were performed on Tunnelbot diameter and length, but it was found that the thermal flux at the Tunnelbot tip needed to be about 20 W_{th}/cm^2 to provide the desired 20 km in 3 yr. The diameter and length design considerations are discussed in Section 5.0.

The concept designs were targeted for a 2032 launch with a NASA technology readiness level (TRL) 6 cutoff of 2026. Ice temperatures, consistencies, and contamination were assessed and described herein. Given the diurnal cycle, the ice is expected to shift, which adds a large risk to cable power and communication approaches. The primary science goals were to sample the ice and water ocean to search for biomarkers and assess habitability. Figures of merit that guided design decisions included ice penetration rate (distance/time), science return, Tunnelbot mass, Tunnelbot cost (including development costs of thermal and/or power system), and Tunnelbot agility.

1.2 Study Approach

The study approach consisted of two phases: an architecture phase and three concurrent engineering point designs. The architecture studies traded several combinations of thermal reactor and Plutonium sources that provided the most benefit for the point designs and are summarized in Section 1.3. The most promising options were a 43-kW_{th} reactor and GPHS bricks (~60). The architecture studies also indicated the

significantly large potential impact of the science instrumentation and cable and repeater equipment on the minimum cross-sectional area. Thus, these systems were added as a focus of the designs. The architecture studies also hinted at the large masses needed for the Tunnelbot systems, indicating that a large launch vehicle would be needed.

1.3 Summary of Requirements and Assumptions

1.3.1 Environment and Mission

- Targeted launch in 2032 (TRL 6 by 2026)
- Consider up to 3 yr of storage for Radioisotope Power Systems (RPS) before launch
- Target: entire landed mass 1,000 kg dry; non-Tunnelbot systems ~40 percent of landed mass
- Given the biodetection science requirements, heavy Space Launch System- (SLS-) class vehicles will be required or very advanced and very small biodetection instruments will be necessary
- Probability of forward contamination of the ocean must be less than 10^{-4}
  - 110 °C sterilization as needed to prevent forward contamination
- Ice thickness estimates range from 5 to 30 km (or more), ~90 K, vacuum at the surface and ~270 K, 20 MPa at the ice and ocean boundary
  - Assumed to be 20 km thick
- Ice properties range from a brittle ice layer at the surface to an underlying ductile layer. Ice includes hydrated salts, porosity, entrained lakes (sills)
- Surface fractures ~100 m deep; 3.5-d diurnal cycle
  - Fractures expected throughout at least the top several hundred meters, during each diurnal cycle

1.3.2 Mission Goals

- Discovery of evidence of life can be sought in the ice shell and liquid water ocean
- Depths >10 m enables sampling of pristine material; this will be almost entirely unaffected by the radiation environment of Europa
- Enables sampling and analysis concentrated biomarkers from past lakes (sills)
- Enables sampling and analysis of liquid water from oceans covered by the shallowest ice thickness or in ice that has been in contact with the liquid oceans in the relatively recent past

1.3.3 Technical Goal

- System-level ice penetration and sampling capability to penetrate ice and reach a subsurface water body on Europa. Within 3 yr, reach:
  - Depths of 20 km to reach the ocean or
  - Depth of 4 km to reach a lake of melted accreted ice

1.3.4 Constraints and Considerations

- Must penetrate dirty ice, for example:
  - Salt, sediment, and sulfur layers, sulfuric acids, and embedded gases
  - Must be able to get unstuck or avoid getting stuck
- Must make forward progress
- Must restart after unexpected, extended (>2 d) stop
- Must retain command authority for the life of the mission, including after entry into liquid (ocean or lake)
  - Some level of obstacle detection and avoidance
  - Surface systems, if any, must survive radiation environment

2.0 Concept of Operations (CONOPS)

2.1 Launch and Transit

- Notional launch, transit, and landing (not evaluated in this study)
  - SLS Block 1B
- Assume reactor loaded cold with Tunnelbot before launcher integration
- Notional landing site: the Puddle (6° N, 323° W), 3.2 km across
  - Expected not to be above a subsurface lake, and not in a fracturing or subduction zone (too active)
- Surface science: conducted by lander-element
- Notional Ice Introduction (to be evaluated in later designs)
  - Lander Enhanced Multi-Mission Radioisotope Thermoelectric Generators (eMMRTGs) prepares a hole ~50 cm in diameter by 6 m deep, and cover hole with dome (to minimize subliming during ice melting)
- The method to load ice from Tunnelbot hole into reactor shield chambers is not yet determined
  - Current radiation estimates during short reactor operation before ice and water is introduced is tolerable
- Reactor activation
  - Startup reactor using control rod (2 hr) ice melts in shield chambers
- Tunnelbot checkout (1 d)

2.2 Tunnelbot Introduction Into Ice (Not Evaluated In This Study)

- Dome to keep the heat in
  - Drill
  - Thermal
  - Laser
- All-in-one
  - Provide the Tunnelbot with counter-rotating auger or other appropriate method to penetrate the top regolith (potentially very porous) layer (power with Radioisotope Thermoelectric Generators (RTGs))
  - Carry the lander avionics and communications (both space and to the Tunnelbot) in the rear of the Tunnelbot, connected with a tether to the lander communication antennas (all equipment that is naturally rad tolerant)
  - Penetrate down to solid ice
  - Use RTG to melt solid ice and fill reactor shield chambers and then start the reactor
  - Separate lander avionics and Tunnelbot acoustic communication receiver (well attached to solid ice)
    - This protects the lander avionics in the ice from Jupiter's radiation and enhances the communications link to the Tunnelbot
  - Reactor-powered Tunnelbot continues descent, communicating to submerged lander package

2.3 Reactor Tunnelbot Descent and Ice Science

- Ice descent: ~0.5 to 1 m/hr rate
  - Desired 20 km tunneling depth in 3 yr, excluding science stoppage time for sampling
- Data collection during descent: melt water temperature, pressure, conductivity, and depth
  - How to take ice temperature (to ±5 K)
    - Calculated with melt rate (based on heat production and descent rate) and conductivity of melt water during descent (conductivity sensor)
    - Put thermocouples into repeaters
  - Ways to determine depth (±0.5 km)/descent rate: pressure (depth), magnetometer (x,y), accelerometers, tilt sensor, calculate amount of melted ice, radiofrequency (RF) location using communication system, and cable unwind counter for distance
- Stop at specific temperatures for sampling: (10 m, 150 K, 200 K, 225 K, 250 K, 250 K (in middle of convective shell), 260 K, and upon entering ocean): takes <1 min to stop (after heat pumps turned off)
- Science during stops
  - Biodetection science (~2 d): one to five (1 cc) samples (16 Mb per sample) at each stop (~3 hr) with waiting for Earth to analyze and command next steps (~9 hr, transmission rate at 1 Kb/s)
  - (Chosen) Option A: 2-cm auger, take a cleansing sample, then a sealed clean sample, pull into examination chamber; chamber needs to be insulated and evacuated
  - (Backup) Option B: scraping during descent into sample chamber; assumes the film veneer is drained
  - Seismometers (listen for quakes); seismometers to work with repeater and lander seismometer to track quakes (need to filter out 100 Hz from Stirling)
- Maneuverability: due to potentially large size of subsurface lakes (kilometers across) and minimal debris sizes, plan on only small deviations (meters, in x and y) during descent (given estimated turn radius of ~3,000 m, can avoid ~100-m objects 500 m away)
  - But due to high center of mass, use tip heat control to keep pointed down (using accelerometer, bubble sensors)

2.4 Repeater

- Deployed at depths of 5, 10, and 15 km
- Connected by fiber optic cable from Tunnelbot to lander avionics
- Repeater provides either signal boost for fiber optic cable communications (max. 10 km if repeater fails) or RF communications (if cable is broken)
- Timely data (two 6-hr relay periods): <700 Mb biodata per biodetection only data stop
  - Assuming full Deep Space Network (DSN) coverage during 48-hr stops, 24 hr to send 1 percent of data (2-hr detection, 6 hr from Tunnelbot to surface, 4 hr to and from Earth trip, plus 12 hr for Earth analysis); highlights would need ~1 Kb/s for repeater, then command a second sample; reactor radiation only affects bioscience ice and water region after 2 weeks
- Non-timely data (picture and seismic data) ~600 Mb stored on Tunnelbot and sent back on daily 1-hr communications link
- Total data for mission: 10.5 Gb (with 50-percent margin, uncompressed over eight stops): with compression ~3:1, 1 Kb/s sufficient for science data and housekeeping and engineering
- Biodetection mode: computer timer activates for 12-hr waiting for biodetection event; once a week
  - Biodetection: 12 hr (two 6-hr periods) of transmit and receive (10 W_e with growth), 12-hr standby (160 mW_e with growth)

- Standby mode every day: timer activated: transmits 1 hr every day
  - 1-hr transmit and receive (10 W_e with growth), 23-hr standby (160 mW_e with growth)
- Repeater science data
  - Temperature, pressure, conductivity, and seismometer

2.5 Reactor Tunnelbot Water Sensing and Entry

- Use front-mounted sonars to
  - Map ice below the Tunnelbot (up to 500 m ahead)
  - Detect water-ice interface: inform Earth of detection, wait for further instructions (stop the Tunnelbot)
  - Allow deploying tether anchor ~200 to 400 m before breakthrough
- Deploy anchor cable, syntactic foam float ~10 cm diameter by 60 cm long to float the weight of the cable
- Turn off heat pumps, Tunnelbot stops <10 cm distance
- Wait up to 3 d (turn down reactor) for ~200 m water cavity above to freeze the anchor float and cable into ice
- Activate anchor cable cam lock
- Reactivate reactor to resume melting and slowly let out tether and use camera to see when breakthrough occurs
- Breakthrough sensed by sonar, camera, and temperature
- Activate anchor cable lock to prevent going deeper; allows for ocean science at ice and water interface (ice ceiling)

2.6 Reactor Tunnelbot Science at Ocean (or Lake)

- Primary target: breakthrough to ocean (possible submerged lakes; if one is encountered then stop after breakthrough)
  - Stop at edge using tether brake
  - Science in ocean: (~25 cm/s estimated current)
    - Continuous: temperature, pressure, conductivity, hydrophone, vehicle data (power, inertial measurement unit): 200 bps
      - Optional: determine ocean depth using sonar? Ways to sense current?
      - Dielectric constant, turbidity: 50 bps
    - Biodetection: take multiple samples (same as stopped ice location) each week for 1 month (16 Mb per sample)
      - Gamma and neutron radiation will not compromise the breakthrough ice for >1 month
  - Sampling ocean water using core sampler (sample ice ceiling by controlling tether playout)
  - Camera and light to image up and down: three cameras with different filters (for color)
    - 1-mm resolution, 1-megapixel camera
  - Option for dropsonde(s) attached to tether: measure temperature, pressure, conductivity, turbidity, etc.
    - Transmit using light
  - Keep reactor up in ice using deployed 200-m anchor
  - Reactor throttled down (only generating power for needed electricity, ~200 We, ~1 kW_{th})
  - Extended mission: lower the Tunnelbot another 100 m using anchor cable (communication tether also extended)
  - End of mission (EOM): put control rod back in to shut off reactor (still radioactive)

3.0 Mission Design

The approach for the mission design for this study was to leverage extensive mission analysis completed for the 2012 Europa Lander Mission Study completed by the NASA Jet Propulsion Laboratory (JPL) (JPL D–71990). In the report, a complete description of all required change in velocity, ΔV, is broken down by mission phase. In addition to the detailed ΔV budget, a detailed master equipment list (MEL) and propulsion performance details enables the calculation of the mass fractions for each stage of the spacecraft. The three stages from the 2012 report include a carrier stage, braking stage, and the lander. With this set of information and the ideal rocket equation, it is possible to estimate the expected lander dry mass for any initial launch vehicle injected mass if the stage mass fractions are assumed to be constant.

The mission assumes a Venus Earth Earth Gravity Assist (VEEGA) interplanetary trajectory to Jupiter with a launch C_3 of 15 km^2/s^2. After 6.37 yr, the carrier stage is used to enter into Jupiter orbit, where a 1.3-yr tour phase is used to reduce energy before Europa orbit insertion. After a not yet determined time in Europa orbit, the carrier stage is separated, and the braking stage uses a solid rocket motor to deorbit the lander and descend to the surface. The descent profile to a soft touchdown is completed by the lander.

Using the assumed mission design and the data available in the 2012 report, the estimated lander dry mass was determined for four launch vehicles (Table 2). The Delta IV Heavy is able to deliver an estimated 767 kg to the surface (which agrees well with the values in the report). An expendable Falcon Heavy is able to deliver 845 kg to the surface. SLS Block 1 is estimated to deliver significantly more mass, 1,559 kg, to the surface. Assumed performance for the SLS Block 1B suggests a possible lander dry mass of up to 2,500 kg. All of these values are considered estimates for planning purposes of this study. Detailed mission design was not the focus of the effort, and additional analysis should be completed to verify the performance in the future.

TABLE 2.—LAUNCH VEHICLE ASSESSMENT

Launch vehicle	Injected mass, kg (10-percent margin)	Estimated lander dry mass, kg
Delta IV Heavy	7,304	767
Falcon Heavy (expendable)	8,048	845
Space Launch System (SLS) Block 1 (70 t low Earth orbit (LEO))	14,850	1,559
SLS Block 1B (105 t LEO)	23,850	2,500

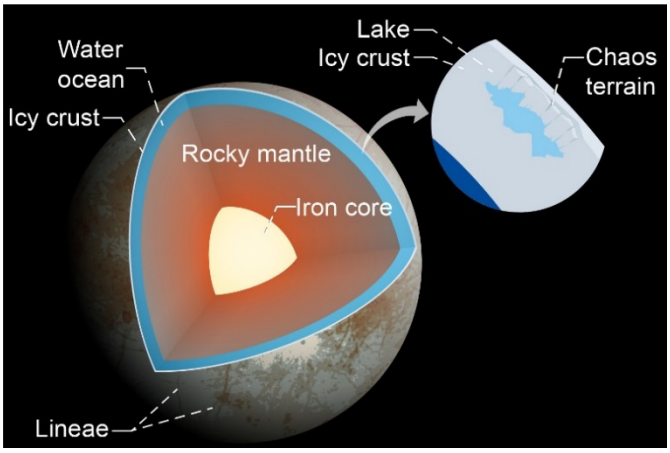

Figure 2.—Illustration of Europa's interior structure, showing relatively thin ice shell overlying a thicker ocean, all around a silicate interior. Zoomed in region highlights potential for pockets of water within ice shell. (Image from https://commons.wikimedia.org/wiki/File:Europa_poster.svg. By Kelvinsong (CC BY-SA 3.0 (https://creativecommons.org/licenses/by-sa/3.0)), from Wikimedia Commons).

4.0 Science

"Because chemical [and physical] information is sparse at present, inferences about the composition [and structure] of the ice-ocean-rock system must rely on reasonable assumptions and idealized models." (Ref. 11)

4.1 Introduction

Below its icy crust, Jupiter's moon Europa, about the size of Earth's Moon, contains more water within its global ocean than all the surface water on Earth. Additionally, that ~100-km-thick ocean has likely existed for most of the lifetime of our solar system, heated by tidal energy as it orbits Jupiter in resonance with Io and Ganymede. The ocean is likely in contact with a silicate-based seafloor where the tidal energy may be supplying chemical elements needed for life (Figure 2 in Ref. 12). In addition, several lines of evidence (Refs. 13 to 15) suggest that there could be mixing of surface components and chemical components from the ocean. All these factors may combine to make Europa's ocean one of the most habitable environments in our solar system.

On Europa, galactic cosmic rays and high energy particles from Jupiter process Europa's surface; however, data and models have shown that the young age of Europa's surface (~10s of Myr) and Jupiter's magnetic field restrict the depth of processing to the order of ~10 cm and less at mid to high latitudes for water ice (Refs. 16 to 18). Cold to suprathermal plasma also processes the surface, although only to very shallow depths, typically < 1 mm (Ref. 19). Therefore, any life or signatures of life within the ice and ocean of Europa would be adequately protected from the harmful radiation, but probing Europa for life requires accessing the subsurface.

To explore this habitable environment within Europa's ice shell and ocean, we present here a robotic mission concept to tunnel into Europa, sample for signatures of life, and assess habitability. The mission would collect samples during descent through the ice shell, analyze the samples for biosignatures and markers of habitability, and achieve a depth of 20 km within 3 yr, possibly reaching Europa's ocean. The mission's science goals and objectives are largely derived from a recent 2016 Science Definition Team (SDT) study for a Europa lander (Ref. 20),which sought to interrogate the nearest subsurface (≥10 cm) for biomarkers and indicators of habitability (Table 3). Additional environmental data will be collected, including seismic, thermal, and chemical. Since the thickness of the ice shell is not known exactly at this time, 20 km will likely enable reaching the ocean or potentially water pockets and/or sills sourced from the ocean. The Europa Clipper mission will visit Europa in the 2020s, with Clipper hosting several instruments, including ice penetrating radar, visual and infrared cameras, and a magnetometer. This Tunnelbot mission concept could utilize these returned data to select and land at the best location at which to travel through the thinnest ice or to shallow liquid water bodies discovered in the subsurface.

TABLE 3.—THE SCIENCE TRACEABILITY MATRIX (STM) FROM THE EUROPA LANDER SCIENCE DEFINITION TEAM REPORT (2016) (REF. 21).

[The first goal is directly applicable to the Tunnelbot. The second goal is directly applicable in a subsurface context, rather than a surface context. The third is complementary and could potentially be addressed by a dedicated lander mission. Boxes with an X indicate baseline model payload instruments chosen to address each objective for the Europa Lander. The Lander Infrastructure Sensors for Science (LISS) column indicates engineering sensors (Descent Imaging and Light Detection and Ranging (LIDAR), thermal sensor(s), telecom, etc.), which the SDT identified as important for the complete science return of the lander mission and are not relevant to the Tunnelbot notional science payload.]

Goals		Objectives	Notional instruments					
			OCA[a]	MLD[b]	VS[c]	CRSI[d]	GSS[e]	LISS
Biosignatures	1. Search for evidence of life on Europa.	1A. Detect and characterize any organic indicators of past or present life.	X	---	X	---	---	---
		1B. Identify and characterize morphological, textural, or other indicators of life.	X	X	X	X	---	---
		1C. Detect and characterize any inorganic indicators of past or present life.	---	---	X	---	---	---
		1D. Determine the provenance of sampled material.	---	---	X	X	---	X
Surface habitability	2. Assess the habitability of Europa via in situ techniques uniquely available to a lander mission.	2A. Characterize the nonice composition of Europa's near-surface material to determine whether there are indicators of chemical disequilibria and other environmental factors essential for life.	X	X	X	X	---	---
		2B. Determine the proximity to liquid water and recently erupted materials at the lander's location.	---	---	---	X	X	X
Surface properties and dynamics	3. Characterize surface and subsurface properties at the scale of the lander to support future exploration.	3A. Observe the properties of surface materials and submeter-scale landing hazards at the landing site, including the sampled area. Connect local properties with those seen from flyby remote sensing.	X	X	X	X	X	X
		3B. Characterize dynamic processes of Europa's surface and ice shell over the mission duration to understand exogenous and endogenous effects on the physicochemical properties of surface material.	X	X	X	X	X	X

[a]Organic compositional analyzer.
[b]Microscope for life detection.
[c]Vibrational spectrometer.
[d]Context remote sensing instrument.
[e]Geophysical sounding system.

4.2 Physical and Chemical Properties of Europa's Ice Shell

The biggest obstacle of any mission to reach Europa's subsurface ocean is the thickness of the ice shell. Unfortunately, analysis of the currently available data and simulations of the evolution of the shell (e.g., Ref. 22 and references therein) have yielded a wide range of values (~2 to 30 km) that would make a tunneling mission either relatively achievable or intractable. Fortunately, the extreme ends of this range are more unlikely. Many analyses indicate that the shell is likely less than 20 km thick, particularly those looking at the formation of Europa's few impact craters (e.g., Ref. 23 and references therein) whose morphology would differ between small craters and large craters that would sense the ocean during their formation. Thus, it is reasonable to design a mission to reach that depth.

Similarly, the temperature structure in the shell is unknown and mostly constrained by models, which suggest surface heat flows of ~20 to 120 $mW_{th}\ m^{-2}$ (e.g., Ref. 24 and references therein). This wide range is a product of the unconstrained state of heat sources. Europa is currently emitting heat from long-lived radiogenic nuclides within the deep silicate interior, which contributes 5 to 10 $mW_{th}\ m^{-2}$ (Ref. 25) and heating from dissipation of tides in the deep ice shell and potentially in the silicate interior. How this heat is transferred through the ice shell to irradiate to space at the surface is likely a combination of near-surface conduction (the thermal lithosphere) and deeper convection.

Indeed, multiple morphological indicators of Europa's surface indicate the presence of convective motions within the ice shell (chaos regions, pull-apart bands, etc.), and these indicators provide some mutual constraint on the thickness and thermal structure of the shell at the time of the surface features' formation. For instance, a shell less than 5 km can pass even the highest estimated heat flow solely by conduction, while the lowest heat flows can pass heat conductively through even the thickest of shells (30 km), leaving no room for a convective interior. Together, estimates of shell thickness and the presence of morphological indicators of convection deep in the ice shell suggest the shell passes ~50 to 100 $mW_{th}\ m^{-2}$ of heat to the surface through a thermal lithosphere 5 to 10 km thick in which

temperatures rise near linearly (the thermal conductivity of ice is inversely proportional to temperature) (Ref. 26), another 5 to 15 km of a convective layer with more isothermal temperatures estimated in the range of 200 to 250 K (Ref. 24), and a thin (<1 km) bottom thermal boundary layer to an ocean at ~270 K (pressure effects and primarily salinity drop the melting point of water at the base of Europa's ice shell by a few degrees) (Figure 3).

The modification of Europa's surface, from tidal forcing and potentially by ongoing internal convection, drives Europa's active surface geology, with implications for the design of a tunneling probe. Models of convection suggest velocities of 1 cm/yr (Ref. 24), and given the coupling of the surface and the convection, it is reasonable to expect average surface velocities of a similar order. Like on Earth, however, this motion would not be continuous everywhere in space and time and will likely be accommodated as discrete stick-slip events along faults. Indeed, Europa even displays evidence for near Earth-like subduction zones (Ref. 15). Tidal motions could also be accommodated along faults. These faults would be shear zones that dip at nonvertical angles in the lithosphere, and thus there is always the possibility that a tunneling probe will be very unlucky and happen to be crossing a fault zone (~1 to 10 m wide) during a slip event of 0.1 to 1 m. Site selection will be critical to mitigate this risk, searching the available data for regions that appear geologically smooth and quiescent, such as the putative frozen pond imaged by Galileo during the E4 encounter (Figure 7 in Ref. 27). Both the Europa Clipper mission and the Europa Lander under study would be able to provide important data on the structure and tidal motions of Europa's ice shell.

The tidal stresses on Europa also generate mode-1 fractures (i.e., pull-apart crevasses). Analysis suggests these cracks could open 0.1 to several km deep into Europa (Refs. 20 and 28), but again, site selection based on prior and upcoming missions will be critical to avoid these hazards.

Beyond faulting and fracturing in the lithosphere, tidal displacements will also stretch the entire ice column. Tides generate horizontal strains of 10^{-5}, which leads to vertical Poisson strains of the same order. Thus, any deployment that is coupled to the shell (e.g., a communications tether) will be subjected to hundreds of cycles of MPa-level stresses over the course of the mission, assuming a reasonable Young's modulus of 100 GPa for the ice.

The consistency of the ice is also a design driver. Fortunately, large voids (i.e., on the scale of the Tunnelbot or larger) are not expected. Like other planetary surfaces, Europa's ice column starts with a regolith ~1 m thick of porous ice that has been pulverized and processed by numerous microimpacts and radiation gardening. This regolith then progressively grades with depth into a fractured bedrock, again with small-scale void spaces, until ductile creep squeezes out the void spaces below the thermal lithosphere (Figure 4.3.5 in Ref. 21).

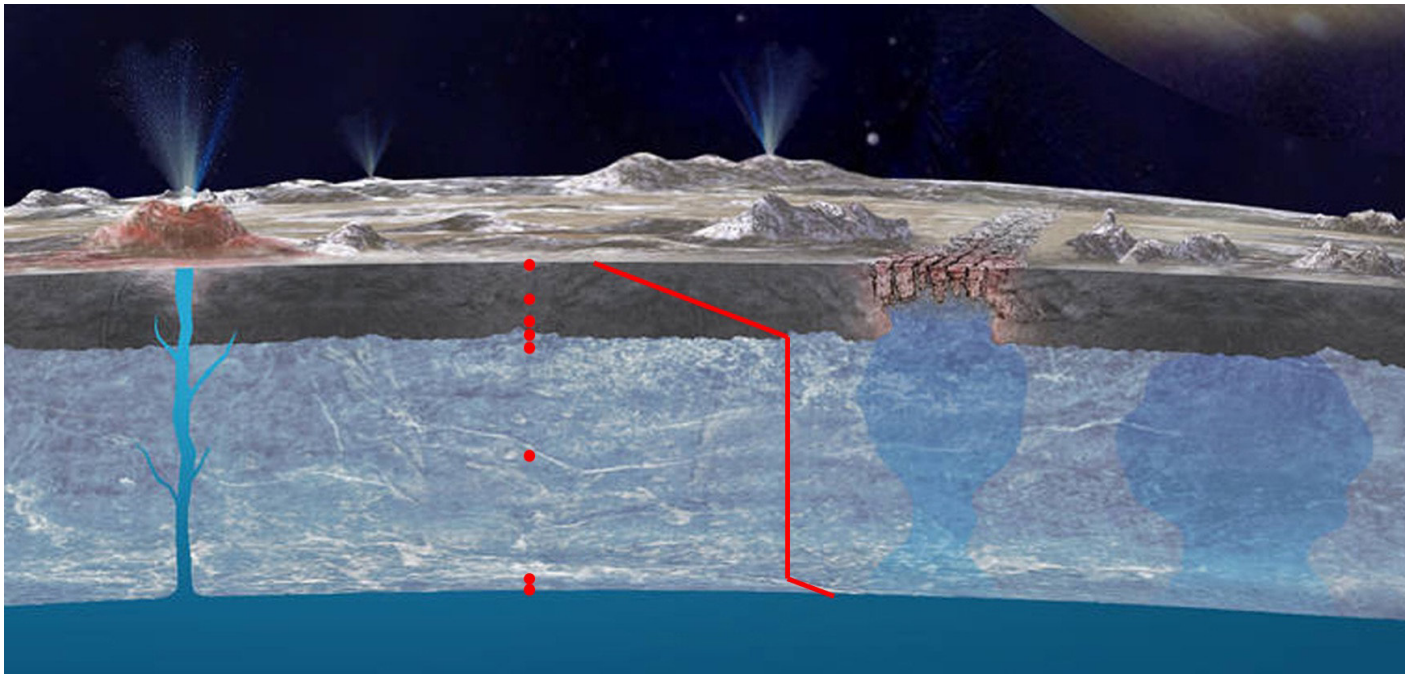

Figure 3.—Ice shell of Europa, artist's conception. Red line traces notional thermal profile through shell, and red dots show nominal sampling locations from initial concept of operations, which are tied to thermal profile. Modified from image courtesy of NASA/JPL-Caltech.

While voids are expected to be absent, the pulverized and fractured nature of Europa's near surface ice introduces a porosity that can affect the thermal conductivity. The 1-m regolith, by analogy to terrestrial regolith and soils, likely has a porosity of 30 to 50 percent (cf. sand), which models (Ref. 29) suggest will result in a 30- to 95-percent reduction in the thermal conductivity. Below the regolith, analogies to fractured (igneous) bedrock and sea ice suggest porosities of 1 to 10 percent, with perhaps up to a 20-percent reduction in thermal conductivity. Below the lithosphere, porosities are <1 percent.

In addition, there exists the possibility of lakes of liquid water within the ice shell. Several models for the formation of surface features have proposed pockets of water within the subsurface, created and potentially continuously fed by the deeper ocean (Ref. 13, 14, and 30). These pockets are potentially kilometers wide, so steering a Tunnelbot around them is problematic. However, like the deeper ocean, these lakes represent potential chemical mixing zones that could be habitable, and so reaching either a lake or the ocean is desirable. Unfortunately, the presence of these lakes are equivocal with the available data; however, data from the Europa Clipper mission could be used to refine landing site selection to either target or avoid any pockets of water.

The composition of the ice shell is also uncertain. While dominated by water ice (like sea ice on Earth), the exact composition is expected to be influenced by endogenous processes from the ocean, exogenous processes from the surface environment, and impact gardening and potential subduction that mix the two. The ocean may provide sulfate or chloride salts, hydrocarbon and nitrogen compounds, and other volatiles like methane and ammonia. Conversely, the Jupiter environment around Europa can provide silicate and carbonaceous chondritic material (including polyaromatic hydrocarbons), sulfur compounds from Io, and radiolysis and photolysis products from the radiation environment interacting with the surface and producing oxidized volatiles (e.g., Ref. 11 and references therein). Consequently, the upper centimeter could be 3 to 5 percent molar salts, with impact gardening mixing the salts into the upper 1 to 10 m of ice. The deeper ice should reflect more the composition of the ocean.

Notably, large hard particles that could impede a tunneling probe are likely absent. Impacts of bolides larger than micrometer-sized dust into Europa are not slowed because of the lack of an appreciable atmosphere, resulting in vaporization of meteorites. Thus, silicate chondritic material is likely limited to dust-sized particles, but volumes are expected to be low. Johnson et al. (Ref. 19) estimated the dust flux to Europa as ~5 ton/d. Integrated over the expected 60-Myr age of the ice shell, the mass of dust is ~10^{14} kg, which is less than one-millionth the mass of the shell. A Tunnelbot sweeping through a 1-m^2 column of the shell should flux through ~3 kg of dust. This dust is also likely limited to the upper gardened zone (<10 m deep).

4.3 Notional Science Concept of Operations (CONOPS)

The science goals and objectives can be met by providing a vertical profile of measurements through the ice shell. The sites of these measurements should be targeted at zones where mixing of redox components occurs and in interim spaces to flesh out the profile. Because these mixing zones are largely controlled by the thermal structure of the ice shell (e.g., the base of the lithosphere), the decision to stop and sample should be guided by temperature. Hence, the Tunnelbot will need to be able to measure temperature of the unperturbed surrounding ice to within 5 K (Figure 3).

A suite of samples at the surface is desirable, but the sampling acquisition mechanisms at the surface could be quite different from when the Tunnelbot is deployed into the shell, which could add unrealistic cost and complexity to the mission. Conversely, surface data could be acquired by a precursor or contemporaneous lander mission (e.g., Europa Lander SDT Report, 2016) (Ref. 21).

Ostensibly, the first mixing zone will be the base of the thermal lithosphere, where convectively upwelling ice from the deep interior flattens against lithosphere. Models suggest the transition from conduction to convection occurs over a range of 200 to 250 K, so several samples (e.g., at 200, 225, and 250 K) are required to ensure sampling near this mixing zone. A previous sample at 150 K will provide context of the geochemical and geophysical state of the lithosphere that is mixing with the convective ice.

Below the lithosphere, the temperature of the ice goes largely isothermal in the convection zone. Presumably, a precursor orbiter mission (e.g., the Europa Clipper) will constrain the thickness of the ice shell prior to deployment of the tunneling probe. This value, coupled with Tunnelbot data on the base of the lithosphere, should allow acquisition of a sample midway through the convective interior of the shell in order to constrain the typical conditions of the material that mixes with the lithosphere above.

The final mixing zone is the base of the shell. A sample within the bottom thermal boundary layer is desired to understand how ocean components might be incorporated into the ice. Thus, this sample site should occur at an intermediate temperature between that of the isothermal convective region and the melting temperature of the ice at ~270 K.

The final suite of samples should directly sample ocean water immediately at the base of the ice shell. This sampling should include the ability to measure the ice at this interface because of the potential for biomarkers (e.g., microbial communities) on the interface ice.

A caveat to this scheme occurs if the Tunnelbot encounters a lake on the way down. Should this possibility occur, the top of the lake should be treated as if the Tunnelbot has reached the

ocean. Because a putative subsurface lake would represent an interface and possible mixing zone where biomarkers could be present, this scenario is also of value towards the science objectives.

4.4 How To Detect and Characterize Biosignatures Within Europa's Ice and Subsurface Ocean

The primary science goal of this concept study is to provide a confidently positive or negative determination of the presence of biosignatures within the ice shell and subsurface ocean of Europa and to assess its potential for habitability. The definition of biosignature is adopted from the Europa Lander SDT Report (2016) (Ref. 21) as a "feature or measurement interpreted as evidence of life," and follow a similar path of using multiple, nested analytical techniques towards providing confidence in the interpretation of results. Individually, no single measurement or analysis can provide irrefutable evidence of the presence of life (past or present) that is distinguishable from a false biosignature produced abiotically. However, combining carefully chosen measurements and analyses supports interpretations and will provide strength to both positive and negative determinations of the presence of biosignatures.

Towards this, there are four main analytical objectives:

(1) Analysis and characterization of a wide range of organic biosignatures.
(2) Detection of amino acids and determination of enantiomeric proportions.
(3) Visualization of the ice and ocean interface (or potential ice and lake interface).
(4) Assessment of the habitability of Europa's ice shell and subsurface ocean.

4.5 Specificity of Life

Life affects the geochemistry of any system in a nonrandom manner. Separating which organic compounds are potentially biosignatures from the matrix of abiological geochemistry found in the same environment requires looking for patterns in types and distribution of organic biomarkers. Abiotic geochemical processes follow thermodynamic patterns and produce smooth distributions of products, often following a Poisson distribution as a function of mass. In contrast, biological processes select for specific compounds, enriching a sample with complex distributions of organic biomarkers. In addition, because it is not known if organic biosignatures on Europa will be identical to those found in Earth systems, determination of life using just compound identification is problematic. It can be expected, however, that even Europan biological processes will specify preferences and produce nonrandom patterns in compound distributions.

As an example, Figure 4 depicts a comparison between the randomized production of hydrocarbons in an abiological process and the nonrandom production in a biological system. The Fischer-Tropsch Type (FTT) synthesis of hydrocarbons produces a smooth distribution of compounds of every length, where the biological production of hydrocarbons in Bacteria and Eukaryotes favors even-numbered carbon chains over odd-numbered carbon chains (Refs. 31 and 32). Identification of carboxylic acids, such as those found in cellular membranes, will be insufficient for positive identification of biosignatures in Europa; rather, the distribution and patterns found will support determination of life (Objective 1).

Similarly, identification of individual amino acids serves as a potential biosignature, but is indeterminate alone. Around 500 members of the same chemical class as amino acids have been identified (Ref. 33), and over 70 have been detected in meteorites (Refs. 34 to 36). However, only 22 amino acids are used by life on Earth, restricting the type of amino acids that are expected to be relevant for the search for life. Furthermore, abiotically produced amino acids are distributed as driven by thermodynamics and kinetics (Ref. 37), while biology demands functionality. As a result, the relative abundance of specific amino acids from biotic sources compared to those from abiotic sources differs substantially (Figure 5), and comparing the proportions of amino acids is a powerful tool for determining biogenicity. In addition, amino acids are chiral and display one of two configurations (L and D). This enantiomeric ratio is also dependent on the source of the amino acids. Abiotic mechanisms produce nearly equal proportions of each enantiomer, or up to 15-percent preference for the L-enantiomer (Refs. 38 and 39), while biological processes produce the L-enantiomer nearly exclusively (Ref. 40), with exceptions (Ref. 41). The powerful combination of analyzing type, abundance, and enantiomeric ratios of amino acids provides confidence in the determination of biological origins (Objective 2).

The end destination of the Tunnelbot is a body of water (ocean or subsurface lake). The interface between ice and fluid represents a transition zone where gradients in geochemistry and energy availability are anticipated to occur. Because this transition will include a physical boundary (between ice and fluid), it is anticipated that organisms living in this transition zone may utilize the solid surface as a nucleation point for biofilm or biomineral formation. Visualization of the solid interface, and analysis of potential biosignatures on the solid surface will confirm this possibility (Objective 3).

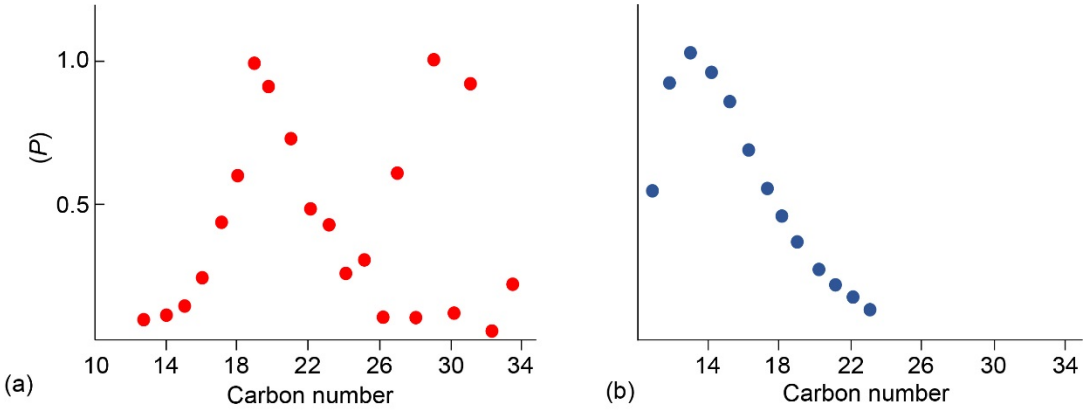

Figure 4.—Comparison between the randomized production of hydrocarbons in an abiological process and the nonrandom production in a biological system. Abiotic production of organic compounds such as *n*-alkanes typically produces a smooth distribution of compounds, while biological processes selectively produce compounds necessary for biological processes. Such data can be found throughout literature, such as in Hartgers et al. (2000) and Lovelock et al. (1965) (Refs. 42 and 43). (a) Produced by biogenic processes and found in wax. (b) Produced from abiotic Fischer-Tropsch Type synthesis process.

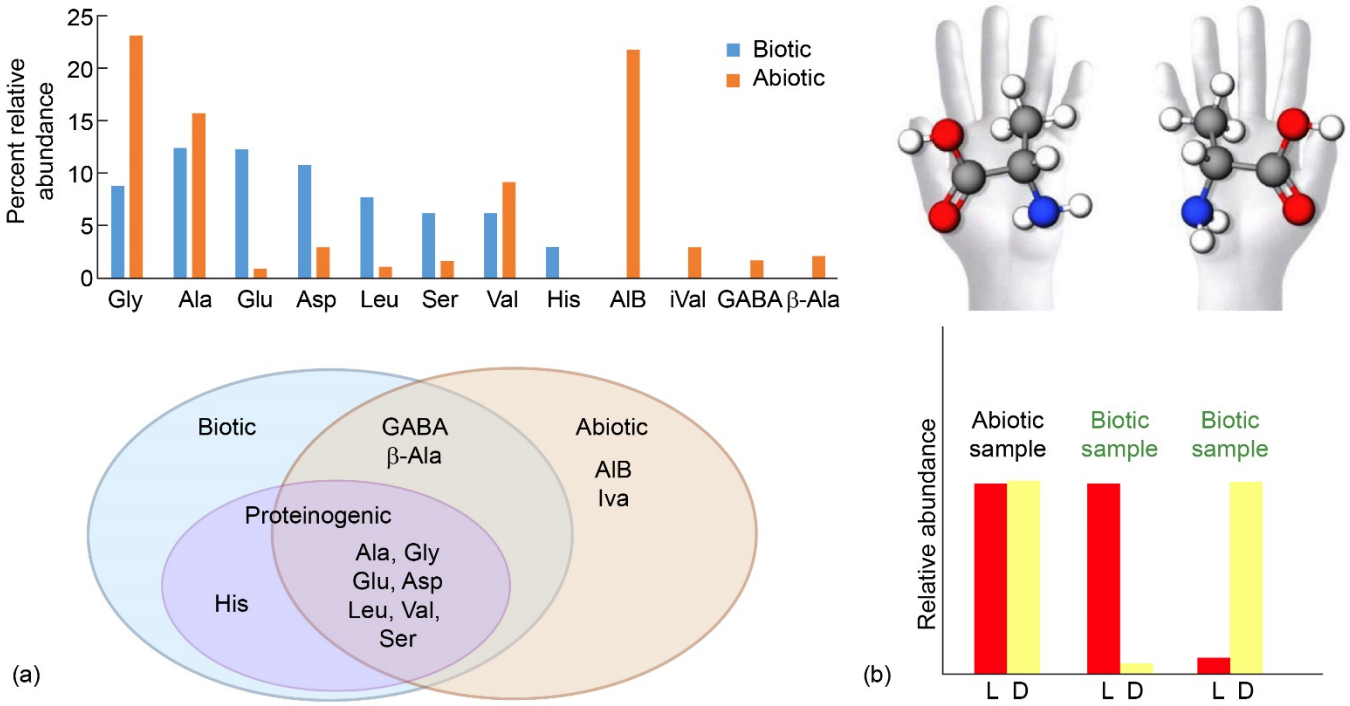

Figure 5.—Type and abundance of amino acids produced is extremely informative. (a) Specific amino acids are only produced abiotically, and ratios of relative abundance of amino acids can help decipher their origin as biological or not. (b) Enantiomeric excess is another diagnostic tool for distinguishing biotic from abiotic amino acid production. Both figures adapted from Europa Lander Science Definition Team Report (Ref. 21).

4.6 Habitability Assessment

All life should require a source of carbon to build biomass and a source of energy to support biomass production. Measurement of the geochemistry and temperature of fluid and solid water on Europa will inform the geologic context of the moon, reveal the degree of water-rock-ice circulation, and provide indications of how the satellite may support active metabolism. A characterization of the habitability of the ice shell and subsurface ocean is as necessary a science mission goal as the measurement of biosignatures (Objective 4). In fact, observance of biosignatures that appear extant would be supported by an assessment of habitability, while a lack of habitability would cast doubt on other potential biosignature observations. Furthermore, in the event of a failure to detect organic biomarkers, the habitability assessment, mission profile, and other data will help guide decisions about future searches for life on Europa.

4.6.1 Instrumentation

To meet these objectives, the following items would need to be measured. For Objective 1, abundances and ratios of carboxylic acids, including phospholipid fatty acids (PLFAs), other lipids, carbohydrates, other hydrocarbons will need to be determined, while Objective 2 will require abundances, ratios, and chirality of amino acids. Objective 3 would need imagery and spectroscopy from the base of the ice shell. Objective 4 will require determination of physiochemical parameters such as temperature, pH, sulfates, carbonates, and silicate minerals as well as dissolved ions, salts, radiolytic products, and volatile compounds.

The minimum specifications for the concept instrumentation are expected to be identical to that of the Europa Lander, as the materials encountered will largely be the same. Improvements on these limitations during instrument development should be considered as well. Based on the Science Traceability Matrix (STM) from the Europa Lander Concept Study (2016) (Ref. 21), the instrument needs and capabilities for the Tunnelbot mission are to be defined as follows.

Organic compounds such as carboxylic acids (including PLFAs), other lipids, carbohydrates, and other hydrocarbons need to be detected in concentrations of at least 1 pM/g of Europan subsurface material (or equivalent). The instrumentation will need to identify compounds with a broad molecular weight distribution of at least 2 to 550 Da at a resolution of $m < 1$ Da across the m/z range for most compounds and 1,000 m/m for some compounds (such as lipid parents). Detection of amino acids requires instrumentation that can identify (at 1 pM/g limit of detection (LOD)) at least four amino acids from the group: Ala, Asp, Glu, His, Leu, Ser, Val, Iva, Gly, β-Ala, GABA, and AIB. Furthermore, at least one representative of each class (abiotic, biotic, and proteinogenic) needs to be identifiable. For chiral molecules, the desired LOD is at least 1 nM/g for each of the two chiral forms. The mass range expected is 18 to 387 Da at a resolution of 1,000 m/m. These biosignatures could be addressed with an instrument such as a quadrupole mass spectrometer (MS) or quadrupole ion trap MS, or a multibounce or impact-ionization time of flight (TOF) MS. Conceptual heritage and additional instrumentation in development is discussed in the following paragraphs.

The bulk geochemical and physical characteristics of the ice and ocean need to be addressed as well. Temperature, Eh, and pH will be necessary to determine solubility and stability of compounds within the matrix measured and to make predictions concerning habitability. Sulfate, chloride and other salts, radiation products (e.g., H_2O_2, CO_2, O_2, SO_2, and S_n), additional volatiles (e.g., H_2S, CH_4, CO, CH_3SH, and DMS), metals and metal hydroxides, and silicates (both hydrous and anhydrous) will need to be detected at levels of at least a few to hundreds of ppt, by mass. These measurements could be achieved with a vibrational spectrometer (VS) (such as a Raman Laser Spectrometer) or a microfluidic device.

When the Tunnelbot meets a body of water, a different set of analyses will be required as solid ice is left behind. The visualization and analysis of the ice-fluid interface will require a pair of cameras and spectrophotometry to identify potential biofilms and biominerals on the surface of the interface. This could be achieved at either high or low focal distance (both are preferable). For example, a combination of an instrument with a field of view (FOV) of 100 by 100 µm to give context imaging and an ultraviolet- (UV-) fluorescence spectrophotometer could achieve the goal at low focal distance. Heritage options could include a SHERLOC+WATSON-like instrumentation. Coarse resolution data could be obtained with a pair of cameras with a resolution of 500 µm/pixel from 2 m away from the surface. Heritage instrumentation includes the SuperCam (Mars 2020) (Ref. 44).

The previous measurement requirements largely build on those detailed in the Europa Lander Concept Study (2016) (Ref. 21). This study identified a suite of instruments that can meet the goals of the Tunnelbot, and thus serve as heritage, some of which were discussed previously.

Heritage instruments that meet the requirements for analysis of organic biosignatures include SAM and SHERLOC. However, these have specifications that would likely exceed the payload capabilities of the Tunnelbot (notably volume), so it is recognized that further instrument design and development will be required for the Tunnelbot for the analysis of organic biosignatures. Potential instrumentation designs that would be miniaturizable could include, in addition to those discussed previously, a high-sensitivity linear ion trap with a high-resolution CosmOrbitrap

analyzer. Such an instrument would allow broadband detection of organic and inorganic compounds as well as ion isolation at very high resolution. Additional options are a Laser Desorption Mass Spectrometer (LDMS) or Linear Ion Trap Mass Spectrometer (LITMS). These instruments have a high mass range capability at high resolution. An instrument with a laser source would also supply geologic context of salts and mineral phases present in the residues that can be analyzed in addition to organic biosignatures. Some of the previous instrumentation options would require the addition of a gas chromatograph to obtain chirality data, critical to the disentanglement of potential amino acid biosignature data.

Note that the instrument package (and scientific objectives) does not include the isotopic and physical biomarkers (such as fossils) selected for the Europa Lander Concept Study. These quantities and their implications for life can be ambiguous and are controversial when studied in Earth-based reference frames (Refs. 45 to 48), much more so than the other measurements. Furthermore, isotopic ratios in carbon on Europa could be subject to environmental conditions without a direct analogue on Earth, such as radiation processing, limiting the ability to provide useful points of comparison. Given that the Tunnelbot is severely restricted on payload mass and volume, these methods for biosignature identification are not included. However, a notional payload that includes an instrument that could supply high-precision isotopic abundances to the scientific return would be an added benefit.

In addition, the stated science objectives do not require a seismometer; however, the Tunnelbot would afford a unique seismic opportunity. Most modern applications of planetary seismology (e.g., InSight, the Europa Lander) consist of a single surface station, utilizing single-station analyses that primarily reveals global structure. Undoubtedly, a seismometer should be included on the surface asset. Beyond that, series of seismometers on the Tunnelbot and the repeaters would effectively create a linear array. Such an array would be able to resolve seismic events in depth (yet would be blind to azimuth), thereby helping to constrain the seismicity and fracturing activity within Europa's ice shell and provide data on ice shell density with depth.

4.6.2 Consequences of Radiation

Although life would be protected from Jupiter's strong radiation impinging on the surface and very shallow (<10 cm) subsurface, the power supply for the Tunnelbot is expected to produce radiation that could impact both the instrumentation and areas from which the samples are gathered. Destruction of organic biosignatures by gamma and neutron radiation can occur by two main paths; direct exposure to radiation and exposure to peroxides formed by radiolytic reactions (Ref. 49). Both of these paths are of concern to the successful collection of samples in the Tunnelbot mission, and instrumentation could be damaged by direct exposure.

While most focus of radiation effects on the formation and destruction of organic compounds in planetary contexts has centered on UV radiation (Ref. 50), much of what is known about the impact of gamma and neutron radiation on biological compounds (such as proteins, membrane lipids, amino acids, and nucleic acids) comes from work exposing whole cells or organisms to specific radiation levels, as relevant to the food processing and health industries. For example, there is extensive interest in how much radiation is enough to kill whole cells or organic components for food safety (Refs. 51 and 52), but there exists very little literature available on what the lower threshold is for bacterial survival. Doses and times of exposure vary widely. Few data exist from testing gamma or neutron radiation effects on Archaea (Refs. 53 and 54). To complicate further a review of available literature, disciplines use different methods to gauge destruction of target compounds, ranging from remaining measurable concentrations, changes in ratios of specific compounds, changes in structure (length, saturation, number of rings, etc.) and function, and percent survivability.

The primary source for determining the impact of gamma and neutron radiation on individual compound classes relevant to this mission comes from the astrobiological literature. Several studies concerned the probability that organic reagents needed for mission experimentation will survive a trip to a planetary surface and how long they will remain viable there (Refs. 55 to 57). Some studies exposed how deeply a spacecraft would have to excavate the Martian regolith before organic biosignatures might be found that were unaltered by billions of years of radiation hitting the surface of the planet (Refs. 49, 58, and 59). Table 4 pulls together the fragments of available information towards reaching a lower threshold of tolerable gamma and neutron radiation exposures relevant to this mission. Variation and limitations on the data are noted in the footnotes of the table.

Lacking available data, values to estimate the resistance of amino acids to gamma radiation in Table 4 within a 99- to 99.99-percent survival rate dosage were calculated. The estimation used radiolysis constants given for four amino acids in Reference 60. These were applied to an equation derived from experimental data in Reference 58, specifically,

$$\ln (N/N_0) = -kD \quad (1)$$

where N and N_0 are the amino acid abundances postradiation and preradiation, respectively, k is a radiolysis constant for individual amino acids in MGy^{-1}, and D is the radiation dose in MGy. The estimates given in Table 4 are the result of calculating 99 to 99.99 percent survival of L-glutamic acid, the amino acid with the highest sensitivity of the four that were explored in Reference 60. In a mission searching for biosignatures in the subsurface of an extraterrestrial planet, the

TABLE 4.—SUMMARY OF AVAILABLE DATA ON THE LIMITS OF EXPOSURE TO GAMMA AND NEUTRON RADIATION ON VARIOUS CELLULAR COMPONENTS RELEVANT TO THE SEARCH FOR BIOSIGNATURES AND WHOLE CELLS

[All data given in kGy unless otherwise indicated, where Gy = a gray unit and 1 Gy = 100 rad. Empty boxes indicate that data pertaining to that specific variable or measurement were not found in the extensive search through the literature of multiple disciplines.]

Gamma radiation	DNA	Amino acids	Lipids	Proteins	Whole cells
Damaging levels	[a]0.2 to 6	[b]0.58 to 58	[c]<0.1 to [d]5 [e]30 to 60	----------	[f]<0.07 to [g]12
Tolerable levels	----------	----------	----------	30 to 150 [h]	----------
Measured effect	Strand breaking	Peroxidation/direct	Peroxidation	Peroxidation	Cell death
Neutron radiation	----------	----------	----------	----------	----------
Damaging levels	----------	----------	[i]0.009 Gy	[i]0.009 Gy	----------
Tolerable levels	----------	----------	----------	[j]0.6 to 6 MeV	----------
Effect	----------	----------	Direct	Direct	----------

[a]Deoxyribonucleic acid (DNA) damage given as double strand breakage, resulting in cell death. Degree of damage is dependent on genome size, with a high degree of variability for species to repair damage and survive (Ref. 61).

[b]Calculated survival rate dosage. Constants were experimentally defined using dry amino acids with a nonreactive atmosphere. Thus, this value represents direct impact on the amino acids, rather than indirect effects from peroxidation (Refs. 58 and 60).

[c]Lowest irradiation dose used = 0.098 kGy; damage measured as a change in the ratios of specific lipids analyzed as well as the structure of the lipids (Ref. 62).

[d]Lowest irradiation dose used = 5 kGy, damage measured as loss of total PLFA concentration; did not look at impact on lipid structure (Ref. 63).

[e]Lowest irradiation dose used = 30 kGy, damage measured as loss of pigment ability to absorb varying wavelengths (radiation at 30 kGy damaged the ability of all tested pigments to absorb light) (Ref. 59).

[f]Data for *Shewanella oneidensis* (Ref. 61).

[g]From References 51, 61, and 64.

[h]Lowest dose used = 30 Gy, damage measured to antibodies intended for detection of organic molecules on Mars. No damage found to preserved antibodies at 30 Gy, but unpreserved antibodies were not tested (Ref. 56).

[i]Damage to lipids and proteins in whole cell membranes of live animals was considerable and involved structural changes (Ref. 65).

[j]Measured as direct damage to antibodies as a test for mission-specific analyses. Fluorescein was also tested. All tests were done on dried and preserved compounds, and the range stated is the only range tested (Ref. 55).

highest survival rate is preferable to avoid contamination of the measurement with irradiated lipid concentrations and structures that would result from a lower survival rate.

Based on the compilation of data from the available literature, the concept team arrived at a maximum dosage of 100 Gy from the Tunnelbot to any sample collected as a target for the mission.

4.6.3 Implications for Sampling Protocol

The reactivity of radiolytic products, dissolved species, and volatiles requires that an ice sample cannot thaw until the sample is safely in a controlled environment. Furthermore, allowing an ice sample to melt external to the Tunnelbot will introduce the potential of contamination with ice that has been previously melted and irradiated as the Tunnelbot moves through the ice medium. Therefore, it is critical to the success of the mission that a solid sample can be retrieved and transferred into a sealed analytical environment before being allowed to melt. This restriction provides challenges to the design of the Tunnelbot body and sample retrieval mechanism.

In addition, once an ice or fluid interface is reached (either the subsurface ocean or an inter-ice lake), fluid samples are desired to characterize the nature of the fluids and the presence of biosignatures.

It is anticipated that solid samples will be obtained in a coring fashion, into the sidewall of the ice shaft created as the Tunnelbot melts its way into the subsurface. To maintain sample integrity between sample locations, providing a pristine sampling device to each sample location will be required. Cross-contamination between sample locations should be avoided to restrict ambiguity of results. Coring into the sidewall of the ice shaft will mean that the first few millimeters of an auger device will pass through the melted ice between the Tunnelbot and the ice shaft, contaminating the front end of the sampled ice core. Therefore, the front end of the cored ice will need to be ejected or otherwise discarded before the sample enters any pristine sample reception container. It is likely that development of a sampling auger will be required to fit the specific engineering restrictions of the Tunnelbot. A device with a dedicated sample acquisition chamber for each sample location, with either a dedicated auger

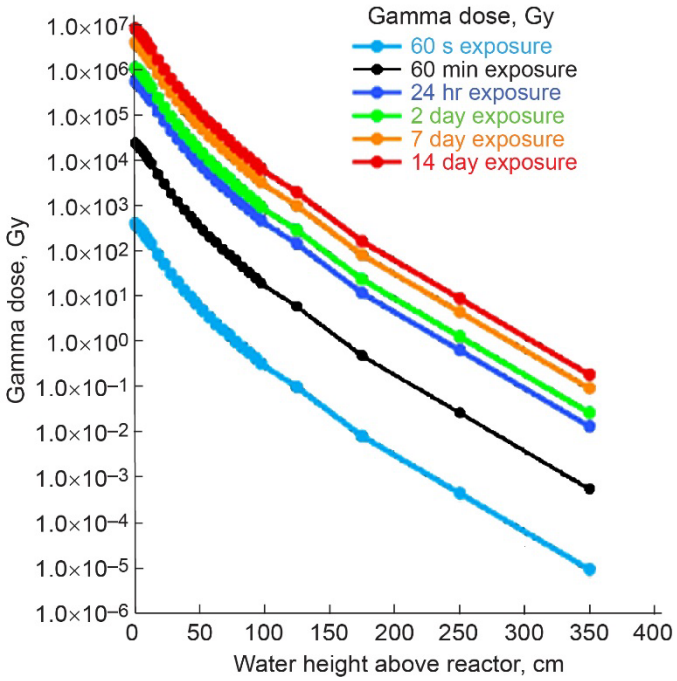

Figure 6.—Gamma ray dose (Gy) as function of water height above 43-kW_{th} nuclear core for different exposure times.

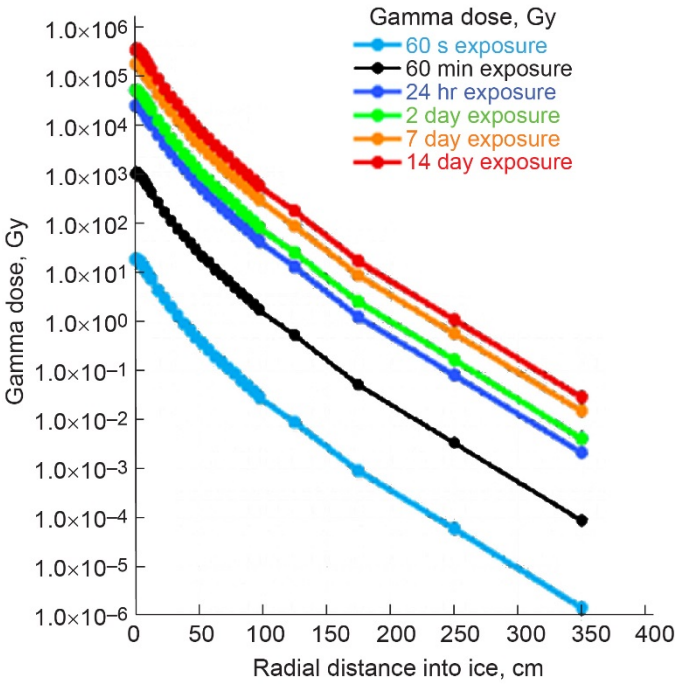

Figure 7.—Gamma ray dose (Gy) as function of radial distance into surrounding ice for different exposure times.

per sample location or an auger that can be cleaned between sample locations, is recommended.

The sampling plan and sample acquisition development should also account for the potential need for duplicate samples to be retrieved at any given sample location. For example, following an analysis of a sample that indicated a biosignature is identified, ideally an Earth-based decision should be made to direct the Tunnelbot to obtain a second sample at the same location. The acquisition of duplicate samples is anticipated to primarily affect the number of pristine sample chambers required, instrument consumables, and the data volume produced.

The concept team arrived at a maximum dosage of 100 Gy from the Tunnelbot to any sample collected as a target for the mission (see the previous discussion). Further estimations revealed that neutron radiation is not expected to be an issue during the mission, and that the exposure of the sample to gamma radiation can be effectively controlled by using a water buffer between the radiation source and the sample collection area. The radiation source will be kept above the sample collection area (downstream of the sample collection), also limiting sample exposure to radiation. Figure 6 and Figure 7 illustrate the time allowable at given gamma radiation exposures. It can be seen in Figure 6 that with a configuration of 1.5-m meltwater between the reactor and sampling area, the Tunnelbot can sit for ~2 d before the sample area reaches 100 Gy dosage. Figure 7 estimates the distance into the solid ice wall for given exposure times before 100 Gy dosage is reached; here, samples are safe at a 30 cm distance from the Tunnelbot for only ~60 min, but up to 2 d at 1 m distance. These data will need to be considered fully as the coring and sampling device are developed, taking into account the possible need for Earth-based decisions concerning resampling of the same area.

See Table 5 to Table 7 for the Science MELs for the reactor Tunnelbot, the GPHS Tunnelbot, and the repeater, respectively.

TABLE 5.—REACTOR TUNNELBOT SCIENCE MASTER EQUIPMENT LIST FOR CASE 1

Description	Quantity	Unit mass, kg	Basic mass, kg	Growth, percent	Growth, kg	Total mass, kg
Science	-	-----	26.9	30.0	8.1	34.9
Raman and camera	1	3.1	3.1	30.0	0.9	4.0
Organic compound analysis package and pump	1	10.5	10.5	30.0	3.2	13.7
Seismometer	1	0.3	0.3	30.0	0.1	0.4
Sample acquisition	1	10.0	10.0	30.0	3.0	13.0
Raman and camera electronics	1	1.8	1.8	30.0	0.5	2.3
Organic compound analysis package and pump electronics	1	1.0	1.0	30.0	0.3	1.4
Temperature sensor	1	0.0	0.0	30.0	0.0	0.0
Pressure sensor	1	0.1	0.1	30.0	0.0	0.1

TABLE 6.—GENERAL PURPOSE HEAT SOURCE TUNNELBOT SCIENCE MASTER EQUIPMENT LIST FOR CASE 2

Description	Quantity	Unit mass, kg	Basic mass, kg	Growth, percent	Growth, kg	Total mass, kg
Science	-	-----	26.9	30.0	8.1	34.9
Raman and camera	1	3.1	3.1	30.0	0.9	4.0
Mass analyzer and linear ion trap and pump	1	10.5	10.5	30.0	3.2	13.7
Seismometer	1	0.3	0.3	30.0	0.1	0.4
Sample acquisition	1	10.0	10.0	30.0	3.0	13.0
Raman and camera electronics	1	1.8	1.8	30.0	0.5	2.3
Mass analyzer and linear ion trap and pump electronics	1	1.0	1.0	30.0	0.3	1.4
Temperature sensor	1	0.0	0.0	30.0	0.0	0.0
Pressure sensor	1	0.1	0.1	30.0	0.0	0.1

TABLE 7.—REPEATER SCIENCE MASTER EQUIPMENT LIST FOR CASES 1 AND 2

Description	Quantity	Unit mass, kg	Basic mass, kg	Growth, percent	Growth, kg	Total mass, kg
Science	-	-----	0.4	30.0	0.1	0.5
Science package group one	-	-----	0.4	30.0	0.1	0.5
Temperature sensor	1	0.01	0.0	30.0	0.0	0.0
Pressure sensor	1	0.10	0.1	30.0	0.0	0.1
Seismometer	1	0.30	0.3	30.0	0.1	0.4

5.0 Configuration

5.1 Reactor Vehicle Design

The configuration for the reactor case of the Europa Tunnelbot resembles that of a test tube with a hemispherical tip, a constant diameter cylindrical section, and an open back end. Overall dimensions of the Tunnelbot can be seen in Figure 8.

The 51.76 cm outer diameter, along with structural wall thicknesses, insulation thickness, and hot plate thickness, provides a cross-sectional area that allows many of the science instruments, other electronics, and the three communication repeaters (their configuration is discussed later) to be placed alongside one another rather than stacking. Having to stack the science instruments and system electronics would increase the overall length of the Tunnelbot. This diameter selection also provides enough width to allow the Stirling assembly to lay horizontally rather than vertically, which again, would increase the overall length. Reducing the diameter is a potential option, but the potential increase in length due to the packaging of components and resulting melting rate based on the new surface area would need to be further examined in detailed trades.

The overall length of 526.22 cm for the Tunnelbot reactor case is a result of science instruments, system electronics, and repeater packaging within the 51.76 cm diameter as well as providing the proper distances between the reactor and electronics to ensure the radiation dosage for the electronics stays below the desired levels. The 200 cm distance shown in Figure 9 is between the pressure vessel containing the science instruments and system electronics (instrument pressure vessel) and the pressure vessel containing the reactor. This section is designed to fill with water from the melted ice, providing sufficient shielding to reduce the radiation dosage the electronics will experience from the reactor to acceptable levels. The 113.7 cm distance shown in Figure 9 is the distance between the end of the reactor and the electronics contained in the repeaters. This distance is driven by the repeater design (length), the 9-cm-long (13-cm-diam.) lead shield located on the end of the reactor, and a 50 cm distance between the bottom of the repeater and the tip of the reactor pressure vessel dome. This 50-cm section will also be filled with water from the melted ice, which when combined with the lead shield on the end of the reactor, the pressure vessel structure, and a 2-cm-thick steel shield placed at the base of the repeaters, will reduce the radiation dosage the repeater electronics will experience to acceptable levels.

Two section views of the Tunnelbot reactor case are shown in Figure 10. In these section views, the reactor and instrument pressure vessels along with a tunnel connecting the two are

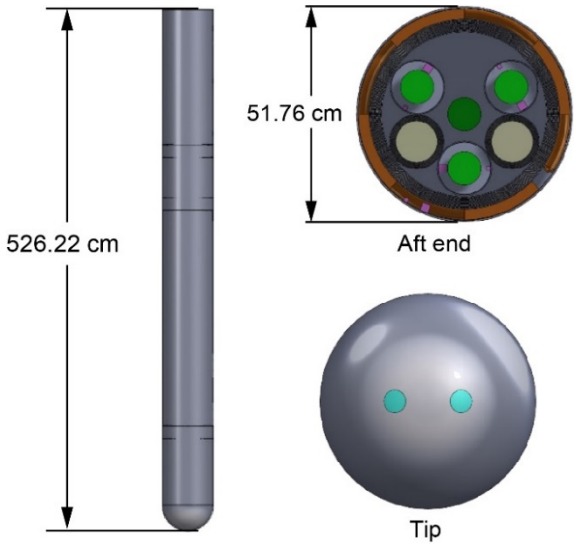

Figure 8.—Overall dimensions of Europa Tunnelbot nuclear design.

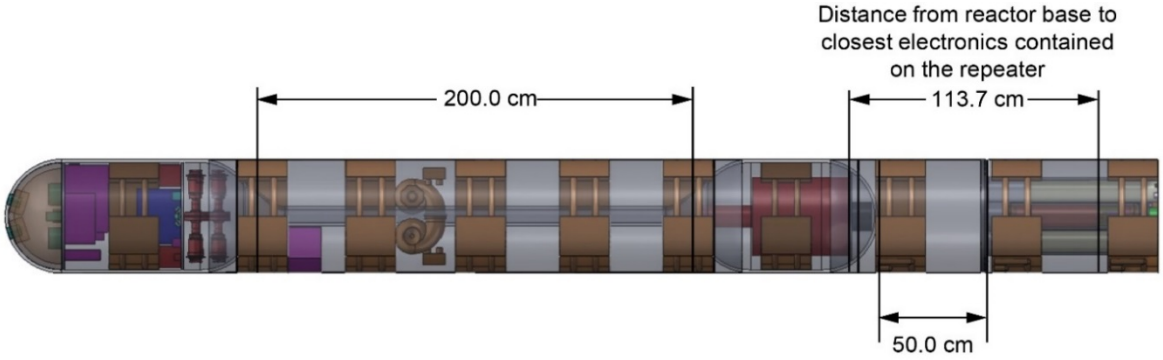

Figure 9.—Distances between reactor and electronics for Europa Tunnelbot nuclear case.

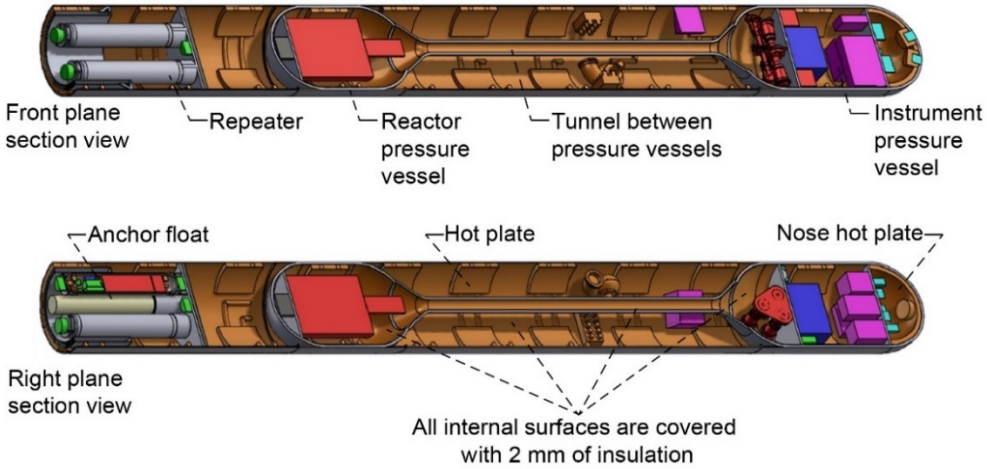

Figure 10.—Section views of Europa Tunnelbot nuclear case.

easier to see, essentially creating a single dumbbell-shaped pressure vessel. This tunnel contains the heat pipes that run between the reactor and the Stirling assembly and keeps them in a dry, low-pressure environment. All of the internal surfaces of both pressure vessels, the tunnel, and the two water chambers contain 2 mm of insulation. Inside of the insulation are the hot plates that are used to evenly distribute the waste heat to the external surface in order to ensure that the entire Tunnelbot will be surrounded by water during its descent into the ice. These hot plates cover about 25 percent of the entire surface area in the cylindrical section, while a single hemispherical hot plate is contained in the nose.

Those components contained within the instrument pressure vessel include most of the science instruments, all of the GN&C components, the Command and Data Handling (C&DH) System, the communication system electronics, power system battery and regulation and control units, the Stirling assembly, and five hot plates, including the nose hot plate. These components are shown in Figure 11.

Those science instruments contained in the instrument pressure vessel include the Raman and camera unit and the associated electronics box; the organic compound analysis package and pump unit and the associated electronics box; and the seismometer. The sample acquisition unit is located in the 200-cm-long water section shown in Figure 11, while the pressure and temperature sensors are located on the aft end of the Tunnelbot, as shown in Figure 12.

All of the components contained in the instrument pressure vessel are mounted to two 12.7-mm-thick honeycomb structural decks, with the exception of the two sonar transducers of the attitude determination and control (AD&C) system and the hot plates (mounted to the outer surface through the insulation). The two sonar transducers are located in the nose of the Tunnelbot and are mounted to the pressure vessel structure. They are each encapsulated in a hot plate that is connected to the hemispherical hot plate and must transfer the heat evenly from the hot plate to their surface that is flush with the pressure vessel external surface in order to prevent any cold spots on the nose while descending into the ice.

The 200-cm-long water section of the Tunnelbot is shown in Figure 13. This section contains the sample acquisition unit of the science system, two fluid loop manifolds, two fluid loop pumps, and 20 hot plates. The pumps move the fluid throughout the thermal system (hot plates) while the manifolds control the flow in order to control the external surface temperature of the Tunnelbot. It should be noted that the heat pipes for the thermal system were not modeled in this study and need to be examined in more detail to determine how they would be routed between the hot plates, pumps, and manifold within the Tunnelbot design. This exercise was beyond the scope of this study.

The reactor pressure vessel components are shown in Figure 14. This section contains the reactor assembly, the reactor instrumentation and controls, the lead shield, and four hot plates. The reactor is mounted to a 12.7-mm-thick honeycomb structural deck located in the dome of the pressure vessel.

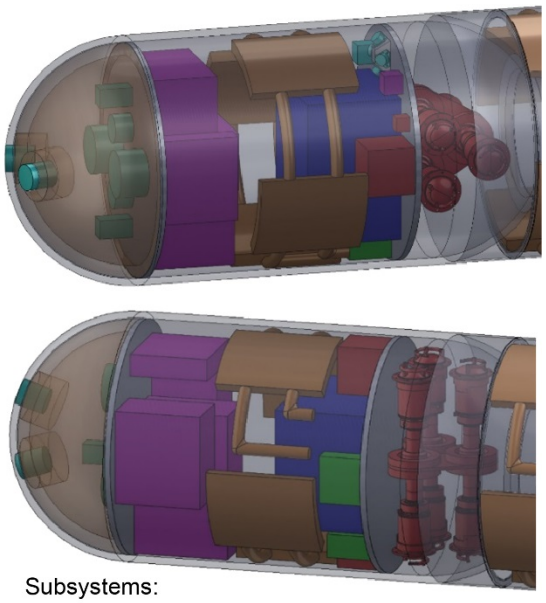

Figure 11.—Instrument pressure vessel components for reactor case.

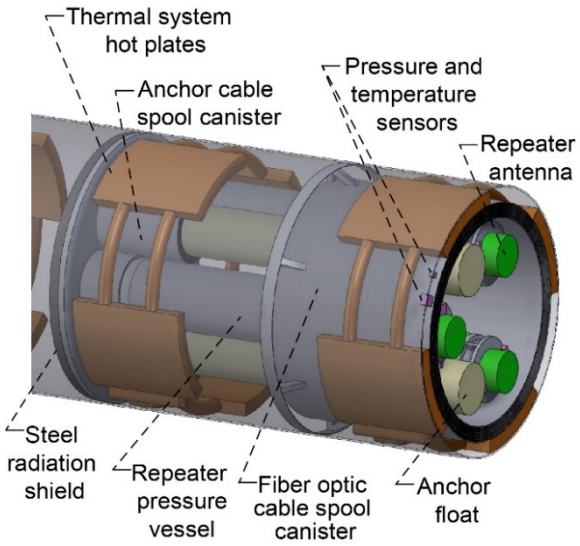

Figure 12.—Aft end of Europa Tunnelbot reactor case.

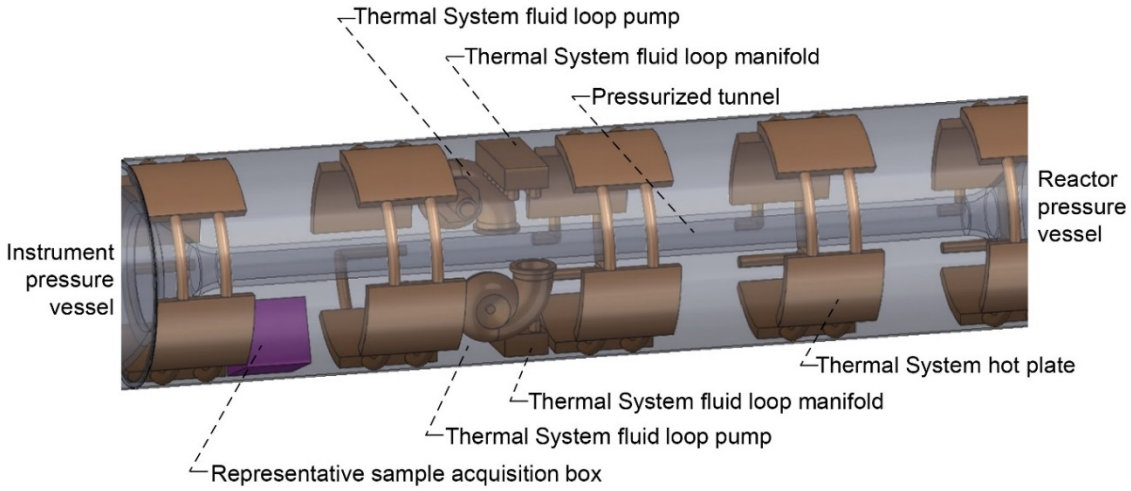

Figure 13.—Tunnelbot reactor case 200-cm-long water section.

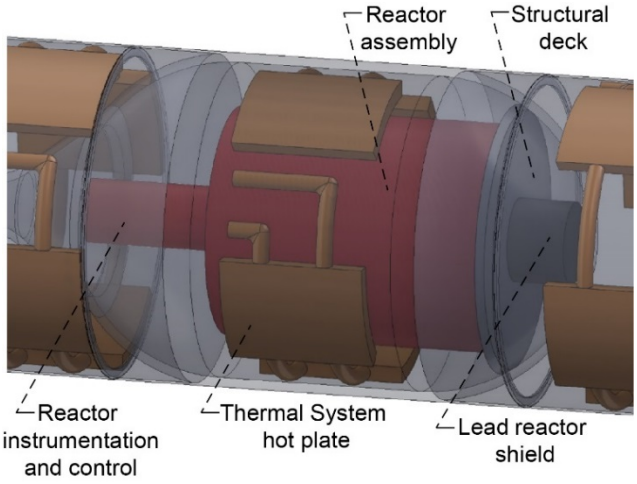

Figure 14.—Reactor pressure vessel components for reactor case.

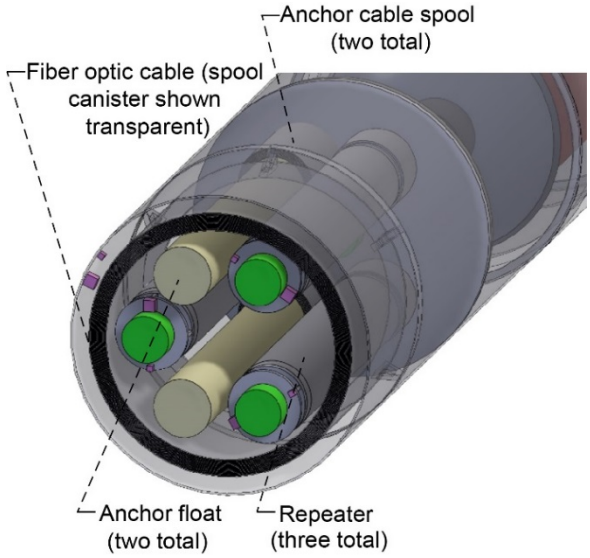

Figure 15.—Additional image of aft end of Europa Tunnelbot reactor case.

Mounted to the other side of this deck is the lead shield. The lead shield is 13 cm in diameter to match the diameter of the reactor core and is 9 cm long.

The aft end of the Tunnelbot contains the three repeaters, the repeater fiber optic cable spool, two anchor floats, two anchor cable spools, the Tunnelbot antenna, pressure and temperature sensors, and eight of the hot plates. This section of the Tunnelbot is shown in Figure 12.

The three repeaters, used for communications between the Tunnelbot and the lander, are each mounted inside a small cylindrical structure contained on a 12.7-mm-thick honeycomb structural deck. A c-channel structure is used for the spool containing the fiber optic cable that connects, in series, the Tunnelbot to the three repeaters and finally to the lander. The spools inner diameter encompasses the three repeaters while the outer diameter stays within the hot plates contained in the aft section. Additional structure is added to the base of the spool to mount the spool to the inside of the outer shell of the Tunnelbot. The two anchor floats (one for redundancy) are mounted on top of their individual spools that contain the structural cable used to stop the Tunnelbot once the anchor float is released, and the ice refreezes around it. The two anchor spools are in turn mounted to the same structural deck as the repeaters. Also mounted to the deck, in the center, is the Tunnelbot antenna used for communicating to the last repeater in the event that there is a break in the fiber optic cable. Located at the very end of the Tunnelbot and mounted to the inside surface of the outer wall are the temperature and pressure sensors. An additional image of the aft end of the Tunnelbot is shown in Figure 15.

Additional transparent images of the Europa Tunnelbot reactor case are shown in Figure 16 while the two water chamber sections of the Tunnelbot can be more easily seen in Figure 17.

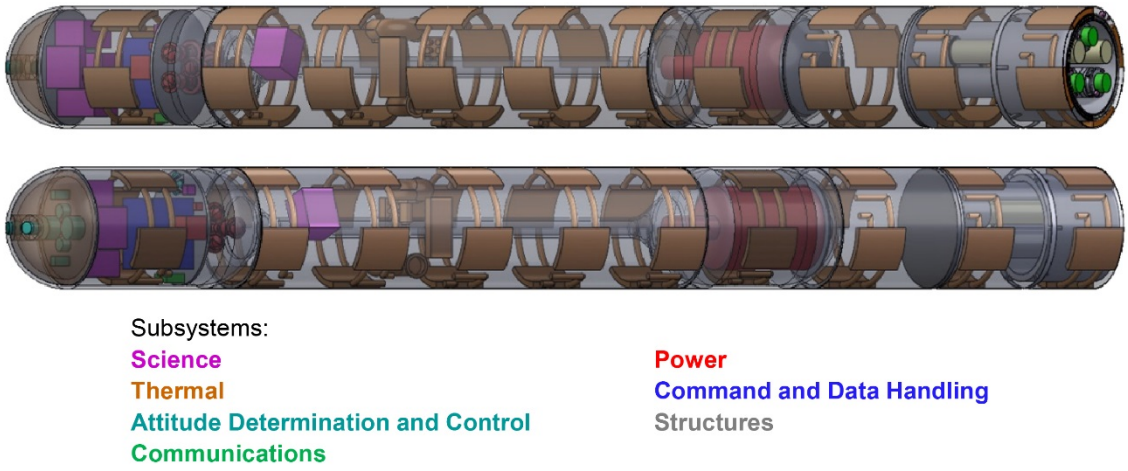

Figure 16.—Additional transparent views of Europa Tunnelbot reactor case.

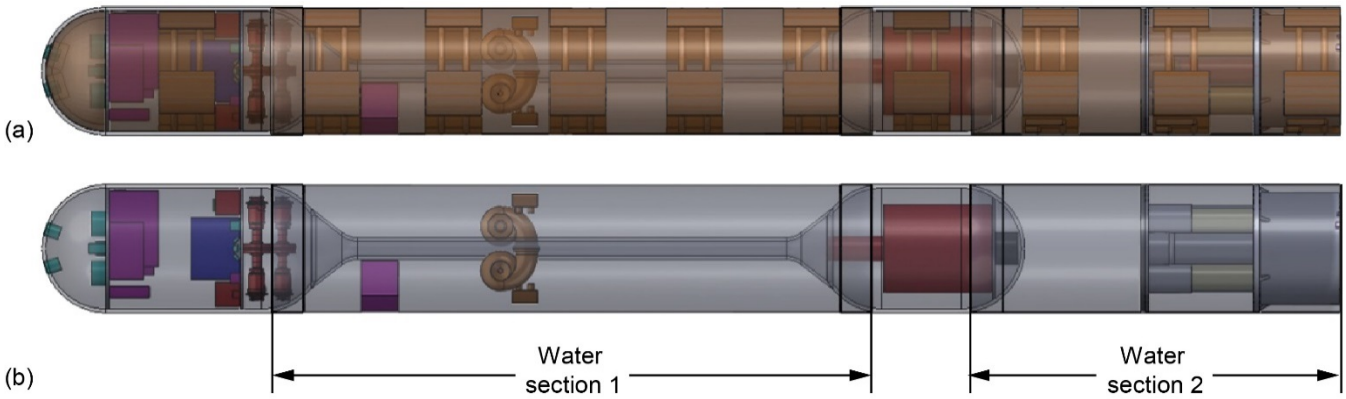

Figure 17.—Better view of water chambers on Europa Tunnelbot reactor case. (a) With insulation and hot plates. (b) Without insulation and hot plates.

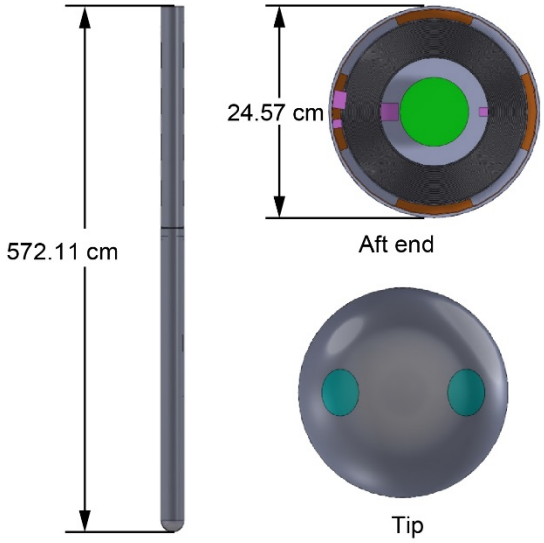

Figure 18.—Europa Tunnelbot general purpose heat source case overall dimensions.

5.2 General Purpose Heat Source (GPHS) Vehicle Design

Similar to the reactor case, the GPHS case has a test-tube shape but at a smaller diameter and longer length. The overall dimensions of the Europa Tunnelbot GPHS design are shown in Figure 18.

The 24.57 cm outer diameter is a result of the packaging selected for the GPHS bricks used to provide the heat distributed to the Tunnelbot surface in order to melt the ice. The five-brick layout for each GPHS layer shown in Figure 19 fits within a minimum diameter of 22.93 cm. This diameter, in addition to the 1 mm of insulation required on the inside surfaces of the Tunnelbot and the 0.72-cm wall thickness of the pressure vessel containing the GPHS stack, results in the 24.57 cm outer diameter of the Tunnelbot. The overall length of 572.11 cm for the GPHS case is a result of the GPHS stack height (10 layers of the five-brick layout), the heights and packaging efficiency of all the electronics and science instruments, and the length of the three repeaters.

As opposed to the two pressure vessel design for the reactor case, most of the science instruments, all of the power system, and all of the electronics for the various other systems are contained in a single pressure vessel. This can be done for the GPHS case because no water is required for additional shielding, and the wall of the pressure vessel is not required to be as thick given the smaller diameter, resulting in a lighter pressure vessel mass per unit of length. The unpressurized section contains the three repeaters, the cable spools (fiber optic and anchor cables), the Tunnelbot antenna, and the temperature and pressure sensors. Hot plates are again placed on the inside of the insulation that covers the internal surface area of both the pressurized and unpressurized sections, with the exception of the volume containing the GPHS stack. The hot plates are resized from the reactor case to cover approximately 25 percent of the surface area for the GPHS case. Both the pressure vessel section and unpressurized section can be seen in the section views shown in Figure 20.

Almost of the components contained in the pressure vessel are the same as those in the reactor case. One exception is the sample acquisition unit that was located in the unpressurized section for the reactor case. This unit is now located within the pressure vessel for the GPHS case. Another exception is the Radioisotope Thermoelectric Generator (RTG) used to generate the power for the GPHS case and its associated controls. While all of the other components are carried over from the reactor case, many of the science instruments, along with the C&DH enclosure, were resized to fit within the smaller diameter while maintaining the same volume. All of the components for the various systems can be seen in Figure 21.

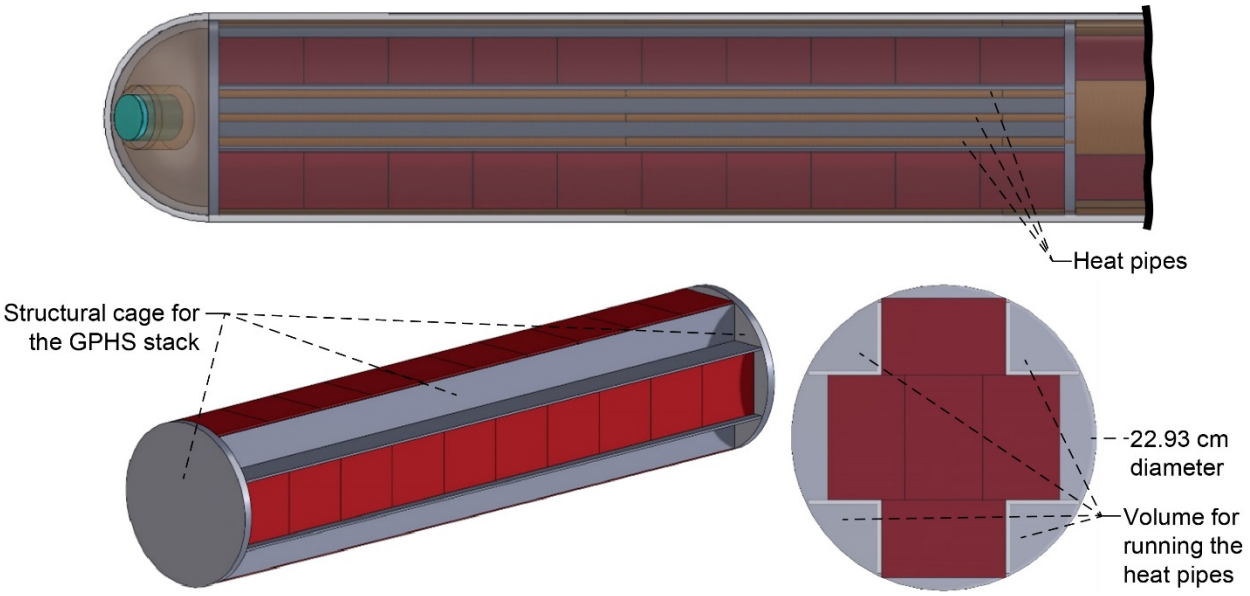

Figure 19.—General purpose heat source (GPHS) stack layout.

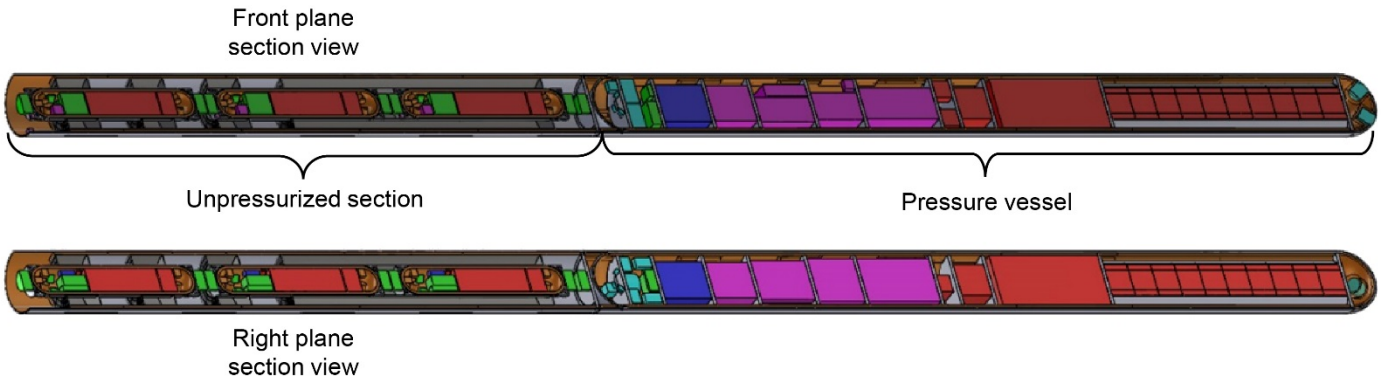

Figure 20.—Section views of general purpose heat source case.

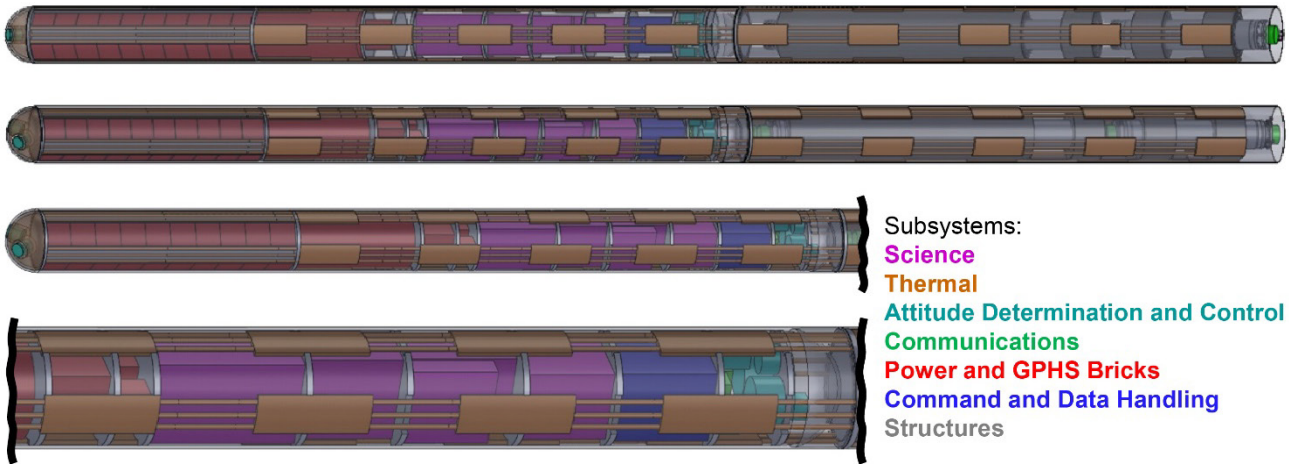

Figure 21.—System components of Europa Tunnelbot general purpose heat source (GPHS) case.

Figure 22 focuses on those components of the power system that are contained within the pressure vessel, while Figure 23 focuses on the science instruments and electronics. Those components that comprise the communications, AD&C, and C&DH systems can be seen in Figure 24. All of these components are mounted to 12.7-mm-thick honeycomb decks (nine total) rather than to the pressure vessel wall, minimizing the thermal leaks through the insulation. Note that the two sonar transducers of the AD&C system are located in the nose as they are for the reactor case.

The repeater design for the GPHS case is identical to that used in the reactor case (repeater design discussed in the next section). Given the smaller diameter for the GPHS case, the repeaters needed to be stacked rather than all three being mounted on the same deck. The layout of the repeaters and their associated spools in the unpressurized section (aft end) can be seen in Figure 25.

A thin structural cylinder is mounted to a deck located in the forward section of the unpressurized section and runs the length of all four spools. The outer diameter of this cylinder is just inside the hot plates that run throughout the unpressurized section. This cylindrical structure provides the interface between the mounting interface for all four spools. The spool canisters (c-channel structure) are then used to help guide the repeaters when they are pulled out of the Tunnelbot by the cables. Spacing of the spools is such that during deployment, prior to a repeater exiting one spool canister, it will have already entered the next spool canister, thus having a guided exit from the Tunnelbot.

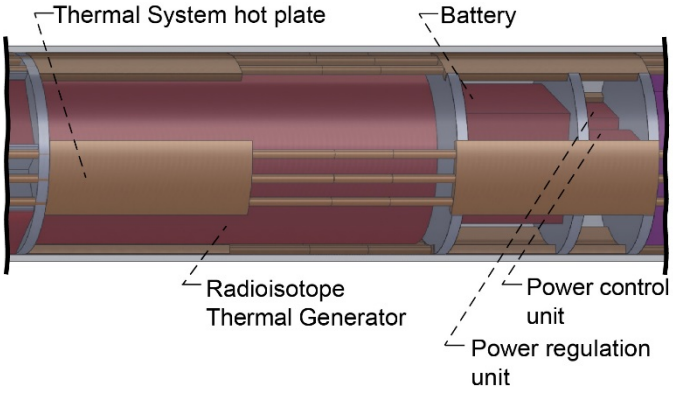

Figure 22.—Power system components for general purpose heat source case.

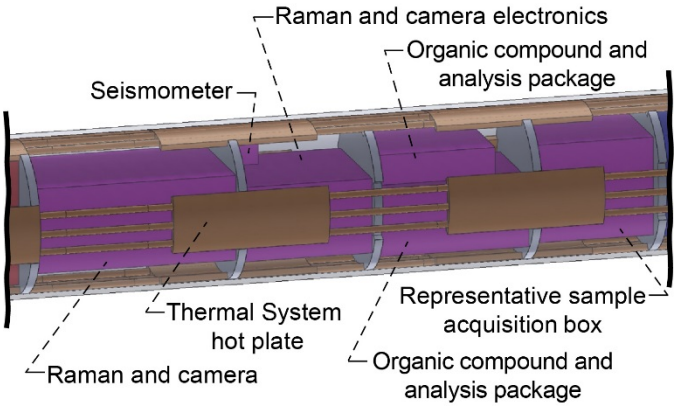

Figure 23.—Science components in pressurized section for general purpose heat source case.

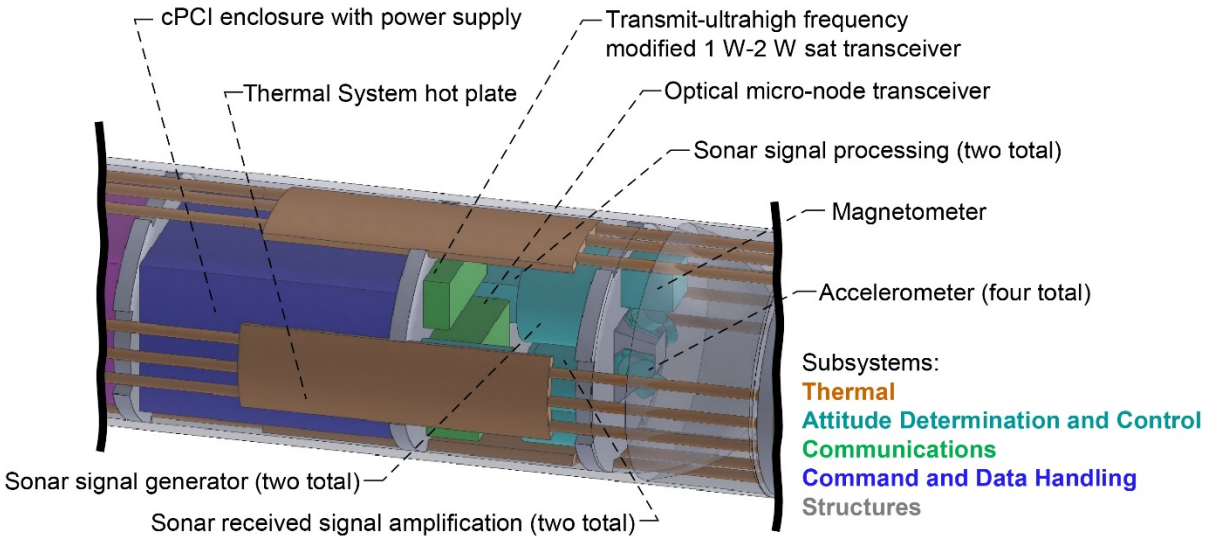

Figure 24.—Communications, attitude determination and control, and Command and Data Handling components for general purpose heat source case, where cPCI is Compact Peripheral Component Interconnect.

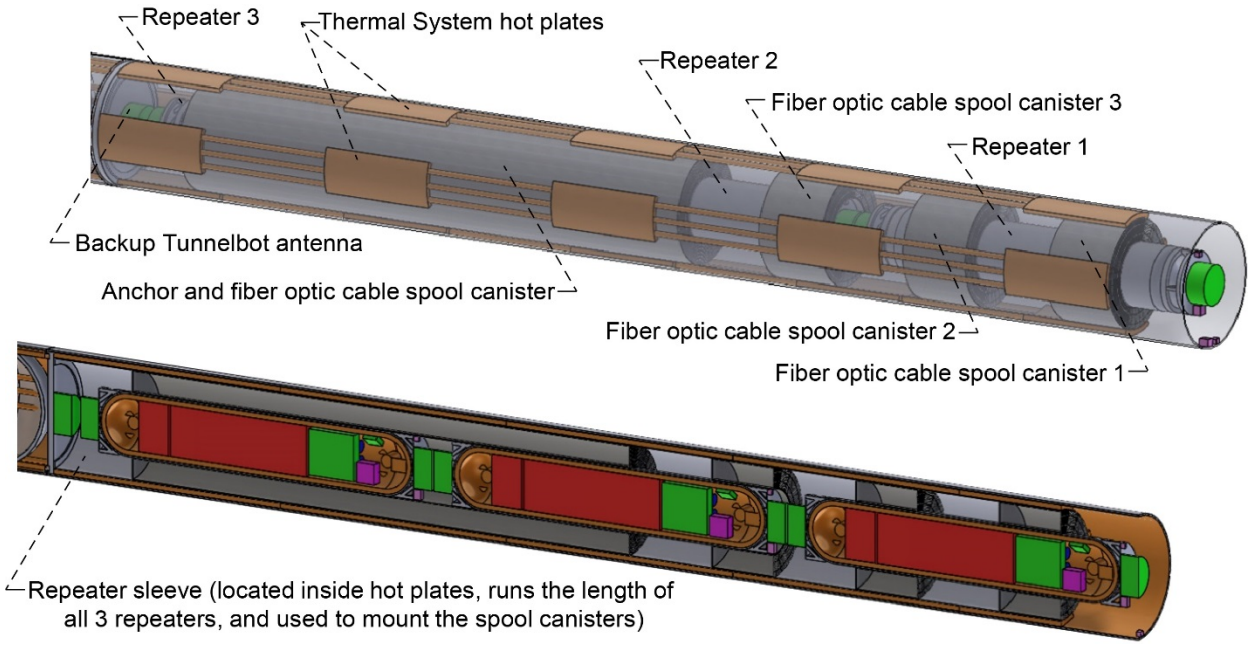

Figure 25.—Unpressurized repeater section for general purpose heat source case.

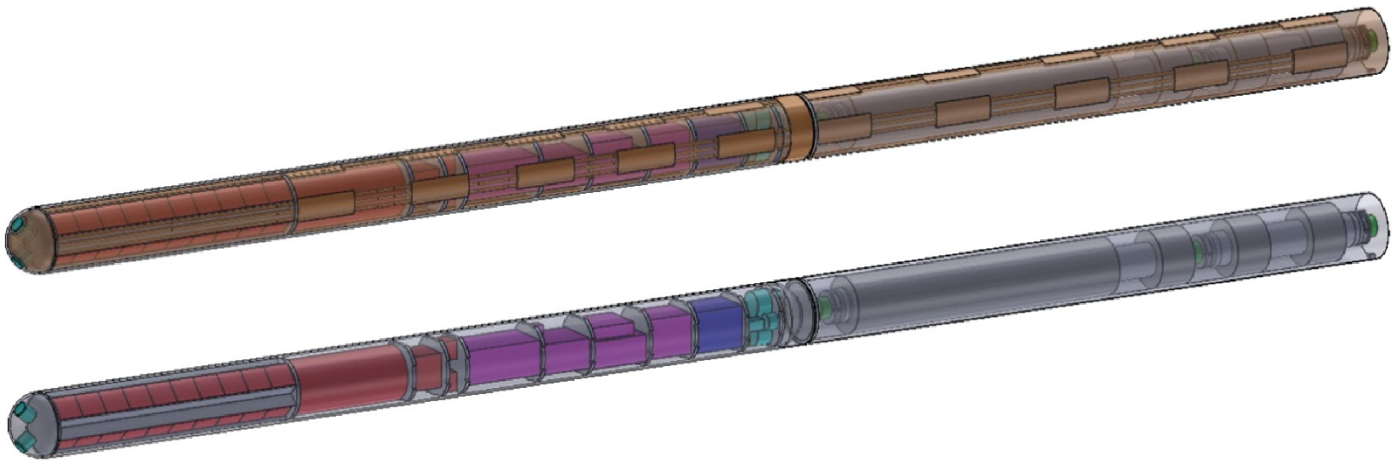

Figure 26.—Additional transparent views of general purpose heat source case.

Spool canister 1 contains 5 km of fiber optic cabling linking repeater 1 to the lander. Spool canister 2 contains 5 km of fiber optic cabling linking repeater 2 to repeater 1. Spool canister 3 contains 5 km of fiber optic cabling linking repeater 3 to repeater 2. Finally, the larger spool contains 5 km of fiber optic cabling combined with 5 km of anchor cabling connecting the Tunnelbot to repeater 3. Repeater 3 plays a similar role to the anchor floats from the reactor case in that when deployed, it will freeze in the ice, thus stopping the Tunnelbot. The mechanisms used to control the cable deployment and rapid repeater deployment in the event anchoring is required prior to reaching a 20 km depth are not shown in the computer-aided design (CAD) graphics.

The Tunnelbot antenna is mounted in the middle of the same deck as the structural cylinder that holds the spool canisters and is only used in the event of a break in the fiber optic cable connecting the Tunnelbot and repeater 3. As with the reactor case, the temperature and pressure sensors are mounted to the inside surface of the unpressurized section structure at the opening on the aft end.

Additional transparent images of the GPHS case can be seen in Figure 26.

5.3 Repeater Design

The repeaters are used to transfer data between the Tunnelbot and the lander for both the reactor and GPHS cases. A fiber optic cable will be used for the communication, however, patch antennas are contained on the Tunnelbot, repeaters, and the lander in the event there is a break in any of the fiber optic cables.

As with the Tunnelbot designs, all of the electronics and the power system components are contained inside a pressure vessel. Those components not inside the pressure vessel are the two antennas (top and bottom) and the temperature and pressure sensors. Figure 27 shows the overall dimensions of the repeater

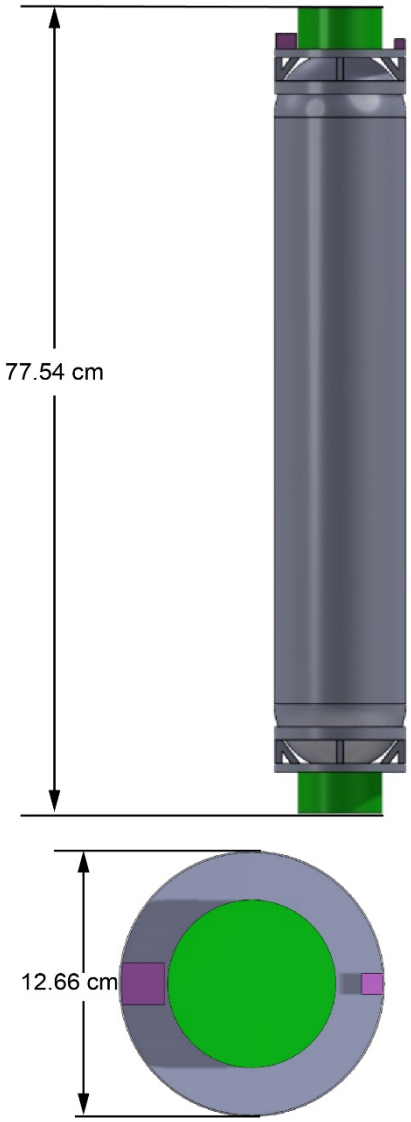

Figure 27.—Overall dimensions of repeater design.

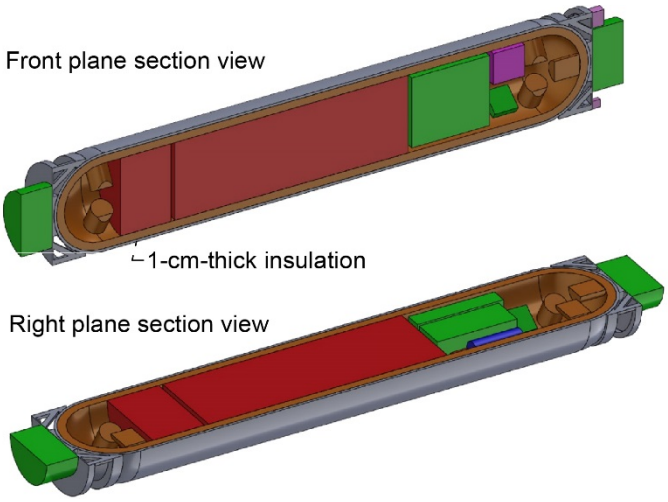

Figure 28.—Section views of repeater design.

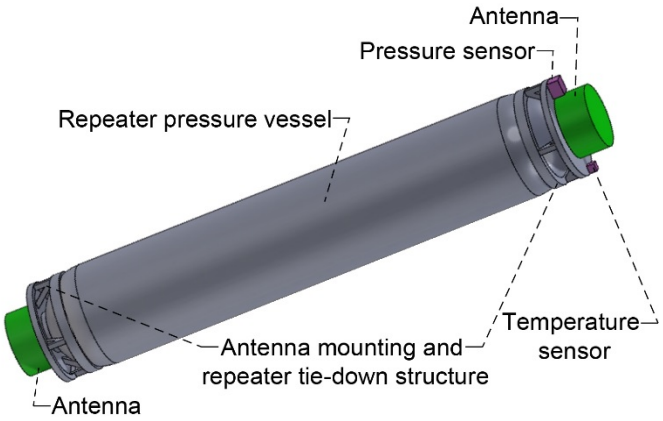

Figure 29.—External components for repeater design.

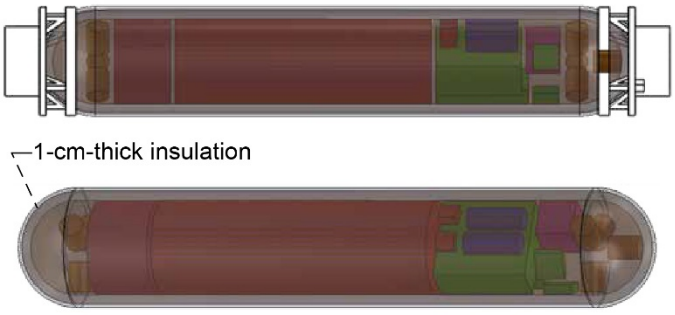

Figure 30.—Internal components for repeater design.

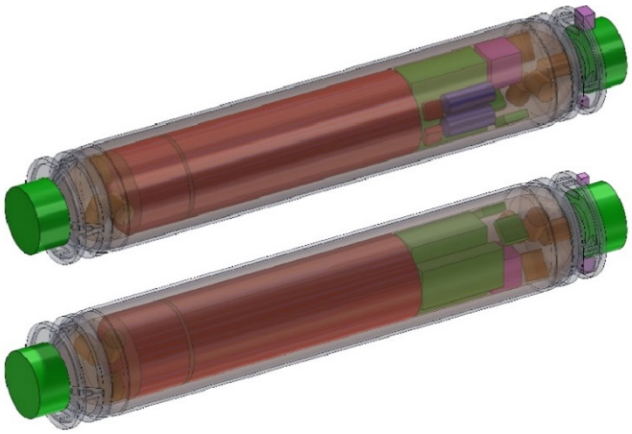

Figure 31.—Additional transparent views of repeater design.

design. The 12.66 cm outer diameter is a result of the 30 cm diameter of the Radioisotope Power Systems (RPS) generator, plus 1 cm of insulation contained on the inside surface of the pressure vessel and 0.33-cm-thick pressure vessel wall. The length of the pressure vessel is driven by the size of those components contained inside and how efficiently they can stack, while the overall repeater length (77.54 cm) includes the thickness of the antennas (one antenna on each end). Section views of the repeater can be seen in Figure 28.

Those components located outside of the pressure vessel are shown in Figure 29. As stated earlier, these include the two antennas and the temperature and pressure sensors. Additional structure is added to the ends of the pressure vessel to provide a physical interface for the antennas and the temperature and pressure sensors. This structure also serves the role as the tie-down structure for the repeaters in the reactor design. In that case, this structure is mounted to the inside of the cylindrical sleeve contained on the repeater deck.

Those components contained inside the pressure vessel include a seismometer, seven radioisotope heater units (RHUs) for thermal control, the communications electronics, the RPS generator, battery, power regulation box, power control unit, and the C&DH system. All of these components are contained within the 1-cm-thick insulation that covers the entire inside surface of the pressure vessel structure. Figure 30 shows those components contained within the pressure vessel.

Two additional transparent views of the repeater design are shown in Figure 31.

6.0 Systems

The Tunnelbot mission requires the vehicle to transit 20 km of ice in 3 yr. There are three fundamental variables that impact the Tunnelbot's ability to transit this ice: heat available to melt ice, vehicle outside diameter, and vehicle length. Provide more heat, and the Tunnelbot will melt through the ice faster. For a

constant heat input, increase the diameter and length, and the Tunnelbot will transit slower, with diameter as the major driver. In order to provide sufficient room for the subsystems and instruments, the team sought to maximize volume while still meeting the 3-yr transit time requirement. Analysis during the architecture study phase determined the optimal balance of diameter and length for the given discrete heat loads provided by the reactor and GPHS units, and served as the guidance for setting the length and diameter.

For the reactor Tunnelbot, with 43 kW_{th} provided by the Kilopower reactor, an outer diameter of 0.52 m and overall length of 5.26 m would allow the Tunnelbot to melt through 20 km of ice in 3 yr. As described in Section 2.0, the Tunnelbot utilizes three communication repeaters. The system-level mass summary is shown in Table 8 and includes the Tunnelbot mass, single repeater mass, and system total mass, including the three repeaters.

For the GPHS Tunnelbot, 54 GPHS ^{238}Pu bricks were utilized to provide 12 kW_{th} of melting power. This melting power corresponded to a permissible vehicle outer diameter of 0.25 m and length of 5.72 m to transit the ice shell within 3 yr. Again, three repeaters were utilized to provide communication relay to the surface. The system-level mass summary is shown in Table 9 and includes the Tunnelbot mass, single repeater mass, and system total mass, including the three repeaters.

The system-level powered equipment lists (PELs) for both the reactor and GPHS Tunnelbots are provided in Table 10 and Table 11, respectively. Section 2.0 describes how the vehicles will perform and provides the backbone for the power modes shown in the PEL.

TABLE 8.—REACTOR TUNNELBOT WITH REPEATER SYSTEM-LEVEL MASS SUMMARY MASTER EQUIPMENT LIST SUMMARY FOR CASE 1

Main subsystems	Tunnelbot	Repeater	Total
	Basic mass, kg	Basic mass, kg	Total basic mass, kg
Element total	988.2	12.7	1,026.4
Science	26.9	0.4	28.1
Guidance, Navigation, and Control	2.7	0.0	2.7
Command and Data Handling	9.7	0.4	10.9
Communications and tracking	1.0	1.0	4.0
Electrical power subsystem	330.5	5.0	345.4
Thermal control (nonpropellant)	133.7	1.1	137.0
Structures and mechanisms	483.8	4.8	498.3
Element mass growth allowance (aggregate)	187.3	2.1	193.6
Additional system-level growth (for 30 percent total)	109.1	1.7	114.3
Total wet mass with 30 percent growth	1,284.6	16.6	1,334.3
Number of repeaters	3	-----	---------

TABLE 9.—GENERAL PURPOSE HEAT SOURCE TUNNELBOT WITH REPEATER SYSTEM-LEVEL MASS SUMMARY MASTER EQUIPMENT LIST SUMMARY FOR CASE 2

Main subsystems	Tunnelbot	Repeater	Total
	Basic mass, kg	Basic mass, kg	Total basic mass, kg
Element total	531.7	12.7	569.7
Science	26.9	0.4	28.1
Guidance, Navigation, and Control	3.1	0.0	3.1
Command and Data Handling	6.4	0.4	7.6
Communications and tracking	1.0	1.0	4.0
Electrical power subsystem	50.7	5.0	65.7
Thermal control (nonpropellant)	128.6	1.1	131.9
Structures and mechanisms	315.1	4.7	329.3
Element mass growth allowance (aggregate)	86.2	2.0	92.3
Additional system-level growth (for 30 percent total)	73.3	1.8	78.6
Total wet mass with 30 percent growth	691.2	16.5	740.6
Number of repeaters	3	------	-------

TABLE 10.—REACTOR TUNNELBOT WITH REPEATER SYSTEM-LEVEL POWERED EQUIPMENT LIST FOR CASE 1

Description	Power modes, W_e						
	1	2	3	4	5	6	7
	Transit	Reactor startup	Moving	Active science	Ocean	Repeater, standby	Repeater, relay
	Years	2 d	Days to months	2 hr	1 month	See notes	See notes
Europa Tunnelbot	0.0	195.0	242.5	323.7	222.5	0.1	8.1
Tunnelbot	0.0	195.0	242.5	323.7	222.5	0.0	0.0
Science	0.0	0.0	0.0	117.3	0.0	0.0	0.0
Guidance, Navigation, and Control (GN&C)	0.0	0.0	27.2	1.4	27.2	0.0	0.0
Command and Data Handling (C&DH)	0.0	11.0	31.0	13.0	11.0	0.0	0.0
Communications and tracking	0.0	0.0	0.3	8.0	0.3	0.0	0.0
Electrical power subsystem	0.0	0.0	0.0	0.0	0.0	0.0	0.0
Thermal control (nonpropellant)	0.0	184.0	184.0	184.0	184.0	0.0	0.0
Structures and mechanisms	0.0	0.0	0.0	0.0	0.0	0.0	0.0
Repeater	0.0	0.0	0.0	0.0	0.0	0.1	8.1
Science	0.0	0.0	0.0	0.0	0.0	0.0	0.0
GN&C	0.0	0.0	0.0	0.0	0.0	0.0	0.0
C&DH	0.0	0.0	0.0	0.0	0.0	0.1	0.1
Communications and tracking	0.0	0.0	0.0	0.0	0.0	0.0	8.0
Electrical power subsystem	0.0	0.0	0.0	0.0	0.0	0.0	0.0
Thermal control (nonpropellant)	0.0	0.0	0.0	0.0	0.0	0.0	0.0
Structures and mechanisms	0.0	0.0	0.0	0.0	0.0	0.0	0.0

TABLE 11.—GENERAL PURPOSE HEAT SOURCE TUNNELBOT WITH REPEATER SYSTEM-LEVEL POWERED EQUIPMENT LIST FOR CASE 2

Description	Power modes, W_e						
	1	2	3	4	5	6	7
	Transit	Reactor startup	Moving	Active science	Ocean	Repeater, standby	Repeater, relay
	Years	2 d	Days to months	2 hr	1 month	See notes	See notes
Europa Tunnelbot	0.0	12.0	39.8	141.0	39.8	0.1	8.1
Tunnelbot	0.0	12.0	39.8	141.0	39.8	0.0	0.0
Science	0.0	0.0	0.0	117.3	0.0	0.0	0.0
Guidance, Navigation, and Control (GN&C)	0.0	0.0	27.5	1.7	27.5	0.0	0.0
Command and Data Handling (C&DH)	0.0	12.0	12.0	14.0	12.0	0.0	0.0
Communications and tracking	0.0	0.0	0.3	8.0	0.3	0.0	0.0
Electrical power subsystem	0.0	0.0	0.0	0.0	0.0	0.0	0.0
Thermal control (nonpropellant)	0.0	0.0	0.0	0.0	0.0	0.0	0.0
Structures and mechanisms	0.0	0.0	0.0	0.0	0.0	0.0	0.0
Repeater	0.0	0.0	0.0	0.0	0.0	0.1	8.1
Science	0.0	0.0	0.0	0.0	0.0	0.0	0.0
GN&C	0.0	0.0	0.0	0.0	0.0	0.0	0.0
C&DH	0.0	0.0	0.0	0.0	0.0	0.1	0.1
Communications and tracking	0.0	0.0	0.0	0.0	0.0	0.0	8.0
Electrical power subsystem	0.0	0.0	0.0	0.0	0.0	0.0	0.0
Thermal control (nonpropellant)	0.0	0.0	0.0	0.0	0.0	0.0	0.0
Structures and mechanisms	0.0	0.0	0.0	0.0	0.0	0.0	0.0

7.0 Power

7.1 Kilopower Introduction

A 43-kW_{th} Kilopower nuclear reactor was selected to provide power for the Europa Tunnelbot for this Compass study. Kilopower is a joint NASA and U.S. Department of Energy (DOE) project to develop a family of reactors from 1 to 10 kW_e that can be integrated with a wide range of power conversion technologies. In 2018, the 1-kW_e variant of the Kilopower design was successfully tested at a DOE site in Nevada. This reactor was coupled to eight Stirling convertors (two Advanced Stirling Convertors (ASCs) (Sunpower, Inc.) and six simulators), which converted the reactor generated heat to electrical power. Stirling technology has been under development for many years at NASA Glenn Research Center. The Stirling convertor used in the Kilopower test called the ASC are engineering units developed under the Advanced Stirling Radioisotope Generator (ASRG) program. Each of these convertors produce about 100 W_e of alternating current (AC) power. Table 12 provides some of the constraints and design parameters for the Kilopower design. Figure 32 shows a conceptual drawing of a 1-kW_e system for deep space.

7.2 Kilopower Tunnelbot

Trades revealed that a large amount of heat and a relatively small amount of electrical power are the primary reactor requirements for the Tunnelbot. Because of these unique challenges of developing a nuclear-powered Tunnelbot, changes from the deep space, in-orbit configuration are required. One drawback of fissioning systems is that they often require both neutron and gamma shielding to protect sensitive electronics. The Tunnelbot design, however, is able to use in situ water from the Europa ice and spot shielding in a few locations, which greatly decreases the shielding mass transported from Earth. Additionally, because heat rejection can be accomplished through the Tunnelbot's contact with water, the heat rejection radiator is not needed. The Kilopower reactor generates heat from the fissioning of its highly enriched ^{235}U core. In the space configuration of the Kilopower reactor, the heat is sent to power convertors though heat pipes that in turn generate electricity. The Europa Tunnelbot, however, will use the majority of the reactor supplied heat to melt the ice. Figure 33 shows a drawing of the 24 sodium heat pipes embedded in the reactor core in the 43-kW_{th} design, and Table 13 summarizes the performance.

Six of these heat pipes will be attached to Stirling convertors, while the remaining 18 will go to heat exchangers that move heat around the nose and body of the Tunnelbot. Due to its unique design, the Kilopower reactor is a self-regulating constant temperature heat source. This is important in that the science CONOPS require the Tunnelbot to occasionally stop its descent to take and analyze samples. Variable conductance heat pipes stop the flow of heat from the reactor to the surrounding ice, and the reactor automatically responds by reducing the amount of heat generated while still supplying the high-temperature heat needed to supply the Stirling convertors heat to generate electrical power. Another heat source under consideration for the Tunnelbot is ^{238}Pu in the form of a GPHS. An important difference between isotope systems and Kilopower is that the reactor can be turned on and off while the isotope sources always produce heat. This greatly simplifies Earth ground operations and spacecraft operation on the trip to Europa.

TABLE 12.—DESIGN CONSTRAINTS AND PARAMETERS

Nuclear fuel	93-percent enriched, solid cast ^{235}U Mo alloy
Reactor	fast spectrum, Be reflector, single centered control rod
Heat transport	1,100 K passive Na heat pipes
Power conversion	Stirling convertors scaled from ASRG[a]
Design life	>10 yr
Load bus	120 Vdc

[a]Advanced Stirling Radioisotope Generator.

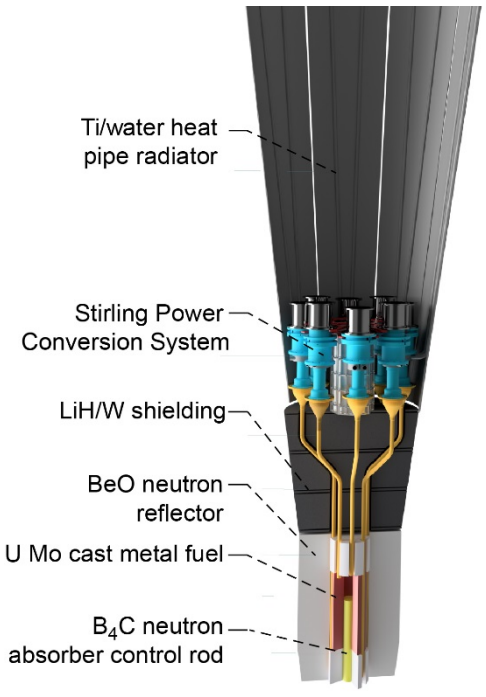

Figure 32.—1-kW_e Kilopower space system.

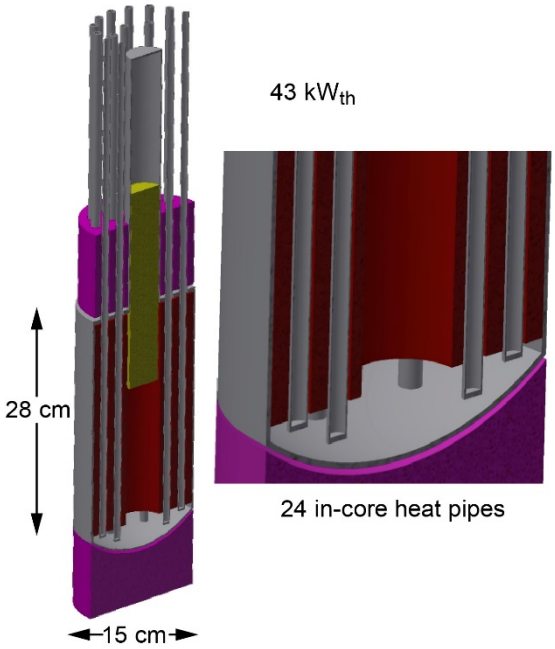

Figure 33.—Kilopower 43-kW_{th} core and reflectors.

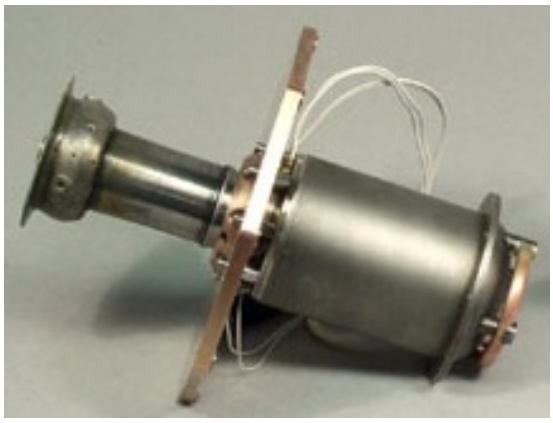

Figure 34.—Sun Power Advanced Stirling Convertor.

TABLE 13.—KILOPOWER TUNNELBOT PERFORMANCE SUMMARY

Item	Kilopower
Thermal output	43.3 kW_{th}
BOM[a]/EOM[b] DC[c] power	420 W_e
Number of Stirling convertors	6/1 spare
Voltage range	28±6 Vdc
Stirling hot end temperature	800 °C
Stirling cold end temperature	50 °C
Conversion efficiency	30 percent
Mass	400 kg
Reactor volume	32-cm-diameter by 50-cm-tall cylinder

[a]Beginning of mission.
[b]End of mission.
[c]Direct current.

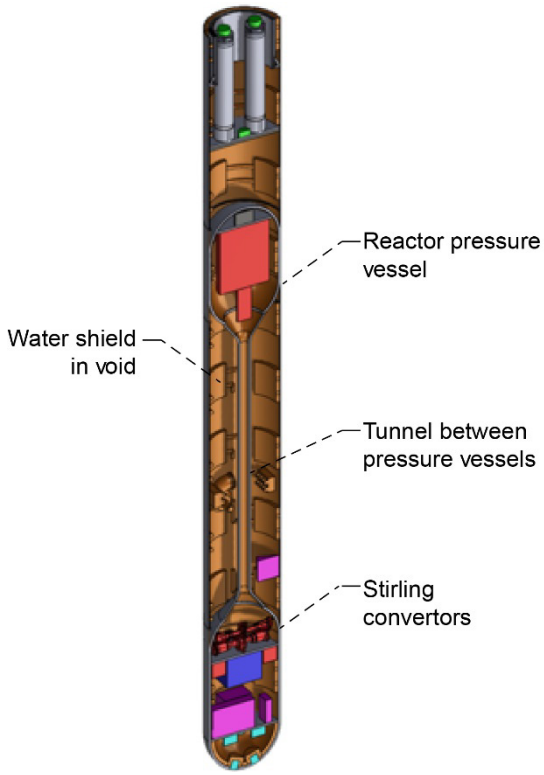

Figure 35.—Kilopower Europa Tunnelbot concept.

The electrical power system consists of six Stirling convertors attached to the reactor core by heat pipes. Five convertors are required for full-power operation with an additional convertor as a spare. Heat rejection from the Stirling convertors is accomplished through heat pipes attached from the Stirling rejector to the Tunnelbot body. These six convertors each have a dedicated balancer. Figure 34 shows a photograph of an ASC. The convertors are attached to a controller that both controls the operation of the Stirling convertors and rectifies the AC to 28 Vdc.

The reactor and Stirling convertors are all placed within Ti pressure vessels to keep the 3,300-psi external pressure away from the power system. These pressure vessels also provide some shielding. Figure 35 shows the layout of the Kilopower Tunnelbot. Meltwater shielding is placed within the void when the Tunnelbot is on the surface. The heat pipes run from the reactor down the tunnel between pressure vessels to the Stirling convertors.

7.3 Kilopower Summary

Kilopower provides a flexible and operationally simple nuclear reactor that can be used in a wide array of NASA missions. When coupled with a Europa Tunnelbot, a highly capable vehicle is envisioned, which could explore Europa's ocean. Kilopower is currently at TRL 5. See Table 14 and Table 15 for the reactor and GPHS MELs.

TABLE 14.—REACTOR TUNNELBOT POWER SYSTEM MASTER EQUIPMENT LIST FOR CASE 1

Description	Quantity	Unit mass, kg	Basic mass, kg	Growth, percent	Growth, kg	Total mass, kg
Electrical power subsystem	-	-------	330.5	20.0	66.1	396.6
Power generation	-	-------	311.0	20.0	62.2	373.2
Total reactor mass	1	226.3	226.3	20.0	45.3	271.6
Stirling assembly	1	46.5	46.5	20.0	9.3	55.8
Instrumentation and control	1	32.2	32.2	20.0	6.4	38.6
Heat rejection assembly	6	1.0	6.0	20.0	1.2	7.2
Power Management and Distribution	-	------	19.0	20.0	3.8	22.8
Power regulation	1	15.0	15.0	20.0	3.0	18.0
Power control unit	1	1.0	1.0	20.0	0.2	1.2
Wiring harness	1	3.0	3.0	20.0	0.6	3.6
Energy storage	-	-------	0.5	20.0	0.1	0.6
Battery	1	0.5	0.5	20.0	0.1	0.6

TABLE 15.—GENERAL PURPOSE HEAT SOURCE (GPHS) TUNNELBOT POWER SYSTEM MASTER EQUIPMENT LIST FOR CASE 2

Description	Quantity	Unit mass, kg	Basic mass, kg	Growth, percent	Growth, kg	Total mass, kg
Electrical power subsystem	-	-----	50.7	20.0	10.1	60.9
Power generation	-	-----	33.6	20.0	6.7	40.4
Six-GPHS Radioisotope Thermoelectric Generator	1	32.0	32.0	20.0	6.4	38.4
Power management and distribution	-	-----	9.3	20.0	1.9	11.2
Power regulation	1	3.5	3.5	20.0	0.7	4.2
Power control unit	1	2.8	2.8	20.0	0.6	3.4
Wiring harness	1	3.0	3.0	20.0	0.6	3.6
Energy storage	-	-----	7.8	20.0	1.6	9.4
Battery	1	7.8	7.8	20.0	1.6	9.4

7.4 Finless Radioisotope Thermoelectric Generator (RTG) Power System

An eight-GPHS, finless RTG was selected to provide electrical power for the second design case. The generator is a scaled-up version of a small RTG Concept. Table 16 provides the top-level characteristics of the finless RTG design. The most critical parameter being the diameter from a mission perspective. Figure 36 shows power output as a function of time from fueling. Estimated TRL for the finless RTG is 3.

TABLE 16.—FINLESS RADIOISOTOPE THERMOELECTRIC GENERATOR (RTG) CHARACTERISTICS

Item	RTG
Nuclear fuel	Eight-GPHS[a]
Thermal inventory BOL[b], when the RTG is fueled	2,000 W_{th}
BOM[c] power, up to 3 yr after fueling	110 W_e
EODL[d] power, 14 yr after BOM	73 W_e
Power conversion	PbTe/TAGS[e]
Environment	Multimission capable
Voltage range	23 to 36 Vdc
Degradation rate	2.5 percent/yr
Efficiency	5 percent
Mass	49 kg
Volume	23 cm diameter by 59 cm height

[a]General purpose heat source.

[b]Beginning of life.

[c]Beginning of mission.

[d]End of design life.

[e]Te/Sb/Ge/Ag.

7.5 Repeater Power System

A 1-W_e direct current (DC) Stirling lightweight radioisotope heater unit (LWRHU) generator (smallSTEP) was selected to power the Europa Tunnelbot communication repeater. Stirling technology has been under development for many years, and Glenn is building this 1-W_e Stirling convertor with a simulated eight-RHU heat source. The RHU shown in Figure 37 is fabricated by the DOE and have been used for decades on NASA spacecraft.

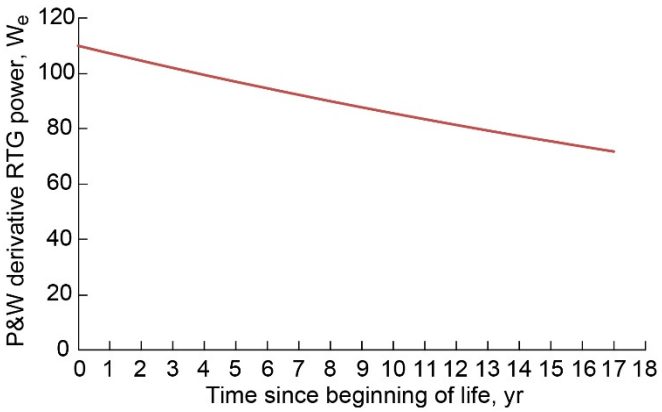

Figure 36.—Direct current power output for beginning of life and end of life for finless Radioisotope Thermoelectric Generator (RTG) eight-general purpose heat source variant.

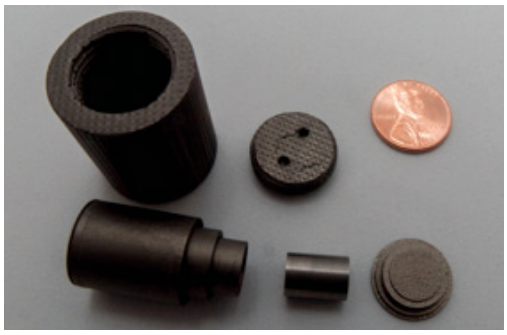

Figure 37.—Lightweight radioisotope heater unit.

RHUs use ^{238}Pu as the primary source of energy, which decays via alpha emission and has a half-life of approximately 90 yr. The RHU is designed to produce about 1 W_{th} of heat at fueling and weigh 40 g (Ref. 66). Each RHU is 2.6 cm in diameter and 3.2 cm in height. Figure 38 shows a 1-W_e Stirling convertor coupled to an eight-RHU heat source assembly that is surrounded by multilayer insulation (MLI).

MLI is the highest performing insulation, but requires a vacuum to operate effectively and is required because of the low heat flux provided by RHUs. The heat source assembly is a vacuum-evacuated canister to support the use of MLI. The Stirling convertor operates at 100 Hz and is rectified to provide a 5-Vdc output to the repeater power bus from the smallSTEP controller. Helium generated from the RHUs is contained within the RHU assembly. Based upon experience with past Stirling isotope power systems, the smallSTEP is assumed to have a degradation rate of 1.2 percent per year, including the 0.8 percent per year degradation from the ^{238}Pu. Expected power output at beginning of life (BOL) is 1 W_e and decays to 0.83 W_e after 17 yr or end of design life (EODL). Figure 39 shows DC power output as a function of time after BOL.

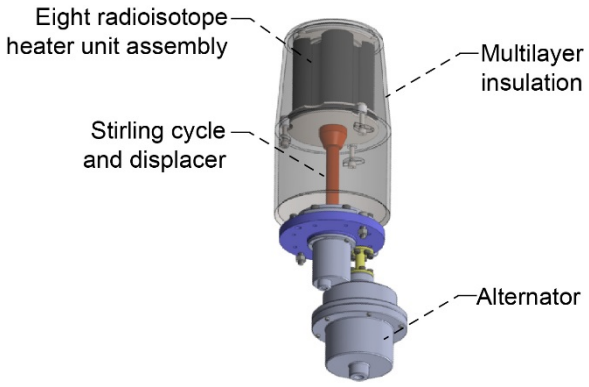

Figure 38.—Stirling convertor coupled to radioisotope heater unit heat source assembly and surrounded by multilayer insulation.

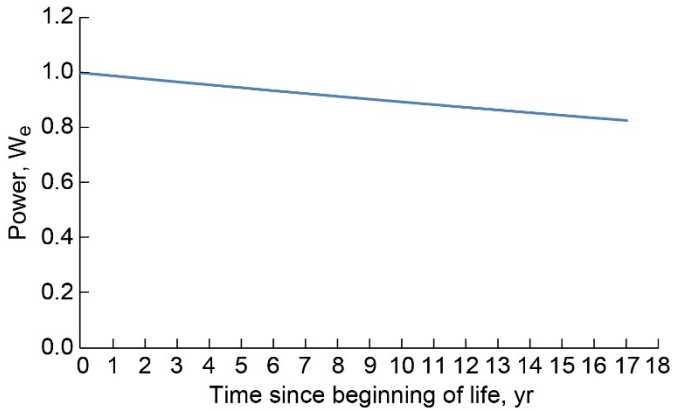

Figure 39.—Power output of Stirling radioisotope heater unit as function of time from fueling.

Total mass of the smallSTEP is 3.0 kg with an overall efficiency of 13 percent. The Stirling convertor and heat source assembly fit into a 3U CubeSat form factor and is 32 cm long by 11 cm in height and width. A performance summary is shown in Section 7.6 (Table 17).

Figure 40 shows the conceptual design for the smallSTEP placed within the Tunnelbot repeater for the NASA Compass Tunnelbot study.

7.6 Repeater Power System Summary

The 1-W_e smallSTEP fills a power gap in space power systems between the mW_e class of RHU-based RTGs and 100-W_e class of GPHS-based generators. While early in its development cycle, the smallSTEP may provide NASA with a new power system for future exploration of the outer planets and the Moon. The smallSTEP is currently at TRL 3. Table 18 lists the Repeater Power System MEL.

TABLE 17.—PERFORMANCE SUMMARY

Item	RHUSTIR[a]
Thermal inventory	eight-RHU[b] producing 8 W_{th} BOL[c]
BOM[d] power	1 W_e
EODL[e] power	0.83 W_e
Voltage range	5 Vdc
Stirling hot end temperature	500 °C
Stirling cold end temperature	50 °C
Efficiency	13 percent
Mass	3.0 kg
Volume	11- by 11- by 32-cm cube

[a]Stirling radioisotope heater unit.

[b]Radioisotope heater unit.

[c]Beginning of life.

[d]Beginning of mission.

[e]End of design life.

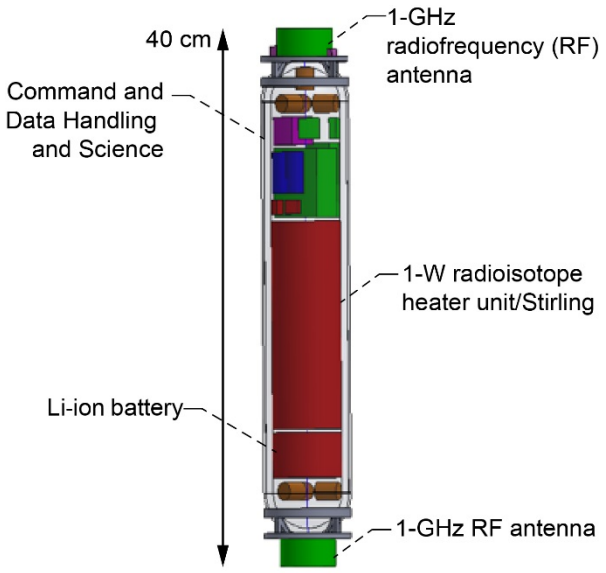

Figure 40.—Tunnelbot repeater.

TABLE 18.—REPEATER POWER SYSTEM MASTER EQUIPMENT LIST FOR CASES 1 AND 2

Description	Quantity	Unit mass, kg	Basic mass, kg	Growth, percent	Growth, kg	Total mass, kg
Electrical power subsystem	-	-----	5.0	17.8	0.9	5.9
Power generation	-	-----	5.0	17.8	0.9	5.9
RPS generator	1	3.00	3.0	20.0	0.6	3.6
Battery	1	1.44	1.4	20.0	0.3	1.7
Power control unit	1	0.24	0.2	0.0	0.0	0.2
Power regulation	1	0.30	0.3	0.0	0.0	0.3

8.0 Radiation Modeling

8.1 Environmental Radiation About Jupiter

The vicinity of Jupiter is an extremely harsh radiation environment due to Jupiter's radiation belts. Europa's orbit about Jupiter places it within this high radiation environment, as shown in Figure 41. The unshielded radiation dose at Europa's orbital location is approximately 3 Mrad/d. On the surface of Europa, this dose is estimated to be half that due to the shielding provided by the moon itself.

The pressure vessels used for the Tunnelbots and repeaters to enable them to survive the high pressure experienced beneath the ice are constructed of Ti. Ti will provide good radiation shielding for the electronics and equipment housed within these pressure vessels when entering Europa's orbit and while on the surface. It is estimated that a 25-Mrad dose would be attenuated to 25 krad with 1 cm of Ti shielding. This corresponds to a dose ratio between Al shielding and Ti shielding of 2.72 to 1. Based on this, the unshielded dose rate from entering Europa's orbit and operating on the surface prior to entering the ice is estimated as

- 7-d operation on the surface: 10.5 Mrad (unshielded)
- Orbital dose: 11.0 Mrad (3.66 d, unshielded)
- Total dose: 21.5 krad (behind 1 cm of Ti)

This total dose would then translate into an environmental dose of 21.5 krad for items within the 1-cm-thick Ti pressure vessels used with the reactor Tunnelbot prior to the ice phase of the mission beginning.

The isotope-powered Tunnelbot has a thinner pressure vessel due to its smaller diameter when compared to the reactor-powered Tunnelbot. The wall thickness for the isotope-powered Tunnelbot is 0.7 cm. Therefore, the estimated environmental dose for the isotope-powered Tunnelbot is 39.5 krad as detailed here.

- 7-d operation on the surface: 52.5 krad (behind 0.7 cm Al)
- Orbital dose: 55.0 krad (behind 0.7 cm Al)
- Total dose: 107.5 krad (behind 0.7 cm Al)
- Total dose: 39.5 krad (behind 0.7 cm of Al)

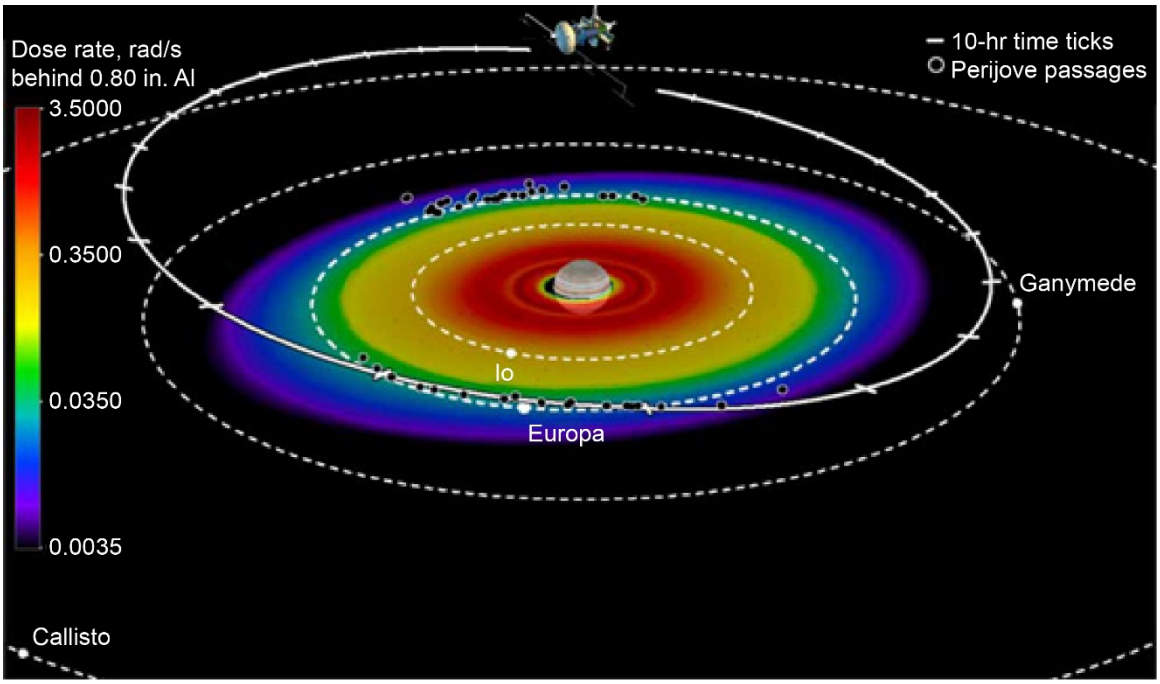

Figure 41.—Radiation belt intensity surrounding Jupiter.

The repeater will have the highest environmental dose since its pressure vessel is the thinnest at 0.26 cm thick. For the repeater, this total dose is 112 krad as detailed here.

- 7-d operation on the surface: 148.75 krad (behind 0.26 cm Al)
- Orbital dose: 155.8 krad (behind 0.26 cm Al)
- Total dose: 304.6 Mrad (behind 0.26 cm Al)
- Total dose: 112 krad (behind 0.7 cm of Ti)

In addition to the environmental radiation dose, the reactor system will be exposed to a high dose level upon the reactor startup prior to the water chambers being filled. The water chambers are used to shield the components within the pressure vessels from the radiation produced by the reactor. However, during initial startup, the reactor will operate for 1 d without water in the tanks to shield from neutrons, as illustrated in Figure 42. This dose, in addition to the environmental dose of 21.5 krad, is still well below the dose limit of 300 krad for the electronics. There was, however, concern that because this 100-krad dose will occur over a short period of time there may be additional damage effects in addition to the standard dose limits. From exposure data, there are indications that a high dose rate will damage the electronics in addition to the cumulative dose. However, the electronics are tested at dose rates of 1 rad/s up to 100 rad/s during initial qualification testing to determine their cumulative dose capability. This indicates that the electronics will be able to tolerate the 1-d dose rate of 1.16 rad/s without any additional damaging effects due to the high dose rate.

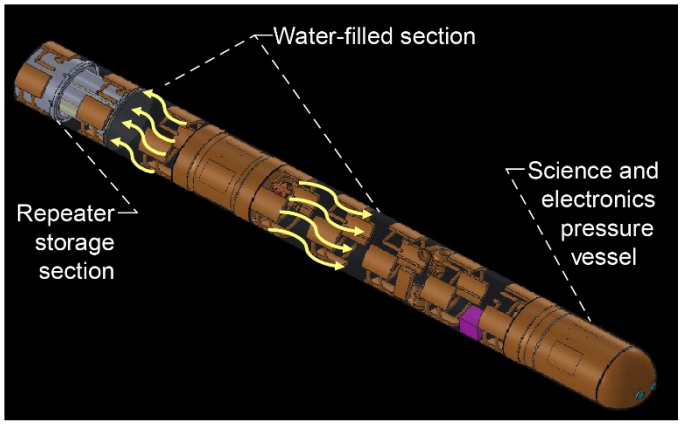

Figure 42.—Reactor startup operation radiation dose. High levels of radiation from reactor will reach the science and electronics section and the communication relays if the shielding sections are empty of water when the reactor is turned on.

8.2 Reactor

A 43-kW_{th} reactor was proposed as a heat source to melt through the Europa ice sheet and to provide some onboard electricity using Stirling engines. The chosen reactor concept is a fast-spectrum reactor based on a Los Alamos National Laboratory (LANL) design concept (Refs. 67 and 68). Slight modifications to the LANL design concept were made in order to fit the reactor within the confines of the Tunnelbot diameter (50 cm). Accommodations were also made for 24 heat pipes (1.59 cm diam.) along with core length and reflector thickness

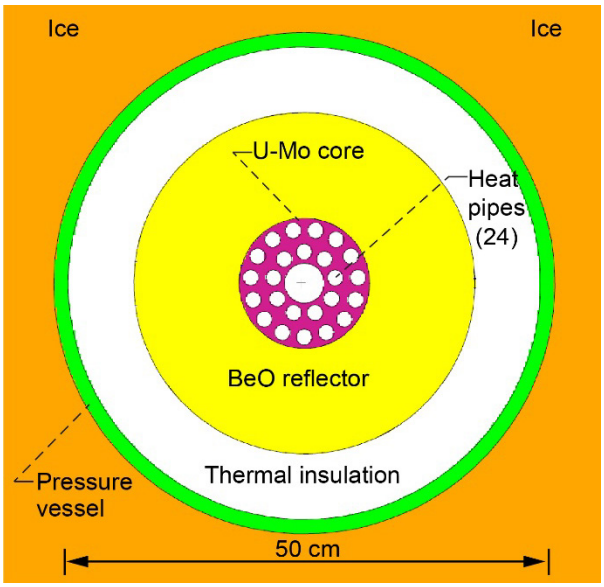

Figure 43.—Radial cross section of reactor core.

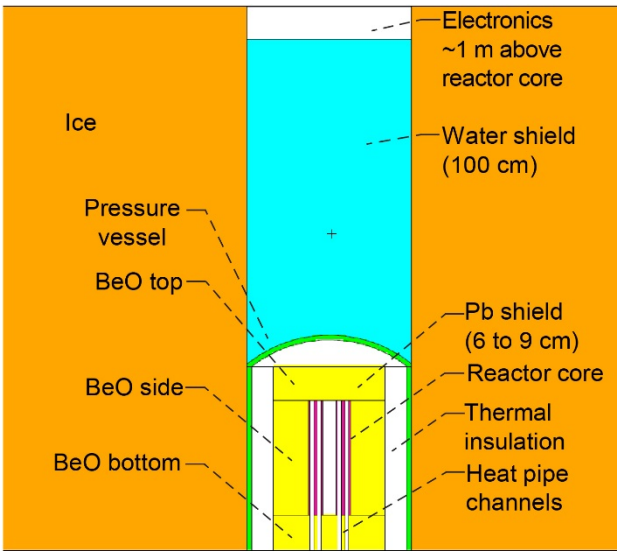

Figure 44.—Axial cross section of reactor core.

adjustments to obtain sufficient core excess reactivity for a 3-yr operation at full power.

The core is a cylindrical annulus of U-Mo with an inner and outer diameter of 4 and 13 cm, respectively. The axial length is 25 cm. The metallic U-Mo annulus is 8 wt% Mo and 92 wt% U with a density of 17.476 g/cm^3 and an enrichment of 93 wt% ^{235}U. The central hole will accommodate both regulating and shutdown control rods. Twenty-four axial channels are drilled in the U-Mo for heat extraction using liquid metal heat pipes (sodium). The total U-Mo mass is approximately 44.4 kg with a corresponding ^{235}U mass of 38.0 kg. Surrounding the core on the top, bottom, and sides are BeO neutron reflectors to boost core reactivity. The side reflector has a 34 cm outer diameter. Both the top and bottom reflectors are 10.5 cm thick. Monte Carlo N-Particle® (MCNP®) (Ref. 69) code (Triad National Security, LLC) was used to model the reactor and perform the radiation transport calculations; Figure 43 and Figure 44 are MCNP® plots showing cross-sectional views of portions of the reactor model and component configuration within the Tunnelbot.

To minimize radiation exposure and damage to organic molecules in the ice, the ice-sampling science instruments were placed more than 2 m below the bottom of the reactor in the nose of the Tunnelbot. This arrangement ensures the molecules in the ice will not be overirradiated prior to sampling. The separation distance, the Pb gamma shielding on the bottom of the core, the melted ice water internal to the Tunnelbot, and the surrounding ice sheet all combine to effectively attenuate the harmful reactor radiation, such that the dose to important organic molecules is <1 Gy (neutron) and <100 Gy (gamma) for a 14-d exposure at full reactor power.

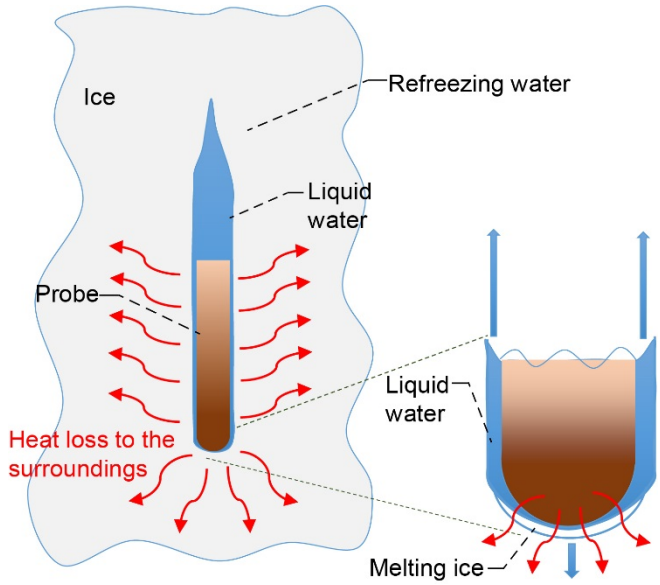

Figure 45.—Tunnelbot descent process. A thermal model was used to determine heat loss to surroundings and heat needed to raise temperature of ice and melt it. Iterating, a descent rate was determined as function of depth.

Sensitive electronics will also need to be protected from reactor radiation with accumulated doses not to exceed 500 krad (silicon). Science instruments in the Tunnelbot nose are shielded from gammas by 4 to 6 cm of lead below the reactor core and neutrons by 2 m of melted ice water pumped into the space around the heat pipes and Stirling engines inside the Tunnelbot. The heat pipes are intentionally curved to prevent direct radiation streaming paths to the instruments.

Gamma shield credit can also be gained from the metallic components of the Stirling engines and heat pipe walls. However, local electronic box shielding will also be required to reduce 2.2-MeV gammas generated by radiative capture from hydrogen in the melted water and ice. Similar shielding considerations are required for sensitive electronics located 1 m above the reactor core. These electronics are closer to the core and will require 6 to 9 cm of lead shielding (gamma) on top of the reactor. The 1 m length of melted ice water pumped into the Tunnelbot between the core and electronic boxes will provide good neutron shielding. Local gamma shielding will also be required around the electronic boxes.

During reactor startup on the surface of the moon, melted ice water will not be available as a neutron shield for the electronics. However, for a 1-d startup, the maximum silicon dose from neutron and gamma radiation is expected to be <20 and <10 krad, respectively, at full power. The gamma dose is mitigated by the lead shielding already in place above and below the reactor core. Longer reactor startup times on the surface will accumulate significant dose from both reactor operation and from the natural radiation fields engulfing Europa.

The preliminary reactor design here can easily provide the necessary heat and power requirements for the Europa mission. The initial excess core reactivity is more than sufficient to maintain core criticality over the 3-yr period with a ^{235}U burnup of only 0.12 percent. Further core and Tunnelbot design studies are needed to optimize the core reactivity and control and to minimize core and shield mass.

9.0 Thermal

9.1 Thermal System Descent Process

The Tunnelbot is designed to melt from the surface of Europa through the ice to reach the liquid ocean below the ice. The thermal system for the Tunnelbot is used to control the ice melting process and regulate the descent of the Tunnelbot. The Tunnelbot must be capable of moving through the ice and stopping periodically to perform science during the descent. The thermal environment the Tunnelbot will operate within is frozen salt water ranging in temperature from 100 to 271 K at the ice water interface.

The Tunnelbot descends through the ice by slowly melting the ice in contact with the Tunnelbot tip. Once melted, the liquid water flows along the sides of the Tunnelbot to the void created behind the Tunnelbot as it descends. Eventually the liquid water melted by the Tunnelbot tip will refreeze behind the Tunnelbot as it is descending. This process is illustrated in Figure 45.

A thermal model was used to determine the heat loss to the surroundings and the heat needed to raise the temperature of the ice and melt it. Iterating, a descent rate was determined as a function of depth. The probes' sides are heated to offset the heat loss to the surroundings and keep the water moving up along the sides from freezing. As the water is formed, it is pushed along the sides of the probe as the probe descends. Heat is transferred to the tip to raise the ice temperature melting point, melt the ice, and overcome the losses to the surroundings.

The descent rate will depend on the amount of heat available and the heat losses to the surroundings. Similarly, the time it takes for the water behind the Tunnelbot to refreeze is also dependent on the surroundings temperature. As the Tunnelbot descends, this time increases and the water column behind the Tunnelbot becomes longer because the surrounding ice is getting relatively warmer with depth.

A thermal analysis was set up to model the heat flow from the Tunnelbot into the ice. This model broke the heat transfer into three segments: the heat loss to the surroundings for the surface area of the Tunnelbot, the heat needed to bring the temperature of the ice nearest the tip up to the melting point, and the heat needed to change the state of the ice from solid to liquid. The total of these three heat transfer mechanisms was equated to the total heat available from the Tunnelbot power source. The amount of heat that went into each of these three mechanisms varied as the Tunnelbot descended. This is shown in Figure 46 for the reactor-powered Tunnelbot. The analysis method was verified using data from the Philberth probe used for melting through the ice in Greenland (Ref. 70). The Philberth probe dimensions, heating power, and surroundings temperature were put into the analysis model and a descent rate was calculated. The calculated descent rate was 2.5 m/hr, whereas the measured descent rate from the probe data was 2.7 m/hr. This is a difference of 7.5 percent between the calculated and experimental rates.

Figure 46 illustrates that as the Tunnelbot descends and the surroundings warm up, the heat loss to the surroundings and that needed to bring the ice up to the melting temperature decrease. This leaves more heat for melting the ice, causing the Tunnelbot to speed up as it descends. The descent rate for the reactor-powered Tunnelbot along with the estimated surrounding temperature is shown in Figure 47.

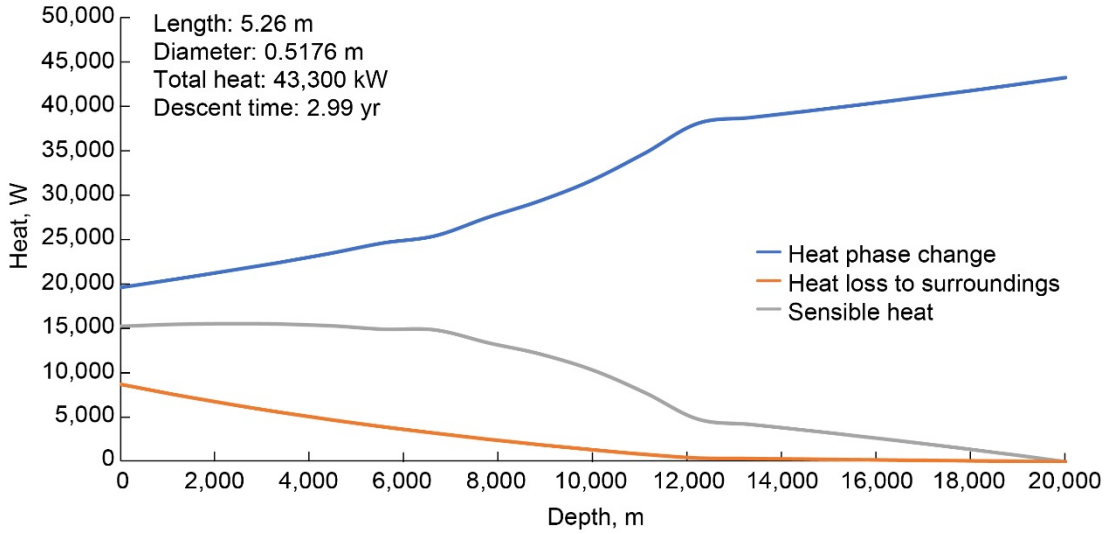

Figure 46.—Reactor-powered Tunnelbot heat flow breakdown during descent.

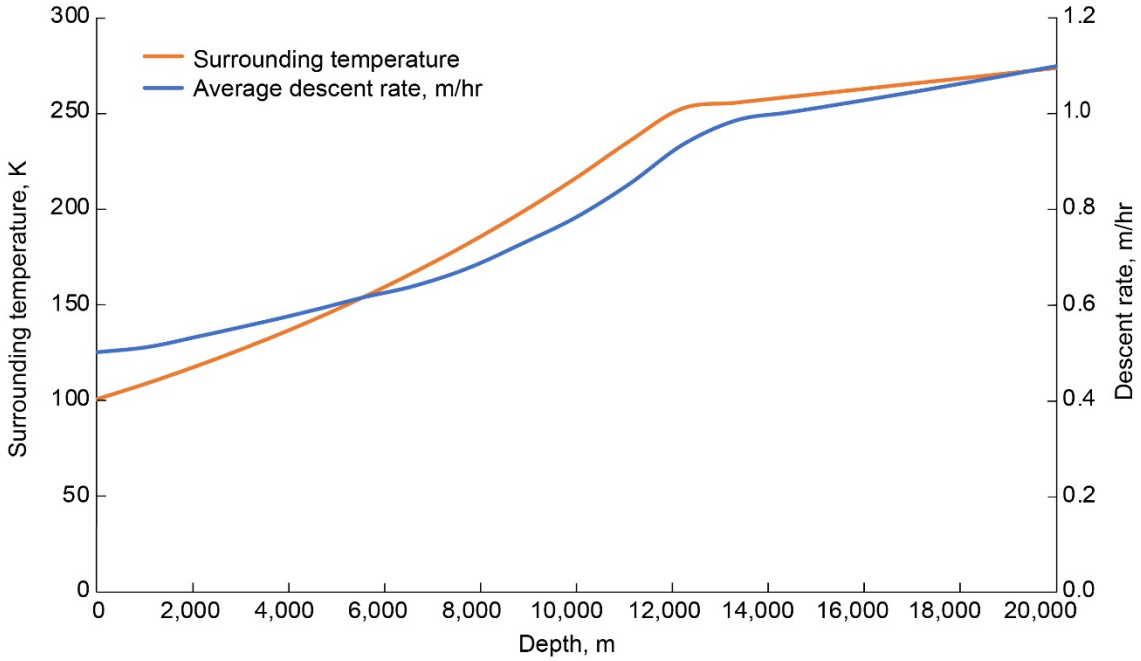

Figure 47.—Reactor-powered Tunnelbot descent rate and surrounding temperature.

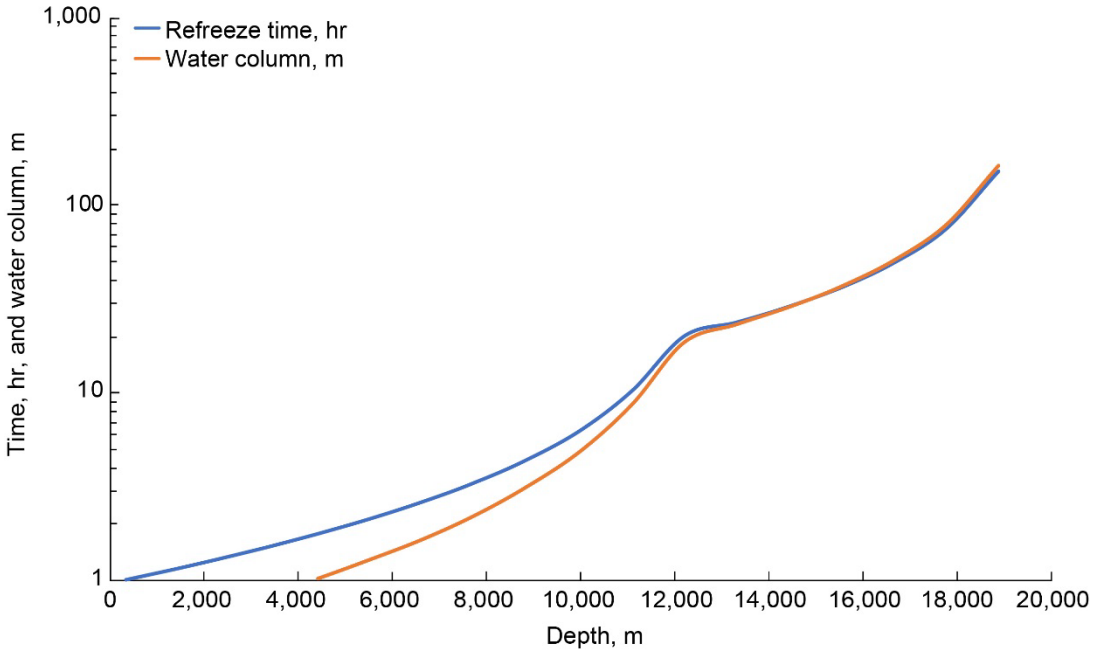

Figure 48.—Reactor-powered Tunnelbot water column length and refreeze time as function of depth.

The refreeze time of the water column behind the Tunnelbot is a critical item in the overall design process. This water column affects the ability to broadcast to the surface if needed due to the large difference is signal attenuation through the water as opposed to the ice. It also affects the ability to securely anchor the Tunnelbot into the ice. If the time for the water column to refreeze is long, the Tunnelbot will need to slow down when it nears the ocean and ice interface in order to allow the water behind the Tunnelbot to freeze, anchoring the Tunnelbot for its descent into the ocean. The water column length and the refreeze time of water in the column are shown in Figure 48 for the reactor-powered Tunnelbot.

9.2 Reactor-Powered Tunnelbot Thermal Design

To melt through the ice, the thermal system moves heat generated by the reactor to a series of hot plates located throughout the Tunnelbot to enable the tip of the Tunnelbot to melt the ice as well as maintaining the exterior wall temperature so that the water produced does not freeze along the sides of the Tunnelbot. The heat from the reactor is moved through a pump loop system that can vary the heat flow to the different sets of heating plates, thereby controlling the heat flow to the surroundings. Controlling the heat flow enables the Tunnelbot to descend, stop, and freeze in place if desired. The Tunnelbot would also be able to be unfrozen and continue its downward descent. The main heat flow components are illustrated in Figure 49.

Side wall hot plates are for spreading heat along the Tunnelbot exterior to maintain a liquid film along the body and preventing the Tunnelbot from being frozen in place and consist of 40 side wall hot plates broken into 10 groups of 4. The heat flow to each group is controlled individually.

Tip hot plates are plates located in the tip for melting the ice in contact with the tip, allowing the Tunnelbot to descend. The tip comprises four individually controllable hot plates.

Insulation is used along the outer wall surfaces to help maintain the interior temperature around 300 K during the descent.

The high-temperature heat pipe system is for moving heat from the reactor to the heat distribution manifold.

The heat distribution liquid loop is the means for distributing and controlling heat flow from the reactor to the various hot plates consisting of an interface manifold with the heat pipes, flow control valves, heating fluid lines, and pumps.

Figure 50 is a diagram of the heat flow components and Table 19 lists the reactor Tunnelbot MEL.

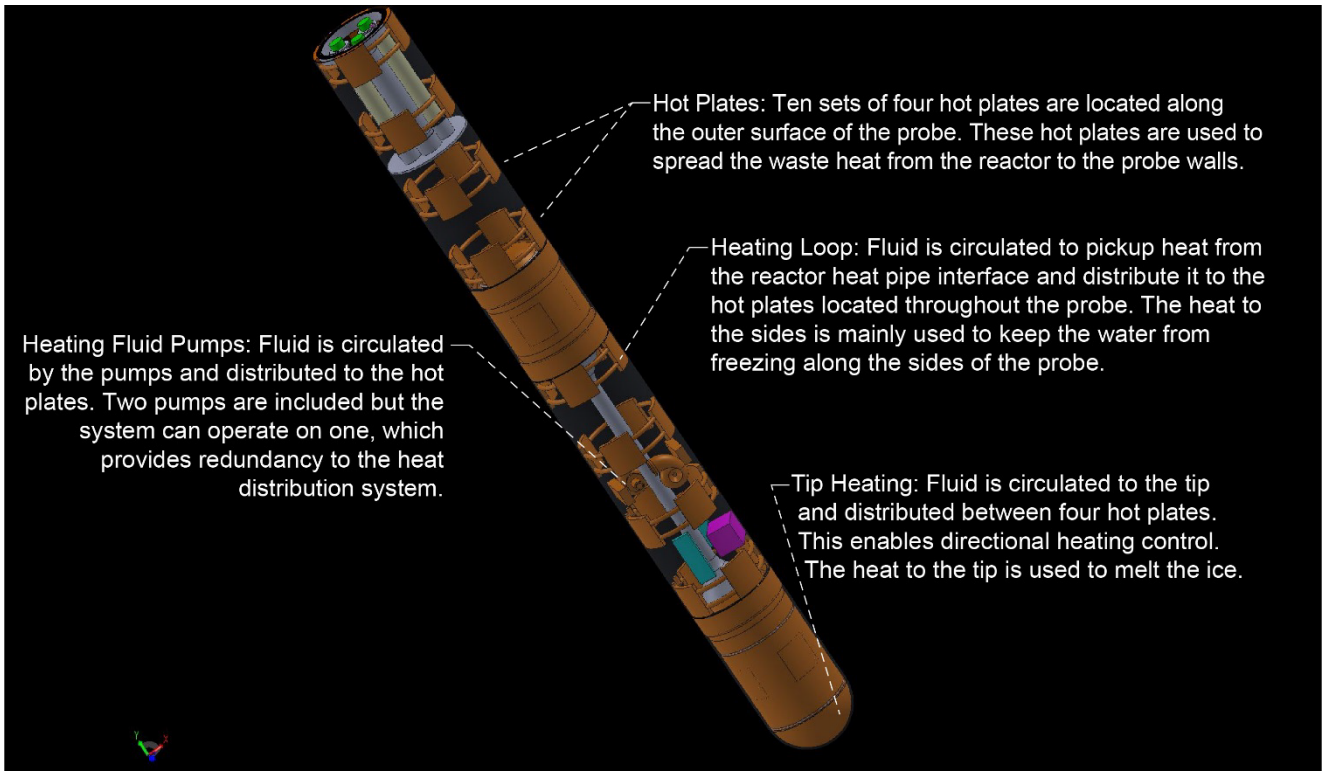

Figure 49.—Reactor-powered Tunnelbot thermal system layout.

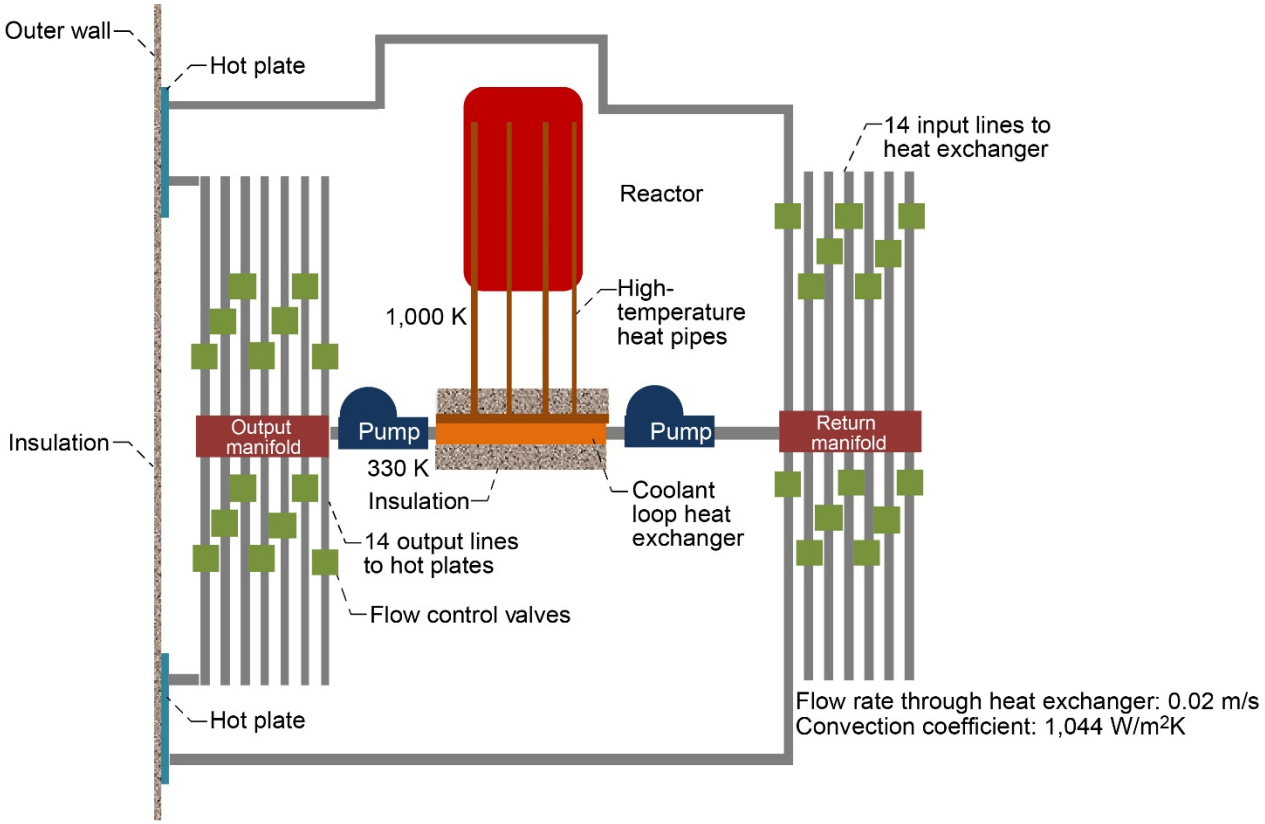

Figure 50.—Reactor-powered Tunnelbot heat flow control diagram.

TABLE 19.—REACTOR TUNNELBOT THERMAL CONTROL SYSTEM MASTER EQUIPMENT LIST FOR CASE 1

Description	Quantity	Unit mass, kg	Basic mass, kg	Growth, percent	Growth, kg	Total mass, kg
Thermal control (nonpropellant)	---	-------	133.7	16.9	22.6	156.2
Active thermal control	---	-------	0.5	0.0	0.0	0.5
Thermocouples	50	0.01	0.5	0.0	0.0	0.5
Passive thermal control	---	-------	133.2	16.9	22.6	155.7
Insulation	1	1.1	1.1	18.0	0.2	1.3
Hot plates	40	0.6	25.3	18.0	4.6	29.9
Heat pipes	1	3.0	3.0	18.0	0.5	3.5
Cold plate	1	0.8	0.8	0.0	0.0	0.8
Heating lines	14	1.9	26.2	18.0	4.7	30.9
Heating pump	2	6.8	13.5	18.0	2.4	15.9
Heating loop manifold	2	2.5	5.1	18.0	0.9	6.0
Flow control valves	14	0.5	7.0	0.0	0.0	7.0
Tip hot plate	1	23.3	23.3	18.0	4.2	27.5
Coolant	14	2.0	27.8	18.0	5.0	32.9

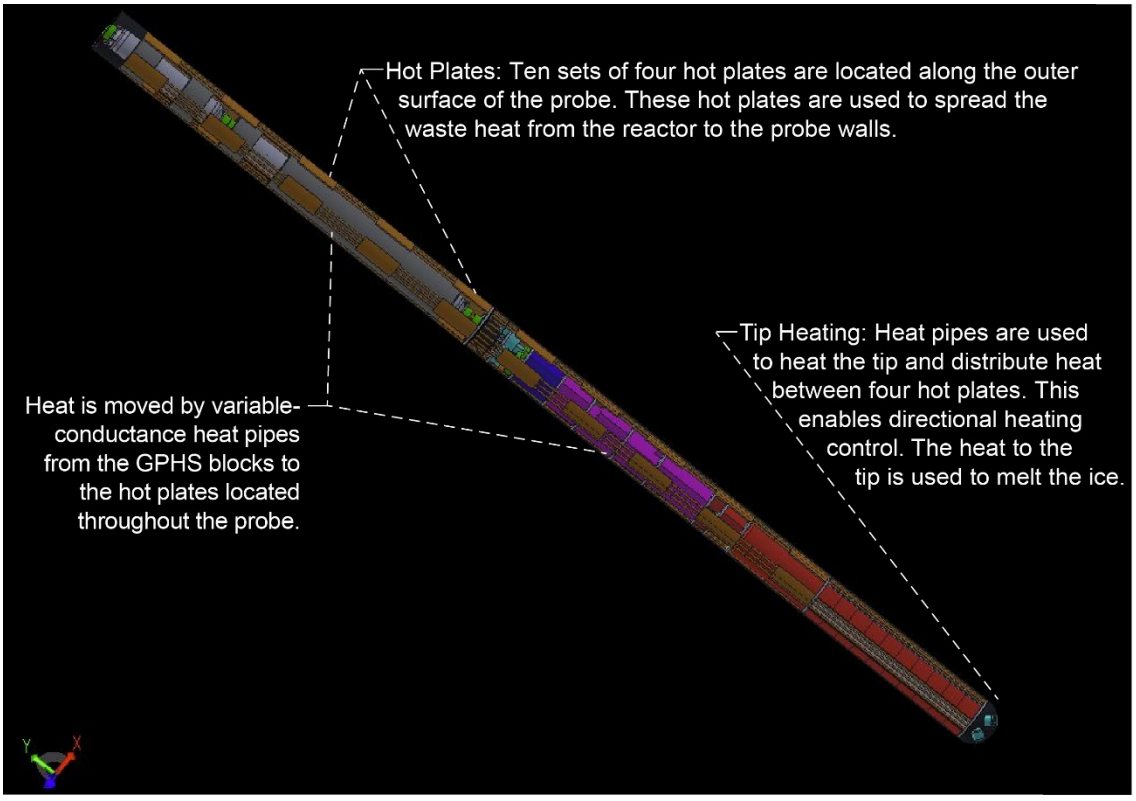

Figure 51.—Isotope-powered Tunnelbot thermal system layout, where GPHS is general purpose heat source.

9.3 Isotope-Powered Tunnelbot Thermal Design

The isotope-powered Tunnelbot thermal system functions in a manner similar to the reactor-powered Tunnelbot, except for the fact that the plutonium heat cannot be turned off. The system consists of a series of hot plates that are used to control the heat flow to the surroundings. The main difference between the thermal systems of the two Tunnelbots is that the isotope system uses variable-pressure heat pipes instead of a pump loop system to move the heat from the isotope heat source to the hot plates. The variable-pressure heat pipes were chosen due to the lower heat transport level of the isotope-powered Tunnelbot and because the orientation of the power system within the Tunnelbot was favorable to heat pipe operation.

In the isotope-powered Tunnelbot, the GPHS blocks are located toward the front of the Tunnelbot, as shown in Figure 51. This enables the fluid within the heat pipe to flow with gravity, eliminating the need to wick the fluid against gravity over the length of the Tunnelbot. The liquid in the heat pipe would vaporize near the tip of the Tunnelbot and rise up to the various plates located along the sides of the Tunnelbot where it condenses rejecting its heat and flows with gravity back toward the tip.

Each heat pipe is connected to four hot plates that are operated together as a zone, conducting heat to the outer wall of the Tunnelbot, as illustrated in Figure 52. The heat flow to each zone can be controlled independently by varying the internal pressure within the heat pipe. Heat is also rejected to one of the zones by the Stirling engines. The waste heat from the engines is conducted to the hot plates in a zone by a pressure-controlled heat pipe.

Pressure-controlled heat pipes are used to move heat from the GPHS blocks and Stirling engines to the hot plates located through the Tunnelbot. Pressure-controlled heat pipes are similar to variable conductance heat pipes in that the vapor and noncondensable gas interface position in the condenser moves to vary the conductance of the heat pipe. However, for a pressure-controlled heat pipe, the control mechanism is active. This provides much closer control of conductance and can allow changing of the set point temperature after assembly of the heat pipe. This is necessary for the Tunnelbot since there are times when the heat flow must be turned off to different sections to stop the descent and freeze into the ice.

Two different control mechanisms are possible: actively injecting or removing the noncondensable gas or by varying the volume of the reservoir by contracting or expanding a bellows. The process selected for the Tunnelbot is to vary the volume, and therefore internal pressure of the heat pipe. An illustration of the operation of a variable-pressure heat pipe is given in Figure 53.

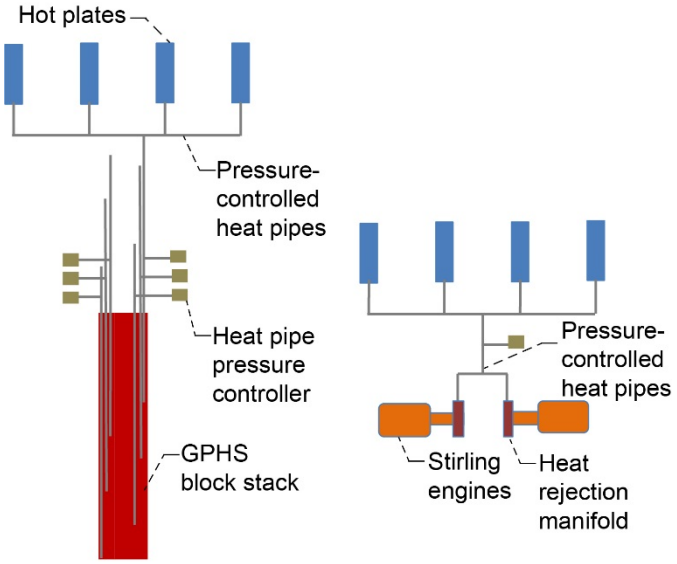

Figure 52.—Isotope-powered Tunnelbot heat flow control diagram, where GPHS is general purpose heat source.

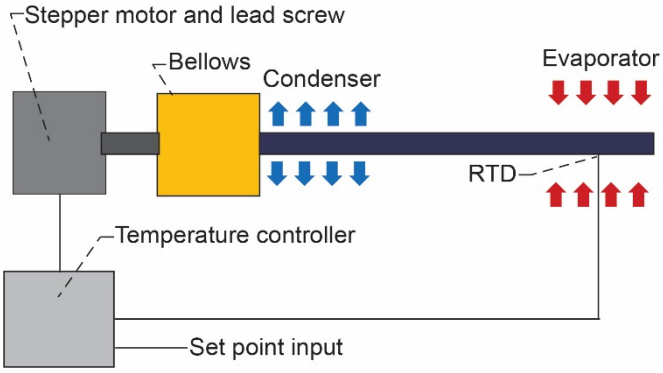

Figure 53.—Operation of variable-pressure heat pipe.

The GPHS Tunnelbot thermal control system MEL is listed in Table 20.

9.4 Repeater Thermal Control

Communication repeaters are periodically dropped off from the Tunnelbot and left to refreeze into the ice. These repeaters need to be capable of maintaining an internal temperature sufficient to enable the electronics to operate while frozen in the ice. This is mainly a concern near the surface where the surrounding temperatures are very low and below the operating temperature of the electronics.

The repeaters consist of an evacuated pressure vessel. MLI is used on the interior of the repeater to reduce the heat loss to the surroundings. Because the repeater is evacuated, MLI is the ideal insulation for limiting heat loss to the surroundings. For the repeater, 15 layers of MLI are used, which limits the heat

loss through the insulation to the surroundings to 0.2 W_{th} at the location of the first repeater dropoff. This location is the coldest ambient environment the repeaters will need to operate in. Additional heat losses to the surroundings occur from the cable that is connected to the repeater (linking it back to the Tunnelbot) and through the internal structural supports that penetrate the MLI to tie the internal and outer structures together. These heat loss components are illustrated in Figure 54. To maintain an operating temperature of at least 271 K and make up for the heat loss to the surroundings, seven RHUs were added to the repeater to supply heat. These seven RHUs, in addition to the eight used to provide power to the repeater, result in 15 W_{th} of total waste heat, which is sufficient to maintain the internal temperature of the repeater within the desired operating range of 271 to 330 K.

Table 21 contains the repeater thermal control system MEL.

TABLE 20.—GENERAL PURPOSE HEAT SOURCE (GPHS) TUNNELBOT THERMAL CONTROL SYSTEM MASTER EQUIPMENT LIST FOR CASE 2

Description	Quantity	Unit mass, kg	Basic mass, kg	Growth, percent	Growth, kg	Total mass, kg
Thermal control (nonpropellant)	---	----	128.6	6.8	8.7	137.3
Active thermal control	---	----	0.5	0.0	0.0	0.5
Thermocouples	50	0.01	0.5	0.0	0.0	0.5
Passive thermal control	---	----	128.1	6.8	8.7	136.8
Insulation	1	0.8	0.8	18.0	0.1	0.9
Hot plates	40	0.4	16.0	18.0	2.9	18.9
Heat pipes	14	1.9	26.2	18.0	4.7	31.0
Cold plate	1	0.8	0.8	0.0	0.0	0.8
Flow control valves	14	0.5	7.0	0.0	0.0	7.0
GPHS blocks	50	1.4	72.0	0.0	0.0	72.0
Tip hot plate	1	5.2	5.2	18.0	0.9	6.2

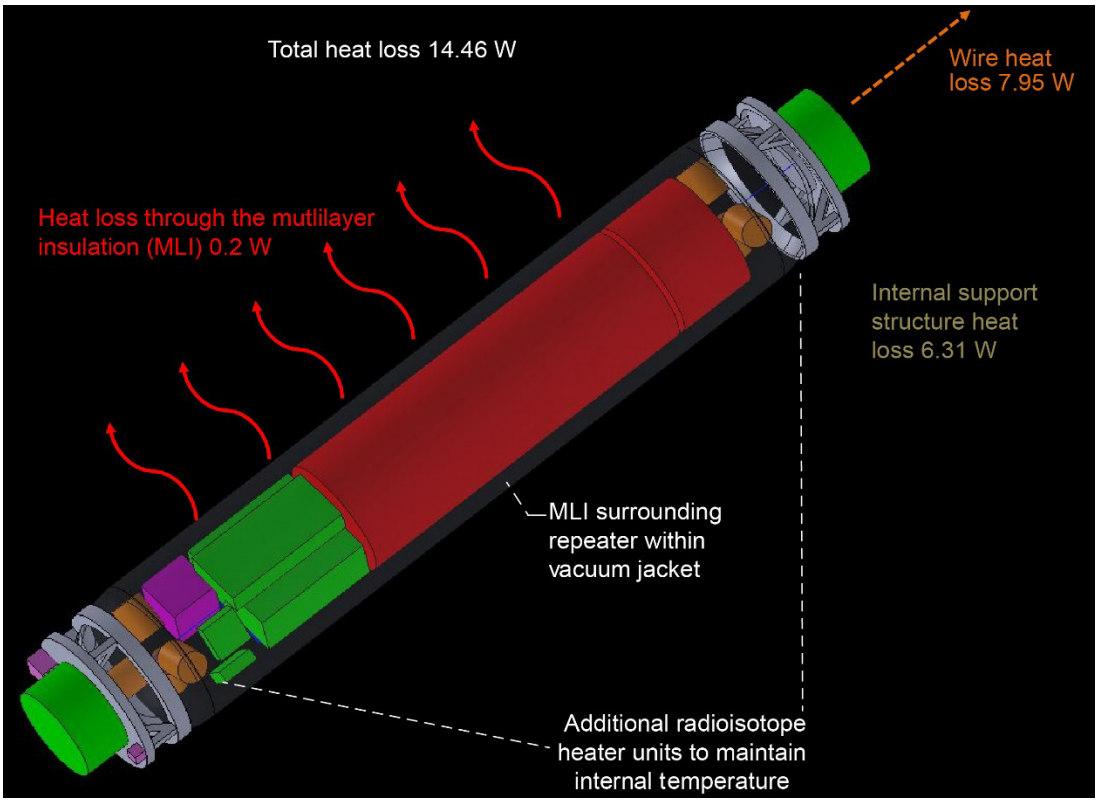

Figure 54.—Repeater thermal layout and heat loss.

TABLE 21.—REPEATER THERMAL CONTROL SYSTEM MASTER EQUIPMENT LIST FOR CASES 1 AND 2

Description	Quantity	Unit mass, kg	Basic mass, kg	Growth, percent	Growth, kg	Total mass, kg
Thermal control (nonpropellant)	---	-----	1.1	0.0	0.0	1.1
Passive thermal control	---	-----	1.1	0.0	0.0	1.1
Insulation	1	0.40	0.4	0.0	0.0	0.4
Radioisotope heater units	18	0.04	0.7	0.0	0.0	0.7

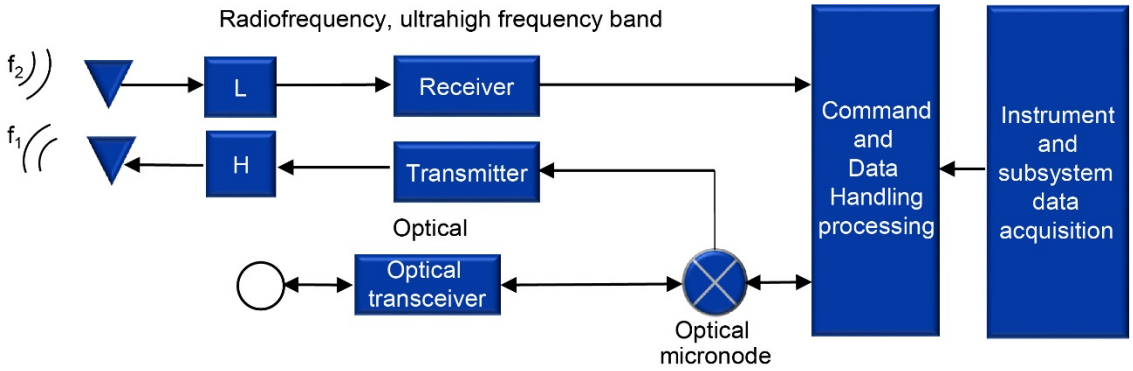

Figure 55.—Communication system block diagram.

10.0 Communication

The communications design requirement for the Europa Tunnelbot is a system to provide at least 1 Kb/s data rate for the duration of the descent through 20 km of ice. Assumptions that were made include single fault tolerance, TRL minimum 5 to 6 hardware, RF communication, and to use the lowest frequency RF signal possible (bounded by practical transmit antenna size) to maximize signal penetration through ice. The combination of Europa ice physical composition, thermal components, and chemistry was assumed to not be greater than 16 dB/km attenuation for an RF signal. The Europa Clipper mission should provide more insight into the characteristics of the ice sheet.

The two trades that were considered were tethered versus untethered descent and operation. The tethered descent involved a metallic conductor cable deployed for the length of descent. However, an analysis of cable mass and resistance per unit length quickly showed this configuration to be prohibitive. Another iteration of the tethered option considered fiber optic cable as a possibility. There was concern over the strength and integrity of the cable sheathing to resist shearing due to unpredictable ice shifting.

Untethered operation involves signal transmission through the ice, throughout descent. This was also a challenge. Two types of untethered operation were considered: acoustic and RF. Acoustic communication uses acoustic waves rather than RF waves and is more unpredictable within unknown compositions of solid, liquid, and quasi-state material than RF. Acoustic is also less efficient for data transmission compared to RF.

An RF link budget communications analysis showed that it would be almost impossible for a transmitter on the surface to communicate with the Tunnelbot probe descending through the ice when it passed 5 km because of the uncertainty of the ice composition and unknown attenuation factors. Therefore, a system model was proposed using communications RF repeaters approximately every 5 km through the ice during descent. The repeaters used the ultrahigh frequency (UHF) band to maximize signal penetration through the ice, while bounding a practical transmit antenna size to optimize signal power transfer. To provide single fault tolerance, a separate fiber optic channel was proposed with optical boosters. This resulted in a hybrid RF and optical repeater. The resulting system configuration and link budget analysis diagrams are detailed in Figure 55 and Figure 56.

The overriding risk of this design is that since the communications link scenarios are based on an ice attenuation of 16 dB/km for RF communications, there is a possibility that the link could be significantly degraded if the resulting ice attenuation is higher. This would result in diminished data rates. The next steps in this design would be to try and further refine and quantify the effects of the ice attenuation coefficients as much as possible, under varying temperatures and RFs, and simulate graceful degradation conditions so that some data may be acquired even under the worst-case circumstances. It is hoped that the Europa Clipper's radar will provide better data on the attenuation.

Table 22 to Table 24 list the MELs for the communication systems' reactor, GPHS, and repeater.

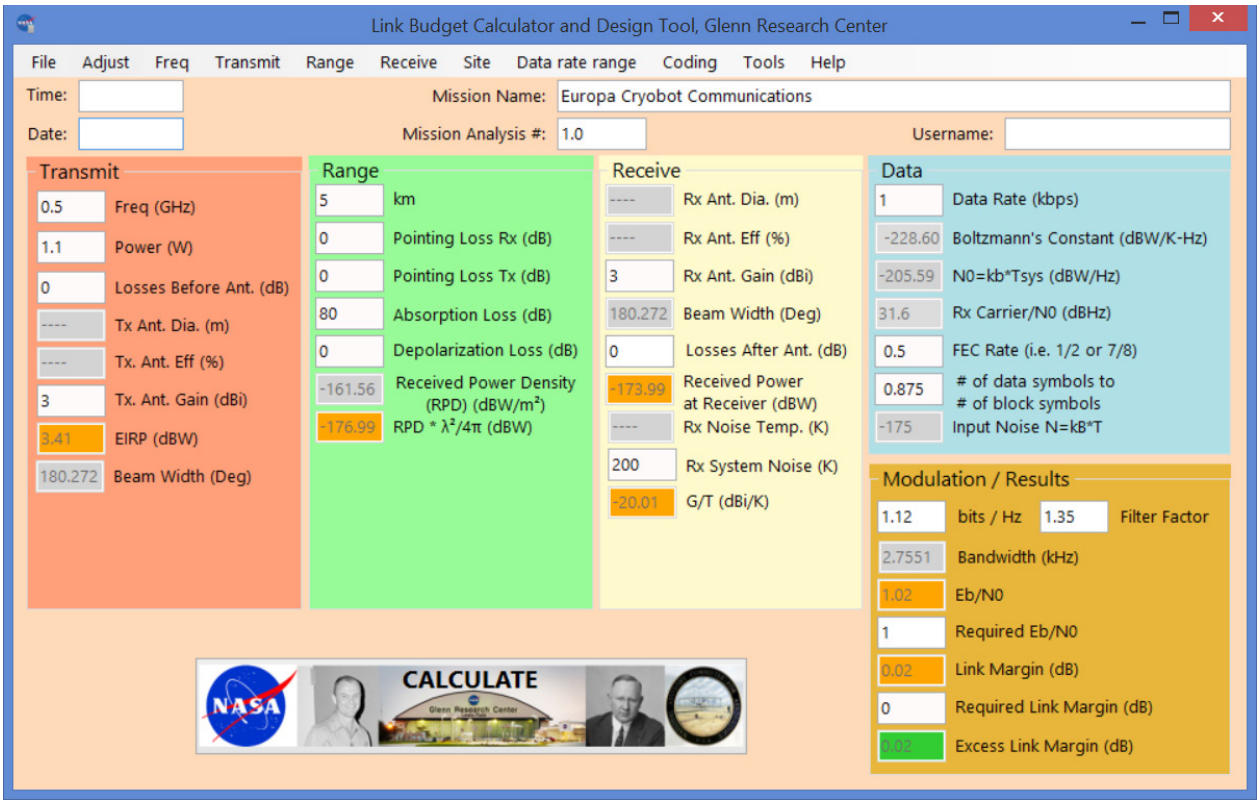

Figure 56.—Communication system link analysis with transmitted frequency of 0.4 to 1 GHz, radiofrequency (RF) output power of ~1 W_e, max. data rate of 1 Kb/s, an RF ice attenuation coefficient of 16 dB/km, and min. antenna gain of 3 dBi.

TABLE 22.—REACTOR TUNNELBOT COMMUNICATION SYSTEM MASTER EQUIPMENT LIST FOR CASE 1

Description	Quantity	Unit mass, kg	Basic mass, kg	Growth, percent	Growth, kg	Total mass, kg
Communications and tracking	-	---	1.0	10.0	0.1	1.1
Ultrahigh frequency (UHF) optical communications system	-	---	1.0	10.0	0.1	1.1
Transmit-UHF modified 1- to 2-W satellite transceiver[a]	1	0.3	0.3	10.0	0.0	0.3
Optical micronode transceiver[a]	1	0.5	0.5	10.0	0.1	0.6
Antenna, multimode	1	0.2	0.2	10.0	0.0	0.2

[a]Mutually exclusive.

TABLE 23.—GENERAL PURPOSE HEAT SOURCE TUNNELBOT COMMUNICATION SYSTEM MASTER EQUIPMENT LIST FOR CASE 2

Description	Quantity	Unit mass, kg	Basic mass, kg	Growth, percent	Growth, kg	Total mass, kg
Communications and tracking	-	---	1.0	10.0	0.1	1.1
Ultrahigh frequency (UHF) optical communications system	-	---	1.0	10.0	0.1	1.1
Transmit-UHF modified 1- to 2-W satellite transceiver[a]	1	0.3	0.3	10.0	0.0	0.3
Optical micronode transceiver[a]	1	0.5	0.5	10.0	0.1	0.6
Antenna, multimode	1	0.2	0.2	10.0	0.0	0.2

[a]Mutually exclusive.

TABLE 24.—REPEATER COMMUNICATION SYSTEM MASTER EQUIPMENT LIST FOR CASES 1 AND 2

Description	Quantity	Unit mass, kg	Basic mass, kg	Growth, percent	Growth, kg	Total mass, kg
Communications and tracking	-	---	1.0	10.0	0.1	1.1
Ultrahigh frequency (UHF) optical communications system	-	---	1.0	10.0	0.1	1.1
Transmit-UHF modified 1- to 2-W satellite transceiver[a]	1	0.3	0.3	10.0	0.0	0.3
Optical micronode transceiver[a]	1	0.1	0.1	10.0	0.0	0.1
Antenna, multimode	2	0.2	0.4	10.0	0.0	0.4
Radiofrequency diplexer and switch	2	0.1	0.2	10.0	0.0	0.2

[a]Mutually exclusive.

11.0 Guidance, Navigation, and Control (GN&C)

11.1 Requirements and Assumptions

The GN&C subsystem has the following requirements for both case studies:

(1) Maintain knowledge of depth to within ±500 m.
(2) Limit transverse dispersions to ±100 m.
(3) Detect obstructions and ice and water interfaces >200 m in front of Tunnelbot.
(4) Maintain knowledge of the Nadir-direction in the Tunnelbot body frame.

Requirements (1) and (2) are satisfied via a combination of measurements from inertial and relative sensors and signal travel time between the closest repeater and the Tunnelbot. Requirement (3) is satisfied via the onboard sonar system. A Synthetic Aperture Radar system that utilizes a log-periodic folded slot array antenna architecture was considered, but the antenna architecture resulted in complications with the Tunnelbot thermal system and configuration. Requirement (4) is satisfied through several inertial and relative sensors mentioned in Section 11.2.

There are several assumptions built into the GN&C subsystem design. First, the rotation about the longitudinal axis is assumed to be passively arrested by fluid dampening and the torsional resistance of the cable. Second, the sonar link budget assumes a 50-percent efficiency between power sent to the transducer and power transmitted into the ice, that the emitted signal is spherically distributed, the ice and water interface is a flat plane, and the ice is free of defects (voids, fissures, and grain boundaries).

11.2 Design Summary

The GN&C subsystem is composed of an inertial and relative sensor suite for state and attitude determination, and a sonar system used for ice and water interface detection and obstacle detection. The sensor suite consists of four high-accuracy accelerometers, two three-axis magnetometers, two single-axis tilt sensors, and one pressure sensor. The three-axis magnetometer makes use of the Europan-induced magnetic field data the Europa Clipper is expected to obtain. The two tilt sensors are mounted orthogonal to each other and are aligned with the yaw and pitch body axes to provide additional orientation measurements. The sensor suite measurements should be filtered to manage error propagation. Additional range/range-rate data can be obtained from RF pings to the nearest repeater, and an independent measurement of distance traveled can be obtained by logging the amount of cable that has been deployed.

The sonar system consists of two transducers. A signal generator forms a pulsed sinusoidal signal, which is amplified to 400 W_e. The signal is transmitted by one transducer, and any returned or reflected signals are sensed by the other transducer. The returned signal is sent through a staged amplification circuit and then processed. The link budget model accounts for transmitted power, signal attenuation through ice, path loss, signal reflectance, and transducer and coupling efficiency. Under the previously listed assumptions, the sonar system is able to detect fluctuations in the propagation medium up to 500 m in front of the Tunnelbot. The system can be tuned to look further ahead at the cost of return margin.

The GN&C subsystem design is identical between the two case studies, except for the orientation of the sonar transducers in the melt head. The reactor design has a larger diameter than the GPHS design, allowing the transducers to point more so in the forward direction. The specified transducers are omnidirectional, but directional transducers would incur a loss from this geometric constraint. The MELs for the GN&C subsystem are shown in Table 25 and Table 26.

TABLE 25.—REACTOR TUNNELBOT GUIDANCE, NAVIGATION, AND CONTROL MASTER EQUIPMENT LIST FOR CASE 1

Description	Quantity	Unit mass, kg	Basic mass, kg	Growth, percent	Growth, kg	Total mass, kg
Guidance, Navigation, and Control	-	---	3.1	20.0	0.6	3.7
Accelerometer	4	0.1	0.3	20.0	0.1	0.4
Neptune T257 communication transducer	2	0.5	1.0	20.0	0.2	1.2
Signal generation and amplification	2	0.3	0.5	20.0	0.1	0.6
Received signal amplification	2	0.3	0.5	20.0	0.1	0.6
Signal processing	2	0.2	0.4	20.0	0.1	0.5
Magnetometer and tilt sensor	2	0.2	0.4	20.0	0.1	0.5

TABLE 26.—GENERAL PURPOSE HEAT SOURCE TUNNELBOT GUIDANCE, NAVIGATION, AND CONTROL MASTER EQUIPMENT LIST FOR CASE 2

Description	Quantity	Unit mass, kg	Basic mass, kg	Growth, percent	Growth, kg	Total mass, kg
Guidance, Navigation, and Control	-	---	3.1	20.0	0.6	3.7
Accelerometer	4	0.1	0.3	20.0	0.1	0.4
Neptune T257 communication transducer	2	0.5	1.0	20.0	0.2	1.2
Signal generation and amplification	2	0.3	0.5	20.0	0.1	0.6
Received signal amplification	2	0.3	0.5	20.0	0.1	0.6
Signal processing	2	0.2	0.4	20.0	0.1	0.5
Magnetometer and tilt sensor	2	0.2	0.4	20.0	0.1	0.5

11.3 Risks and Next Steps

The constant exposure to radiation may degrade the performance of the sensors and sonar system over time. Additional margin and redundancy has been built into the system to attempt to mitigate this degradation.

A preliminary assessment of the turning capability was conducted. Avoiding relatively small obstacles detected ~500 m in front of the Tunnelbot appears to be possible by differentially heating the melt head, causing the Tunnelbot to very slowly build up a tilt angle over time. The reactor design has greater turning capability due to its larger diameter and shorter overall length.

Tilt angle and kinetic friction were varied to determine their effects on forward momentum. Results show only excessively high tilt angles (>80°) and coefficients of kinetic friction would result in forward momentum that was insufficient to keep up with the rate of melting or no forward momentum at all. Excessive tilt and high friction between the metallic Tunnelbot and the ice tunnel is unlikely. Further work on the ability to turn when a nonzero turn angle is present should be considered.

12.0 Command and Data Handling (C&DH)

The C&DH subsystem is responsible for all the onboard processing of the Tunnelbot and repeaters. This includes interfacing to all instruments, routing data to the communications system, processing utilities for GN&C, housekeeping, autonomy, and so on. In a general case, the C&DH subsystem of a terrestrial mission is large. This is often due to the large motor driving requirements as well as complex autonomy and data rates; however, this particular mission allows for some simplification over those systems. First, there are very few onboard electric motors to control, which significantly reduces the size, mass, and power of the system. Secondly, the slow-moving nature and low data rates allow for the required processing to be spread out over long durations, which allows for a dramatic reduction in computer throughput. This throughput reduction allows for a reduction in central processing unit (CPU) clock speed, which then reduces power due to the exponential relationship between clock speed and power. This extra time makes the system more

tolerant to single event upsets (SEUs) because time is available to run error detection and correction algorithms. If an SEU does occur, the slow-moving nature of the Tunnelbot is in no danger if a computer reset is required.

While there are advantages to this design, there are also difficulties. The C&DH system is subject to radiation from the onboard sources. Due to the confined spaces, sensitive avionics cannot simply be moved farther away to solve the problem. There are also radiation concerns related to the approach to Europa and during surface operations. For this project, an assumption of the total ionizing dose (TID) requirement was set at 500 krad (5 kGy). At this level of radiation, no commercial off-the-shelf (COTS) line-replaceable units (LRU) are available. All components, including the single board computer (SBC), must be designed and built from scratch. While this is more expensive, it also offers advantages. Custom LRUs can be designed specifically to mission needs with no unused extras. Also, recent developments have made CPUs tolerant above 1 Mrad (10 kGy) without scrubbing. With this, combined with available radiation-tolerant memory technologies, an extremely robust system is possible. This technology can and should be leveraged for this mission. For the purposes of this design, LRUs tolerant to 100 krad (1 kGy) were selected as references and reduced to TRL 5 to account for the radiation inadequacies. This is based on an assumption that 500-krad LRUs can be produced with comparable performance to those currently available at 100 krad. This also assumes that these new LRUs would comprise technologies that would place the project at TRL 5 when the units are to be developed.

A block diagram of the case Tunnelbot C&DH system is shown in Figure 57. The system is based on the 3U Compact Peripheral Component Interconnect (cPCI) standard, implementing a centralized architecture for fault tolerance. The system is composed of two separate and identical units. This redundancy is intended to provide the required single fault tolerance. Each unit comprises a RAD750®-class SBC (BAE Systems), two digital input output (IO) cards to interface with the digital peripherals, an analog IO card to interface to thermocouples and other analog sensors, four motor drive cards to drive the required heat pumps, valves, and sample acquisition motors. A low-voltage power conditioner (LVPC) is included to provide all required potentials to the C&DH circuits.

A block diagram of the second case (GPHS Tunnelbot) C&DH system can be seen in Figure 58. The second case differs from the first in a few critical ways. Most importantly, the heat pumps are not included, and therefore the motor driving requirements are significantly reduced. Secondly, the system is under much more stringent volume requirements due to the reduced vehicle diameter. To accommodate the volume requirements both redundant systems were placed in the same housing. The system architecture was changed to a federated bus architecture implementing an MIL–STD–1553 bus. This allowed the digital IO cards to be reduced by half. The analog sensors were also changed to digital sensors using Differential Inter-Integrated Circuit (I2C) protocol. This reduces the sensing accuracy slightly, but allows for the removal of the analog interface. The last change is the combination of the valve driver and LVPC capabilities onto a single card. The combination of these changes allows the system to fit within the volume constraints.

Table 27 and Table 28 contain the C&DH MELs for the reactor and GPHS, respectively.

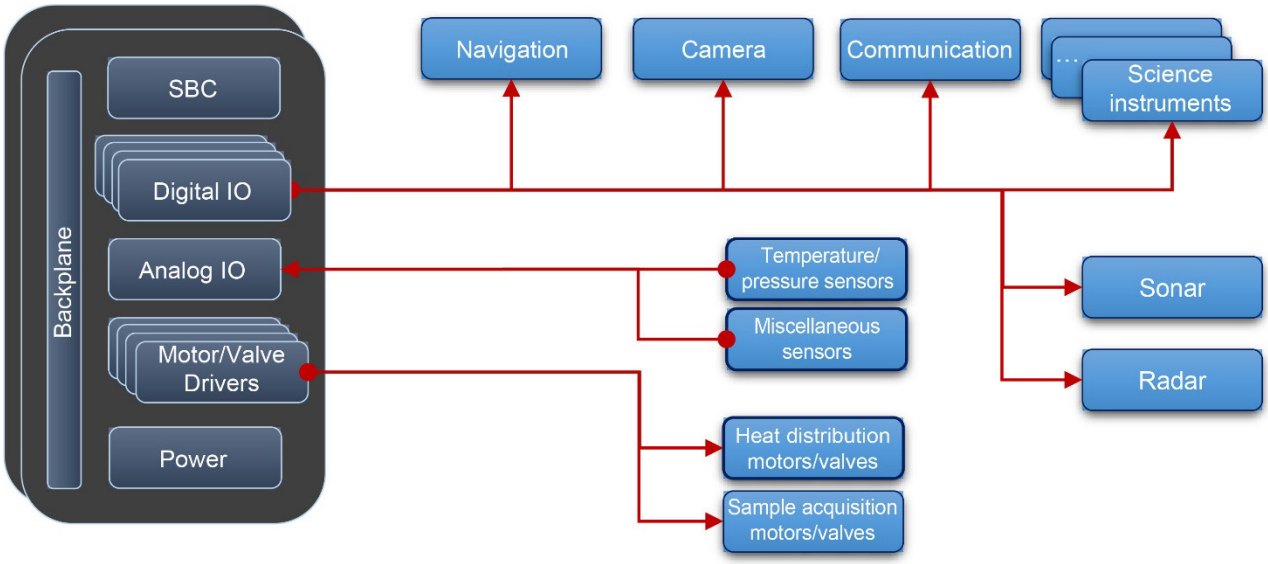

Figure 57.—Reactor Tunnelbot vehicle Command and Data Handling, where IO is input output and SBC is single board computer.

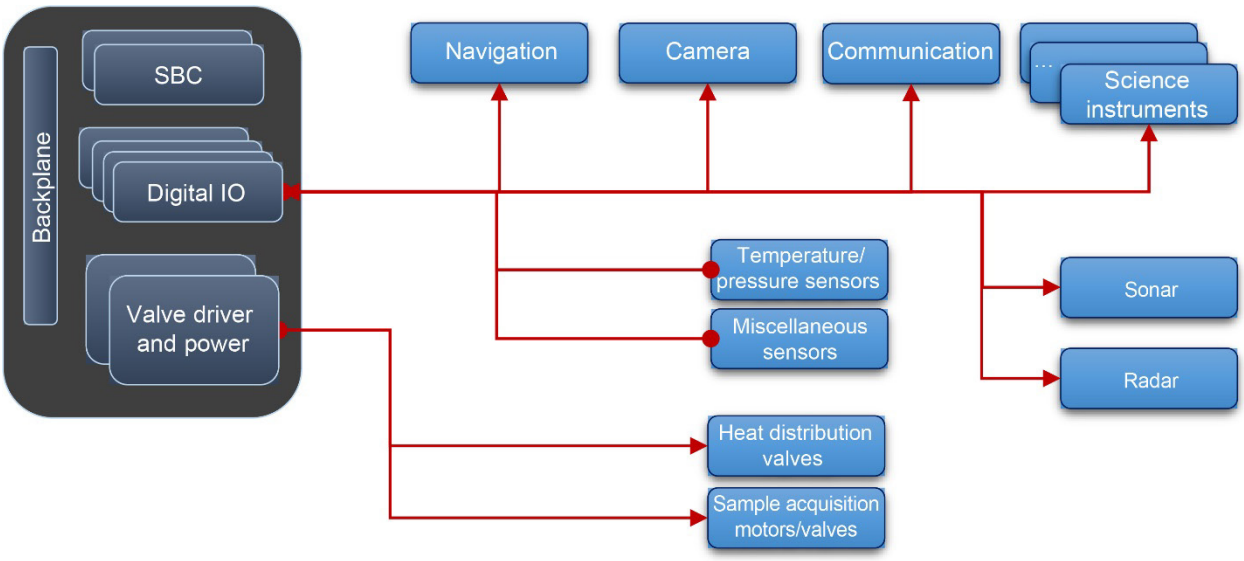

Figure 58.—General purpose heat source vehicle Tunnelbot Command and Data Handling, where IO is input output and SBC is single board computer.

TABLE 27.—REACTOR TUNNELBOT COMMAND AND DATA HANDLING (C&DH) MASTER EQUIPMENT LIST FOR CASE 1

Description	Quantity	Unit mass, kg	Basic mass, kg	Growth, percent	Growth, kg	Total mass, kg
C&DH	-	----	9.7	30.0	2.9	12.6
C&DH hardware	-	----	6.7	30.0	2.0	8.7
RAD750® single bit upset	2	0.6	1.1	30.0	0.3	1.4
Digital MultiOperational Avionics Board input output	4	0.4	1.6	30.0	0.5	2.1
McLASI valve and motor	8	0.2	1.6	30.0	0.5	2.1
Avionics power converter	2	0.3	0.6	30.0	0.2	0.8
Analog MultiOperational Avionics Board	2	0.4	0.8	30.0	0.2	1.0
Avionics enclosure	1	1.0	1.0	30.0	0.3	1.3
Instrumentation and wiring	-	----	3.0	30.0	0.9	3.9
Wiring harness	1	3.0	3.0	30.0	0.9	3.9

TABLE 28.—GENERAL PURPOSE HEAT SOURCE TUNNELBOT COMMAND AND DATA HANDLING (C&DH) MASTER EQUIPMENT LIST FOR CASE 2

Description	Quantity	Unit mass, kg	Basic mass, kg	Growth, percent	Growth, kg	Total mass, kg
C&DH	---	----	6.4	30.0	1.9	8.3
C&DH hardware	---	----	4.6	30.0	1.4	6.0
RAD750® single bit upset	2	0.6	1.1	30.0	0.3	1.4
Digital MultiOperational Avionics Board input output	4	0.4	1.6	30.0	0.5	2.1
Valve driver and power supply	2	0.2	0.4	30.0	0.1	0.5
I2C[a] temperature sensors	50	0.0	0.5	30.0	0.2	0.7
Avionics enclosure	1	1.0	1.0	30.0	0.3	1.3
Instrumentation and wiring	---	----	1.8	30.0	0.5	2.3
Wiring harness	1	1.8	1.8	30.0	0.5	2.3

[a]Differential Inter-Integrated Circuit.

TABLE 29.—REPEATER COMMAND AND DATA HANDLING (C&DH) MASTER EQUIPMENT LIST FOR CASES 1 AND 2

Description	Quantity	Unit mass, kg	Basic mass, kg	Growth, percent	Growth, kg	Total mass, kg
C&DH	-	----	0.4	30.0	0.1	0.5
C&DH hardware	-	----	0.4	30.0	0.1	0.5
Command and telemetry computer	1	0.2	0.2	30.0	0.1	0.3
4-GB memory module	1	0.1	0.1	30.0	0.0	0.1
Data harness	1	0.1	0.1	30.0	0.0	0.1

The repeater C&DH design is a bare bones implementation (MEL in Table 29). The driving force for this design is the need for an extremely low-power system. The system is composed of only two components: ferroelectric random-access memory (FeRAM) and a microcontroller. FeRAM is extremely low power and nonvolatile. It is radiation tolerant above 1 Mrad. The drawback is that the erase and write cycles are limited to roughly a thousand cycles, which places constraints on operations and software. The microcontroller is low power to begin with and is placed in sleep mode for the majority of the mission. When in sleep mode, it is possible to limit the power to several microwatts.

Moving forward, component-level implementations of these subsystems should be explored in greater depth. There is a risk at this point in the design that details related to implementation will change the design dramatically. It is also worth exploring custom circuit board shapes to better fit the cylindrical shape of the Tunnelbot. This is especially true for the second case where the volume constraints are a major driving force. A vertical stack of circular cards may make more sense than rectangular cards with a standardized backplane. The implementation is required to be custom regardless, therefore, a custom shape should have minimal impact on development cost and schedule.

13.0 Structures and Mechanisms

13.1 Structures and Mechanisms Requirements

The Europa Tunnelbot structures must contain all the necessary hardware for science instrumentation, communications, C&DH, and power. The structural components must be able to withstand applied mechanical and thermal loads. In addition, the structures must provide minimum deflections, sufficient stiffness, and vibration damping. The operational loads range from a 23.8-MPa (3,460 psi) maximum external applied pressure (at 20 km depth) for the main structure of the Tunnelbot to the 17.9-MPa (2,590 psi) maximum applied pressure for the repeater container (at 15 km depth).

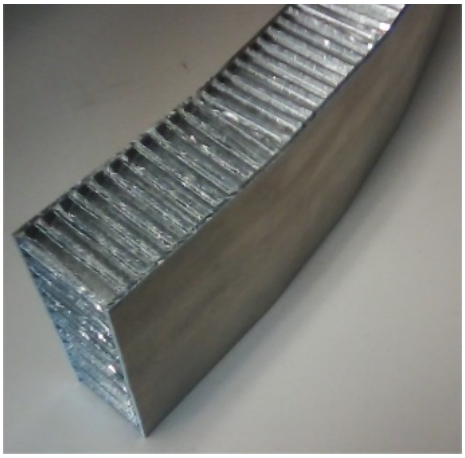

Figure 59.—Typical composite sandwich structure with honeycomb core.

Communication with the lander requires a signal repeater every 5 km along the Tunnelbot's descent path. This requires an estimated 20 km of fiber optic data cable to be deployed as the Tunnelbot descends. Mechanisms consist of a cable deployment system for the repeaters, floats, anchors, and a braking system. The system allows communication with the repeaters. The floats, anchors, and braking system are used to control the Tunnelbot descent upon exiting the ice into the liquid ocean.

13.2 Structures and Mechanisms Assumptions

The bus provides the backbone for the mounted hardware and isolation from the ice and water environment. The primary material for the bus is Ti. Components are of tubular and plate members. Joining of components is by welding, threaded fasteners, and rivets. Composite sandwich structure decks with honeycomb cores are assumed. A typical composite sandwich structure is illustrated in Figure 59.

Mechanisms include cable spools, floats, anchors, and a braking system that is used to stop the vehicle progression as necessary. For the reactor-based design, this cable is wound into a single annular spool, located at the aft end of the Tunnelbot where it surrounds the three repeaters and two syntactic foam

float/anchors. The spool system is designed so that the repeaters are attached to the fiber optic cable at 5 km intervals. Thus, as the cable unwinds from the spool, it extracts the repeaters, as it continuously unwinds from the spool. The repeater deployment sequence is fixed in this design by the unwinding sequence of the fiber optic cable. The two syntactic foam floats/anchors are used to anchor the Tunnelbot into the ice prior to entering the slush-water interface region. They can be deployed at any time during the descent and are designed to float upward into the refreeze cone, freeze into the ice, and thus serve as anchors for the Tunnelbot. Each float is attached to a 500-m anchor cable and braking system that is used to control the Tunnelbot's final descent.

In the GPHS based design, 5 km of cable are stored in four smaller spools located circumferentially around the individual repeaters and are also wound so that each repeater is automatically deployed as the cable is unwound from its respective spool. Instead of floats, the final 5 km of fiber optic cable is reinforced to serve as an anchor cable and is used with the braking system to support the Tunnelbot during its final descent. These two designs and the overall deployment sequence are shown in Figure 60.

13.3 Structures and Mechanisms Design and Master Equipment List (MEL)

Table 30 to Table 32 show the expanded MEL for the structures subsystem. The MELs break down the structures line elements to the lowest work breakdown structure (WBS).

13.4 Structures and Mechanisms Trades

Trades were evaluated with tank materials, tank head configurations, and pressure differentials. Tank material considerations included Al 7075-T73, AISI 304 stainless steel, and Ti-6Al-4V.

The aluminum presents welding difficulties as it loses its temper with the welding process, resulting in a much weaker material. In addition, the low modulus results in a lower resistance to buckling as the tanks are exposed to an external pressure. The low density would help keep the bus mass low. The AISI 304 stainless steel provides good weldability and high stiffness. Unfortunately, the high density and low strength results in excessively heavy components when designed for the given loading conditions.

Lastly, Ti-6Al-4V Ti provides a high modulus, high strength, low thermal conductivity, and good weldability. The higher modulus helps provide greater resistance to buckling of the tanks with the external pressure. The good weldability aids fabrication of the pressure vessels. Also, the Ti provides good radiation shielding. Ti was chosen for this particular design due to its desirable properties. The mass penalty relative to Al was not too significant and it offers a significant advantage when fabricating pressure vessels that require welding.

A few different operating pressure levels within the pressure vessels were investigated. These checks were for the reactor and instrument pressure vessels of case 1. Sizing was set with the pressure vessel stress state at the allowable stress for Ti.

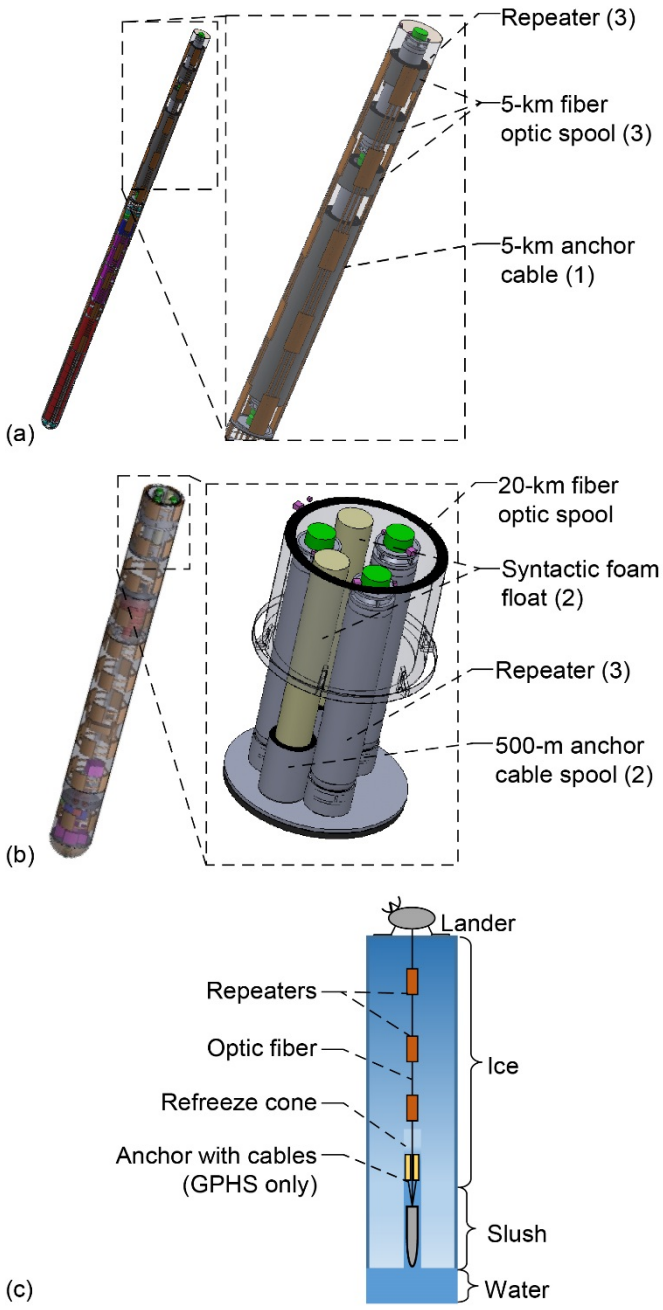

Figure 60.—Cable and repeater deployment designs and overall deployment sequence. (a) General purpose heat source (GPHS) cable and repeater system design. (b) Reactor cable and repeater system design. (c) Deployment sequence.

Internal pressures of 0, 27.6, 11.9, and 23.8 MPa were checked with the external pressure held at the maximum of 23.8 MPa (3.46 psi). Due to the complexity of systems necessary to maintain a pressure other than zero or one, atmosphere was thought to be more problematic than having thicker buckling resistant walls with a near zero internal pressure. As a result, a near zero internal pressure was maintained and the pressure vessel wall thickness was specified to operate at the material allowable stress while staying below the predicted pressure for buckling.

TABLE 30.—REACTOR TUNNELBOT STRUCTURES MASTER EQUIPMENT LIST FOR CASE 1

Description	Quantity	Unit mass, kg	Basic mass, kg	Growth, percent	Growth, kg	Total mass, kg
Structures and mechanisms	-	-------	483.8	18.0	87.1	570.8
Structures	-	-------	459.6	18.0	82.7	542.3
Primary structures	-	-------	367.9	18.0	66.2	434.1
Reactor vessel	1	82.7	82.7	18.0	14.9	97.6
Instrument vessel	1	113.9	113.9	18.0	20.5	134.3
Top cylinder	1	31.1	31.1	18.0	5.6	36.7
Bottom cylinder	1	49.6	49.6	18.0	8.9	58.5
Lead shield	1	13.6	13.6	18.0	2.4	16.0
Flanges	6	0.4	2.1	18.0	0.4	2.5
Tunnel	1	31.4	31.4	18.0	5.7	37.1
Reactor vessel extension	2	3.9	7.7	18.0	1.4	9.1
Instrument vessel extension	1	3.9	3.9	18.0	0.7	4.6
Steel shield	1	31.8	31.8	18.0	5.7	37.6
Secondary structures	-	-------	91.7	18.0	16.5	108.2
Instrument deck	2	1.0	2.1	18.0	0.4	2.4
Reactor deck	1	0.7	0.7	18.0	0.1	0.9
20-km cable assembly	1	57.9	57.9	18.0	10.4	68.3
Repeater deck	1	1.8	1.8	18.0	0.3	2.1
Winch spool	1	0.6	0.6	18.0	0.1	0.7
Anchor cable	2	11.9	23.9	18.0	4.3	28.2
Anchor cable float	2	2.4	4.8	18.0	0.9	5.6
Mechanisms	-	-------	24.2	17.9	4.3	28.5
Adaptors and separation	-	-------	4.0	18.0	0.7	4.7
Cable brake and cutter	2	2.0	4.0	18.0	0.7	4.7
Installations	-	-------	20.2	17.9	3.6	23.8
Command and Data Handling installation	1	0.4	0.4	18.0	0.1	0.5
Communications and tracking installation	1	0.0	0.0	18.0	0.0	0.0
Electrical power installation	1	13.2	13.2	18.0	2.4	15.6
Thermal control installation	1	5.3	5.3	18.0	1.0	6.3
Science installation	1	1.1	1.1	18.0	0.2	1.3
Guidance, Navigation, and Control	1	0.1	0.1	0.0	0.0	0.1

TABLE 31.—GENERAL PURPOSE HEAT SOURCE (GPHS) TUNNELBOT STRUCTURES MASTER EQUIPMENT LIST FOR CASE 2

Description	Quantity	Unit mass, kg	Basic mass, kg	Growth, percent	Growth, kg	Total mass, kg
Structures and mechanisms	-	-------	315.1	18.0	56.7	371.8
Structures	-	-------	304.4	18.0	54.8	359.2
Primary structures	-	-------	149.1	18.0	26.8	176.0
Main vessel	1	74.7	74.7	18.0	13.4	88.1
Top cylinder	1	25.9	25.9	18.0	4.7	30.5
Flanges	2	0.2	0.4	18.0	0.1	0.4
Main vessel extension	1	1.3	1.3	18.0	0.2	1.6
5-km signal cable assembly	3	14.5	43.4	18.0	7.8	51.2
Signal cable spool	3	1.2	3.5	18.0	0.6	4.1
Secondary structures	-	-------	155.3	18.0	27.9	183.2
Instrument deck	9	0.2	1.9	18.0	0.3	2.2
GPHS carriage	1	6.7	6.7	18.0	1.2	7.9
Repeater tube	1	10.2	10.2	18.0	1.8	12.1
Repeater deck	1	0.2	0.2	18.0	0.0	0.3
Anchor cable spool	1	8.1	8.1	18.0	1.5	9.6
5-km anchor cable assembly	1	128.0	128.0	18.0	23.0	151.1
Repeater tube flange	1	0.1	0.1	18.0	0.0	0.1
Mechanisms	-	-------	10.7	17.8	1.9	12.6
Adaptors and separation	-	-------	2.0	18.0	0.4	2.4
Cable brake	1	2.0	2.0	18.0	0.4	2.4
Installations	-	-------	8.7	17.7	1.5	10.2
Command and Data Handling installation	1	0.3	0.3	18.0	0.0	0.3
Communications and tracking installation	1	0.0	0.0	18.0	0.0	0.0
Electrical power installation	1	2.0	2.0	18.0	0.4	2.4
Thermal control installation	1	5.1	5.1	18.0	0.9	6.1
Science installation	1	1.1	1.1	18.0	0.2	1.3
Guidance, Navigation, and Control	1	0.1	0.1	0.0	0.0	0.1

TABLE 32.—REPEATER STRUCTURES MASTER EQUIPMENT LIST FOR CASES 1 AND 2

Description	Quantity	Unit mass, kg	Basic mass, kg	Growth, percent	Growth, kg	Total mass, kg
Structures and mechanisms	-	----	4.8	18.0	0.9	5.7
Structures	-	----	4.5	18.0	0.8	5.3
Primary structures	-	----	4.5	18.0	0.8	5.3
Repeater vessel	1	3.90	3.9	18.0	0.7	4.6
Repeater antenna mount	2	0.30	0.6	18.0	0.1	0.7
Mechanisms	-	----	0.3	18.0	0.1	0.4
Installations	-	----	0.3	18.0	0.1	0.4
Command and Data Handling installation	1	0.02	0.02	18.0	0.00	0.02
Communications and tracking installation	1	0.04	0.04	18.0	0.01	0.05
Electrical power installation	1	0.20	0.20	18.0	0.04	0.24
Thermal control installation	1	0.04	0.04	18.0	0.01	0.05
Science installation	1	0.02	0.02	18.0	0.00	0.02

The repeater pressure vessels were evaluated similarly to the reactor and instrument pressure vessels. Internal pressures of 0, 11.9, 17.9, and 27.6 MPa were evaluated while maintaining the external pressure at the maximum anticipated pressure of 27.9 MPa (2.59 psi). As with the reactor and instrument pressure vessels, the internal pressure was held near zero and the wall thicknesses were sized to operate at the material allowable stress while minimizing potential buckling issues.

In an effort to reduce the volume needed by the pressure vessels an ellipsoid head, relative to a spherical head, was evaluated. A 2:1 ellipsoid head was applied to the Ti reactor pressure vessel of case 1. The result is a mass penalty of 34 kg relative to using spherical heads for the reactor pressure vessel. It was decided that spherical tanks would be utilized for all the pressure vessels as the ellipsoid head did not provide a sufficient advantage in reduced volume relative to the mass penalty incurred.

Alternate anchor cable storage and deployment methodologies were investigated. These included both spool and winch and spool and brake designs. Ultimately, a spool and brake design was chosen for deploying the anchor cable, due primarily to its lower complexity and better volumetric packaging.

Signal conductor cable trades were also executed. Evaluated systems include load-bearing copper conductors, optical fiber with stainless steel rope, and silver-coated aramid ropes. A single optical fiber with a 1×19 AISI 304 rope was chosen for this application, with the optical fiber replacing one of the strands of the 1×19 stainless steel rope.

Various other descent control methods were evaluated, including hooks, wedges, and inflatables using compressed gas, in situ hydrolysis, and both solid and liquid gas generators. Most alternate designs proved too bulky, massive, and/or had a low TRL due to the high inflation pressures required at depth. An integrated cable spool, braking system, and repeater design that would allow for a tailored deployment sequence was devised but was not further evaluated due to study time constraints.

13.5 Structures and Mechanisms Analytical Methods

Ti is specified for the structures material. Per the Metallic Materials Properties Development and Standardization (MMPDS) (Ref. 71), the Ti-6Al-4V ultimate strength is 579 MPa (84 ksi) and the yield strength is 490 MPa (71 ksi) at 467 °C (872 °F). Applying the safety factors of 1.4 on the ultimate strength and 1.25 on the yield strength, as per NASA standard NASA–STD–5001B (Ref. 72), results in a maximum allowable stress of 393 MPa (57 ksi).

Hand calculations and a spreadsheet were utilized to determine approximate stress levels in the pressure vessels. Pressure vessel wall thickness is based on the allowable stress of the material. In addition, a check was made to ensure the wall thickness is sufficient to avoid buckling. Buckling calculations were as presented by Young and Budynas (Ref. 73) for cylinders under an external pressure.

The case 1 reactor vessel has a wall thickness of 14.3 mm and a buckling pressure of 1,140 MPa, which is well above the anticipated operating pressure of 23.8 MPa. The case 1 instrument vessel has a wall thickness of 14.3 mm also and a buckling pressure of 1,350 MPa, which is significantly higher than the maximum operating pressure of 23.8 MPa.

The cases 1 and 2 repeater vessel has a wall thickness of 2.6 mm and a buckling pressure of 55 MPa. The case 2 main vessel has a wall thickness of 6.8 mm and a buckling pressure of 94.3 MPa.

The 1×7 anchor cable has an operating load of 1.1 kN, which is 20 percent of the break load of 5.3 kN. The anticipated load is 872 N for case 1 and 765 N for case 2.

The signal cable is a 1×19 configuration of stainless steel. One strand is replaced by an optical glass fiber with polytetrafluoroethylene (PTFE) coating. Scaling by 18/19, the operating load is 123 N.

An additional installation mass was added for each subsystem in the mechanisms section of the structures subsystem. These installations were modeled using 4 percent of the current best estimate (CBE) dry mass of each of the subsystems. The 4 percent magnitude for an initial estimate compares well with values reported by Heineman (Ref. 74) for various manned systems. This is to account for attachments, bolts, screws, and other mechanisms necessary to attach the subsystem elements to the bus structure, and not bookkept in the individual subsystems.

13.6 Structures and Mechanisms Risk Inputs

Excessive acceleration loads or impact from a foreign object may cause too much deformation, vibrations, or fracture of sections of the support structure. Consequences include lower performance from mounted hardware to loss of mission. The likelihood is 3 of 5. Consequences to cost is 4 of 5, schedule is 4 of 5, performance is 4 of 5, and safety is 1 of 5.

To mitigate risks, the structure is to be designed to NASA standards to withstand expected environment, acceleration, and impact loading, and to have sufficient stiffness and damping to minimize issues with vibrations. Transport and mission trajectories are to be planned to minimize the probability of excessive loads and impact with foreign objects.

13.7 Structures and Mechanisms Recommendation

A stress analysis with finite element analysis (FEA) is recommended. Optimum designs may be accomplished with the use of orthogrid or isogrid panels.

14.0 Cost

14.1 Ground Rules and Assumptions

The following ground rules and assumptions apply to the Tunnelbot cost estimates:

(1) The scope of the estimates is the design and development and flight hardware for the Europa Tunnelbot Vehicle only. This estimate does not include launch services and delivery, mission operations and data analysis, mission level costs (Project Management (PM), Safety and Mission Assurance (SMA), etc.), and any necessary technology development up to TRL 6.
(2) Protoflight development.
(3) Estimates assume the system is contracted to a major aerospace firm; 10-percent fee for a cost-reimbursable contract is included.
(4) Quantitative risk analysis was performed using a Monte Carlo simulation driven by input parameter uncertainty and error statistics of the cost estimating relationships (CERs).
(5) Costs presented are mode values (approximately 35th percentile), in constant fiscal year 2018 dollars.

14.2 Estimating Methodology

The Tunnelbot estimate was developed using a Microsoft Excel-based parametric cost model created for this study. The model uses an approach similar to the NASA Air Force Cost Model (NAFCOM), that is, the subsystem hardware and software elements of a product-oriented WBS were estimated primarily using parametric CERs and the sum of the subsystem costs were used to estimate system integration costs. The primary input to the vehicle cost model was the MEL developed by the Compass team for this study; most of the CERs use mass as at least one of the independent parameters. The WBS in the MEL is mapped to the cost estimate WBS, which in several cases rolls up multiple elements to create elements consistent with the most applicable CERs. The Flight System and National Environmental Policy Act (NEPA) and Nuclear Safety Launch Approval costs are shown for cases 1 and 2 in Table 33. Most CERs were developed in-house using zero-bias, minimum percentage error (ZMPE) or minimum unbiased percentage error (MUPE) regression analysis, and are based on as many relevant data points as available so the standard errors used to develop the risk model have a strong statistical basis. The Tunnelbot flight system breakdown for cases 1 and 2 is provided in Table 34, and the cost estimation curves are provided for cases 1 and 2 in Figure 61 and Figure 62, respectively. The science instruments were estimated using the NASA Instrument Cost Model and should be viewed as representative because they were not robust in technical detail.

TABLE 33.—WORK BREAKDOWN STRUCTURE (WBS) 6.0 AND WBS 8.2 COST

WBS	Vehicle cost summary description	Case 1 fiscal year 2018, $M	Case 2 fiscal year 2018, $M
6.0	Flight system	1,294	562
6.1	Tunnelbot 3	1,208	476
6.2	Repeaters	85	86
8.2	NEPA[a] and nuclear safety launch approval	42	30
	Total vehicle cost	1,336	592
	Reserves (25 percent)	334	148
	Total cost with reserves	1,670	740

[a]National Environmental Policy Act.

TABLE 34.—FLIGHT SYSTEM COST BREAKDOWN

Tunnelbot estimate description	Case 1 total fiscal year 2018, $M	Case 2 total fiscal year 2018, $M
Science payload	58	59
Guidance, Navigation, and Control	9	9
Command and Data Handling	45	41
Communications and tracking	4	4
Electrical power subsystem	613	97
Thermal control (nonpropellant)	51	39
Structures and mechanisms	140	89
Subsystem subtotal	921	338
Systems integration		
Project Management	40	24
Systems Engineering	30	18
Mission Assurance	30	18
Integration, Assembly, and Test	22	17
Ground System Equipment	56	20
Spacecraft total	1,099	433
Fee (10 percent)	110	43
Prime total	1,209	476

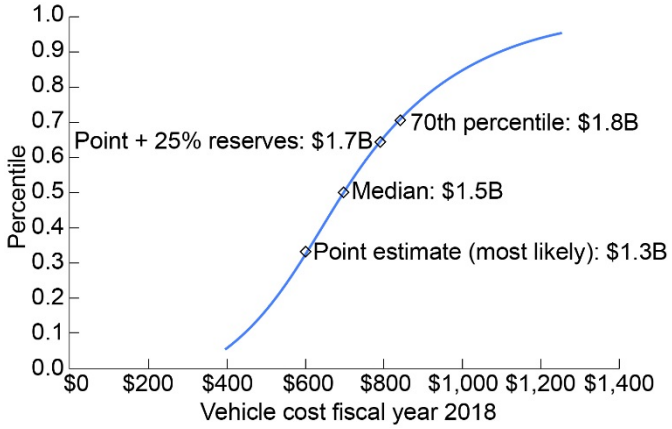

Figure 61.—Cost curve for case 1.

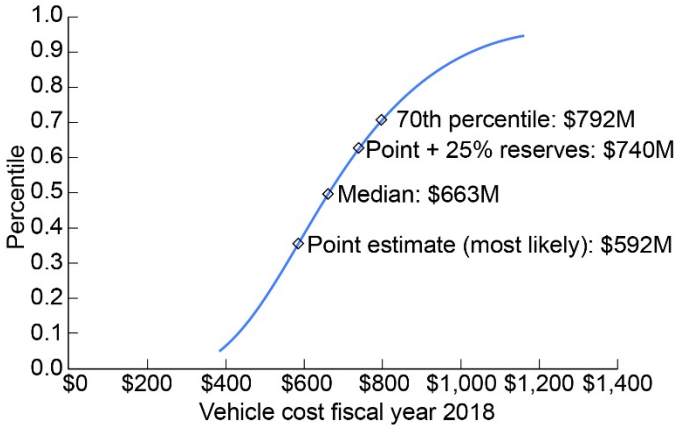

Figure 62.—Cost curve for case 2.

For case 1, the Fission Power System (FPS) was estimated based on the Affordable Fission Power System (AFPS) study that was conducted from 2007 to 2008 as part of the human exploration architecture work being done at the time. The AFPS estimate development was a very thorough and rigorous effort involving representatives from both NASA and the DOE. The AFPS was a landed, 40-kW_e system intended primarily to support a lunar base, with extensibility to human Mars exploration. For the Tunnelbot FPS, the system hardware was estimated at the level of the following subsystem elements:

- Reactor
- Shield
- Heat rejection
- Power conversion
- Power Management and Distribution (PMAD)
- Control system

PRICE H MCPLXS (complexity) factors were derived by calibration using the AFPS estimates for those elements, and then adjustments were made to the factors to account for the Tunnelbot FPS, assuming fabrication using refractory metals instead of the stainless steel as assumed in the AFPS. The costs of the nonhardware elements (PM, system engineering, SMA, flight software, etc.) were taken from AFPS with the only adjustment being for inflation. It was assumed that these activities should not be significantly different for the Tunnelbot FPS than the AFPS.

For case 2, due to lack of technical definition, the GPHS RTG system is cost as if it were a Multi-Mission Radioisotope Thermoelectric Generator (MMRTG). Any additional development costs required to modify the system are not included.

15.0 Conclusion

15.1 Lessons Learned

Overall: While it was known in the architecture studies that the thermal power system footprint would drive the size and mass of the Tunnelbot, it was found in the point designs that the science and repeater minimum footprints and volumes are both of equal importance to the thermal power system in driving the size of the Tunnelbot. Thus, it is recommended to consider the volume impacts in three main areas in future studies equally: (1) thermal and power, (2) science instrumentation, and (3) communication repeaters.

It was also found that the pressures that the Tunnelbot must endure at 20 km of ice depth require a not insignificant structural mass. This pressure vessel thickness was found to be very valuable as a radiation protection shield for the Jupiter orbit and Europa landing exposure times.

Indeed, the Tunnelbot designs are quite dense in order to minimize the heat required to melt holes of certain diameters, thus, making the Tunnelbots several times denser than water and requiring an anchor system to prevent sinking in the ocean.

Communications: Assuming worst-case ice transmission losses (16 dB/km, based on estimates for the Europa Clipper radar) and the unknown risk of cable breakage, repeaters will be required for communications. Use of a combined repeater and fiber optic system reduces unknown environment risks (transmission losses, shifting ice) while providing a completely different backup system. As the Tunnelbot depth increases, the ambient temperature increases, and hence the ice is slower to refreeze behind the Tunnelbot. This results in a column of liquid meltwater in the shaft above the Tunnelbot. This is exacerbated by the fact that the Tunnelbot moves faster through the warmer ice. At great depths, the Tunnelbot could have as much as a 200-m water column above it, making radiofrequency (RF) communications very unlikely.

Reactor Tunnelbot: Reactors do not scale linearly; a 4.3-kW_{th}, 32-cm-diameter reactor does not have sufficient

power, but a 43-kW_{th}, 36-cm-diameter reactor has an approximate 50-percent thermal power margin. The use of melted water nearly eliminated radiation shielding mass for the reactor Tunnelbot but did add length (but not pressurized volume). By placing the instruments in the nose and utilizing a >2-m meltwater chamber, radiation impacts on the science sample region are <100 Gy. A follow-on design for the reactor could utilize a smaller diameter and might save 100 to 200 kg of mass and allow either a 1.8-yr descent time or a lighter, lower power reactor (<30 kW_{th}) and less radiation.

General purpose heat source (GPHS) Tunnelbot: The large biodetection science payload drives a load of GPHS bricks that is equivalent to the Cassini spacecraft in order to achieve the 20 km transit in 3 yr. The required loading of 50 or more GPHS bricks into a pressure vessel on the pad will be very challenging.

Power systems: It was found that the reactor-powered Tunnelbot could base its power conversion systems on other potential planned Kilopower users. Due to the small diameter of the GPHS solution, a new Radioisotope Thermoelectric Generator (RTG) system would be needed. The Repeater Power System drives its volume. An eight-radioisotope heater unit (RHU), 1-W_e dynamic power system was found to have the smallest volume; however, a new single-GPHS thermoelectric (TE) system may be possible if larger diameters are allowed.

15.2 Top-Level Risks

The main risk is the lack of good knowledge on the actual ice and ocean environment; the absence of this data greatly hinders design and adds contingency. It is hoped that they can be mitigated in the coming years using Europa Clipper and perhaps Europa lander data. These environmental unknowns are as follows:

1. **How far below the surface is the ocean?**
   - The design assumes a maximum ice thickness. If the ice shell is thicker than we assume, we may not be able to reach the ocean. If the ice shell is thinner than assumed, on the contrary, a simpler (and hence lower cost) mission could have been designed.
   - Are there locations on the map where the ocean is closer (and hence easier to reach)?
1. **What is the RF transparency of the ice?**
   - RF transparency varies by several orders of magnitude from pure water ice to high-salinity dirty ice. The ability to communicate through ice will depend on the RF transparency, and hence the distance between repeaters (and even whether repeaters are required) will depend on this.
2. **What is the temperature profile of the ice crust?**
   - Models with convection bring warm ice upward. Since the RF transparency of the ice is a very strong function of the temperature, the location of the transition between cold and warm ice is the factor that determines the place of transition between very transparent ice and absorbing ice, and thus the distance and number of repeaters.
   - Temperature will also determine the melt rate.
3. **Do lakes (pockets of liquid water) exist within the ice shell?**
   - If so, how big are they? Meter-scale lakes are significantly different to the design from 100-m-scale lakes.
   - How saline are they (high-salinity lakes will not allow RF transmissions to pass through them)?
   - Can we identify individual lakes as targets for an easy mission?
4. **Is there dust in the ice?**
   - If the ice incorporates significant amounts of dust or sand, this may accumulate at the bottom of the melt pool and prevent the ability to move.
5. **What is the nature of the ice and ocean interface?**
   - Is there a layer of slushy ice at the interface? If so, what are the mechanical properties of this layer? How thick is it?
   - Is the interface specular or rough? This affects the reflectivity of radar (and sonar).

15.3 Next Steps

Due to time constraints, only the designs of the Tunnelbot were completed assuming a starting point below the ice surface. It is imperative that these Tunnelbot designs be incorporated into a lander and avionics package that also addresses how the Tunnelbot is introduced into the ice. Such options may include heat or a mechanical drill that could be integral or separate from the Tunnelbot. These designs should be symbiotic with the need to place the lander avionics package beneath the ice to allow operation for 3 yr (avoids high surface radiation impacts). The design may also help address risks of salt deposits and need for mechanical front end to be added to both Tunnelbots.

Appendix A.—Nomenclature

AC	alternating current
AD&C	attitude determination and control
AFPS	Affordable Fission Power System
AMOAB	Analog MultiOperational Avionics Board
ASC	Advanced Stirling Convertor
ASRG	Advanced Stirling Radioisotope Generator
BOL	beginning of life
BOM	beginning of mission
CAD	computer-aided design
CBE	current best estimate
C&DH	Command and Data Handling
CD	Compass Document
CER	cost estimating relationship
CONOPS	concept of operations
COTS	commercial off-the-shelf
CPU	central processing unit
CRSI	context remote sensing instrument
cPCI	Compact Peripheral Component Interconnect
DC	direct current
DMOAB	Digital MultiOperational Avionics Board
DNA	deoxyribonucleic acid
DOE	Department of Energy
DSN	Deep Space Network
eMMRTG	Enhanced Multi-Mission Radioisotope Thermoelectric Generator
EODL	end of design life
EOM	end of mission
FEA	finite element analysis
FeRAM	ferroelectric random-access memory
FOV	field of view
FPS	Fission Power System
FTT	Fischer-Tropsch Type
GN&C	Guidance, Navigation, and Control
GPHS	general purpose heat source
GSS	geophysical sounding system
I2C	Differential Inter-Integrated Circuit
IO	input output
JPL	Jet Propulsion Laboratory
LANL	Los Alamos National Laboratory
LDMS	Laser Desorption Mass Spectrometer
LEO	low Earth orbit
LIDAR	Light Detection and Ranging
LISS	Lander Infrastructure Sensors for Science
LITMS	Linear Ion Trap Mass Spectrometer
LOD	limit of detection
LRU	line-replaceable unit
LVPC	low-voltage power conditioner
LWRHU	lightweight radioisotope heater unit
MCNP	Monte Carlo N-Particle
MEL	master equipment list
MLD	microscope for life detection
MLI	multilayer insulation
MMPDS	Metallic Materials Properties Development and Standardization
MMRTG	Multi-Mission Radioisotope Thermoelectric Generator
MS	mass spectrometer
MUPE	minimum unbiased percentage error
NAFCOM	NASA Air Force Cost Model
NEPA	National Environmental Policy Act
OCA	organic compositional analyzer
PEL	powered equipment list
PLFA	phospholipid fatty acid
PM	Project Management
PMAD	Power Management and Distribution
PTFE	polytetrafluoroethylene
RF	radiofrequency
RHU	radioisotope heater unit
RHUSTIR	Stirling radioisotope heater unit
RPS	Radioisotope Power Systems
RTG	Radioisotope Thermoelectric Generator
SBC	single board computer
SBU	single bit upset
SDT	Science Definition Team
SEU	single event upset
SLS	Space Launch System
SMA	Safety and Mission Assurance
STM	Science Traceability Matrix
TAGS	Te/Sb/Ge/Ag
TE	thermoelectric
TID	total ionizing dose
TOF	time of flight
TRL	technology readiness level
TRX	transmit
UHF	ultrahigh frequency
UV	ultraviolet
VEEGA	Venus-Earth-Earth gravity assist
VS	vibrational spectrometer
WBS	work breakdown structure
ZMPE	zero-bias, minimum percentage error

D	radiation dose in Gy	k	radiolysis constant for individual amino acids in MGy^{-1}
N	amino acid abundance postradiation		
N_0	amino acid abundance preradiation	ΔV	change in velocity

Appendix B.—Study Participants

Europa Tunnelbot Design Session			
Subsystem	Name	Center	Email
Study PI	June Zakrajsek	NASA Glenn Research Center (GRC)	june.f.zakrajsek@nasa.gov
Science PI	Kate Craft	Johns Hopkins University Applied Physics Laboratory	kate.craft@jhuapl.edu
Science PI	Andrew Dombard	University of Illinois at Chicago	adombard@uic.edu
Science PI	D'Arcy Meyer-Dombard	University of Illinois at Chicago	drmd@uic.edu
Kilopower PI	Lee Mason	GRC	lee.s.mason@nasa.gov
Compass Team			
Lead	Steve Oleson	GRC	Steven.R.Oleson@nasa.gov
Lead Systems Engineer	J.Michael Newman	GRC	j.m.newman@nasa.gov
Science	Geoffrey Landis	GRC	geoffrey.landis@nasa.gov
Mission	Steven McCarty	GRC	steven.mccarty@nasa.gov
Guidance, Navigation, and Control	Brent Faller	GRC	brent.f.faller@nasa.gov
Mechanisms	James Fittje	GRC	james.e.fittje@nasa.gov
Structures and Mechanisms	John Gyekenyesi	GRC	John.Z.Gyekenyesi@nasa.gov
Thermal	Anthony Colozza	GRC	Anthony.J.Colozza@nasa.gov
Power	Paul Schmitz	GRC	paul.c.schmitz@nasa.gov
Power	James Sterbentz	Idaho National Laboratory	James.Sterbentz@inl.gov
Communications	Robert Jones	GRC	rejones@nasa.gov
Command and Data Handling	Nicholas Lantz	GRC	Nicholas.c.lantz@nasa.gov
Configuration	Thomas Packard	GRC	Thomas.W.Packard@nasa.gov
Planetary Protection	Terri McKay	GRC	terri.l.mckay@nasa.gov
Cost	Elizabeth Turnbull	GRC	elizabeth.r.turnbull@nasa.gov

References

1. Aamot, Haldor W.C.: Special Report 119—The Philberth Probe for Investigating Polar Ice Caps. U.S. Army Materiel Command Special Report, 119, 1967.
2. Winebrenner, D.: Applied Physics Laboratory Ice Diver. 2016. http://kiss.caltech.edu/workshops/oceanworlds/presentations/Winebrenner.pdf Accessed March 22, 2019.
3. Benson, T., et al.: IceCube Enhanced Hot Water Drill Functional Description. Ann. Glaciol., vol. 55, no. 68, 2014, pp. 105–114.
4. French, L.C., et al.: Subsurface Exploration Technologies and Strategies for Europa. Innovative Approaches to Outer Planetary Exploration 2001–2020, 2001. https://www.lpi.usra.edu/meetings/outerplanets2001/pdf/4008.pdf Accessed March 22, 2019.
5. Wilcox, B.: Deep Ice Probes. 2017. https://www.lpi.usra.edu/opag/meetings/feb2017/posters/Wilcox.pdf, Accessed March 22, 2019.
6. Elliott, J.O.; and Carsey, F.D.: Deep Subsurface Exploration of Planetary Ice Enabled by Nuclear Power. Presented at the 2004 IEEE Aerospace Conference, Big Sky, MT, 2004.
7. Maise, George: Multi-MICE: A Network of Interactive Nuclear Cryoprobes to Explore Ice Sheets on Mars and Europa. Presented at the NIAC Phase 1 Fellows Meeting, Atlanta, GA, 2005. http://www.niac.usra.edu/files/library/meetings/fellows/mar06/1059Maise.pdf Accessed March 22, 2019.
8. Stone, W.C., et al.: Progress Towards an Optically Powered Cryobot. Ann. Glaciol., vol. 55, no. 65, 2014, pp. 2–13.
9. Cwik, Tom: Going to the Water—Challenges in Designing a Mission That Travels Through Europa's Crust: Deployment, Operations, Communication. Presented at the California Institute of Technology Keck Institute for Space Studies Study, 2017. http://kiss.caltech.edu/workshops/oceanworlds/presentations/Cwik.pdf Accessed March 22, 2019.
10. Gibson, Marc: Kilopower Reactor Development and Testing. Presented at the Kilopower Press Conference, 2018. https://www.nasa.gov/sites/default/files/atoms/files/kilopower_media_event_charts_16x9_final.pdf Accessed March 22, 2019.
11. Zolotov, M. Yu.; and Kargel, J.S.: On the Chemical Composition of Europa's Icy Shell, Ocean, and Underlying Rocks. Europa, Robert T. Pappalardo, William B. McKinnon, and Krishan K. Khurana, eds., University of Arizona Press, Tuscon, AZ, 2009, pp. 431–458.
12. Kelvinsong: Image available in Wikimedia Commons, The Free Media Repository, 2013. https://commons.wikimedia.org/wiki/File:Europa_poster.svg Accessed March 22, 2019.
13. Schmidt, B.E., et al.: Active Formation of 'Chaos Terrain' Over Shallow Subsurface Water on Europa. Nature, vol. 479, 2011, pp. 502–505.
14. Dombard, Andrew J., et al.: Flanking Fractures and the Formation of Double Ridges on Europa. Icarus, vol. 223, no. 1, 2013, pp. 74–81.
15. Kattenhorn, Simon A.; and Prockter, Louise M.: Evidence for Subduction in the Ice Shell of Europa. Nat. Geosci., vol. 7, 2014, pp. 762–767.
16. Selesnick, R.S.: Cosmic Ray Access to Jupiter's Magnetosphere. Geophys. Res. Lett., vol. 29, no. 9, 2002.
17. Patterson, G. Wesley; Paranicas, Chris; and Prockter, Louise M.: Characterizing Electron Bombardment of Europa's Surface by Location and Depth. Icarus, vol. 220, no. 1, 2012, pp. 286–290.
18. Nordheim, T.A.; Hand, K.P.; and Paranicus, C.: Preservation of Potential Biosignatures in the Shallow Subsurface of Europa. Nat. Astron., vol. 2, 2018, pp. 673–679.
19. Johnson, R.E., et al.: Radiation Effects on the Surfaces of the Galilean Satellites. Jupiter: The Planet, Satellites and Magnetosphere, Fran Bagenal, Timothy E. Dowling, and William B. McKinnon, eds., Cambridge University Press, Cambridge, England, 2004, pp. 485–512.
20. Poinelli, Mattia: Toward a Better Understanding of Europa Crevasses. Master's Thesis, Delft Univ. of Technology, 2017.
21. Hand, K.P., et al.: Europa Lander Mission. Europa Lander Study 2016 Report, Science Definition Team, 2016.
22. Nimmo, F.; and Manga, M.: Geodynamics of Europa's Icy Shell. Europa, Robert T. Pappalardo, William B. McKinnon, and Krishan K. Khurana, eds., University of Arizona Press, Tuscon, AZ, 2009, pp. 381–404.
23. Schenk, P.M.; and Turtle, E.P.: Europa's Impact Craters: Probes of the Icy Shell. Europa, Robert T. Pappalardo, W.B. McKinnon, and K. Khurana, eds., University of Arizona Press, Tuscon, AZ, 2009, pp. 181–198.
24. Barr, A.C.; and Showman, A.P.: Heat Transfer in Europa's Icy Shell. Europa, Robert T. Pappalardo, William B. McKinnon, and Krishan K. Khurana, eds., University of Arizona Press, Tuscon, AZ, 2009, pp. 405–430.
25. Moore, W.B.; and Hussmann, H.: Thermal Evolution of Europa's Silicate Interior. Europa, Robert T. Pappalardo, William B. McKinnon, and Krishan K. Khurana, eds., University of Arizona Press, Tuscon, AZ, 2009, pp. 369–380.
26. Petrenko, Victor F.; and Whitworth, Robert W.: Physics of Ice. Oxford University Press, Oxford, England, 2002.

27. Fagents, Sarah A.: Considerations for Effusive Cryovolcanism on Europa: The Post-Galileo Perspective. J. Geophys. Res., vol. 108, no. E12, 2003, p. 5139.
28. Gudmundsson, Agust: Rock Fractures in Geological Processes. Cambridge University Press, Cambridge, England, 2011.
29. Shoshany, Yossi; Prialnik, Dina; and Podolak, Morris: Monte Carlo Modeling of the Thermal Conductivity of Porous Cometary Ice. Icarus, vol. 157, no. 1, 2002, pp. 219–227.
30. Manga, Michael; and Michaut, Chloe: Formation of Lenticulae on Europa by Saucer-Shaped Sills. Icarus, vol. 286, 2017, pp. 261–269.
31. Balkwill, David L., et al.: Equivalence of Microbial Biomass Measures Based on Membrane Lipid and Cell Wall Components, Adenosine Triphosphate, and Direct Counts in Subsurface Aquifer Sediments. Microb. Ecol., vol. 16, no. 1, 1988, pp. 73–84.
32. Steger, Kristin, et al.: Microbial Biomass and Community Composition in Boreal Lake Sediments. Limnol. Oceanogr., vol. 56, no. 2, 2011, pp. 725–733.
33. Gutiérrez-Preciado, Ana; Romero, Hector; and Peimbert, Mariana: An Evolutionary Perspective on Amino Acids. Nature Education, vol. 3, no. 9, 2010, p. 29.
34. Lu, Yi; and Freeland, Stephen: On the Evolution of the Standard Amino-Acid Alphabet. Genome Biology, vol. 7, no. 102, 2006.
35. Cronin, J.R.; and Pizzarello, S.: Amino Acids in Meteorites. Adv. Space Res., vol. 3, no. 9, 1983, pp. 5–18.
36. Ehrenfreund, Pascale; and Charnley, Steven B.: Organic Molecules in the Interstellar Medium, Comets, and Meteorites: A Voyage From Dark Clouds to the Early Earth. Annu. Rev. Astron. Astrophys., vol. 38, 2000, pp. 427–483.
37. Higgs, Paul G.; and Pudritz, Ralph E.: A Thermodynamic Basis for Prebiotic Amino Acid Synthesis and the Nature of the First Genetic Code. Astrobiology, vol. 9, no. 5, 2009, pp. 483–490.
38. Pizzarello, Sandra: The Chemistry of Life's Origin: A Carbonaceous Meteorite Perspective. Acc. Chem. Res., vol. 39, no. 4, 2006, pp. 231–237.
39. Elsila, James E., et al.: Meteoritic Amino Acids: Diversity in Compositions Reflects Parent Body Histories. ACS Cent. Sci., vol. 2, no. 6, 2016, pp. 370–379.
40. Aubrey, Andrew D.: Amino Acid Biosignatures—Implications for the Detection of Extinct or Extant Microbial Communities on Mars. Ph.D. Thesis, University of California, 2008.
41. Kaiser, Karl; and Benner Ronald: Major Bacterial Contribution to the Ocean Reservoir of Detrital Organic Carbon and Nitrogen. Limnol. Oceanogr., vol. 53, no. 1, 2008, pp. 99–112.
42. Hartgers, Walter A., et al.: 13C-Contents of Sedimentary Bacterial Lipids in a Shallow Sulfidic Monomictic Lake (Lake Cisó, Spain). Org. Geochem., vol. 31, no. 9, 2000, pp. 777–786.
43. Lovelock, James E.: A Physical Basis for Life Detection Experiments. Nature, vol. 207, no. 4997, 1965, pp. 568–570.
44. Instruments—Mars 2020 Rover. 2015. https://mars.nasa.gov/mars2020/mission/instruments/ Accessed March 25, 2019.
45. Garcia-Ruiz, J.M., et al.: Self-Assembled Silica-Carbonate Structures and Detection of Ancient Microfossils. Science, vol. 302, no. 5648, 2003, pp. 1194–1197.
46. House, C.H.; Schopf, J.W.; and Stetter, K.O.: Carbon Isotopic Fractionation by Archaeans and Other Thermophilic Prokaryotes. Org. Geochem., vol. 34, 2003, pp. 345–356.
47. Nihous, Gerard C.: Notes on the Temperature Dependence of Carbon Isotope Fractionation by Aerobic CH4-Oxidising Bacteria. Isot. Environ. Health Stud., vol. 46, no. 2, 2010, pp. 133–140.
48. Cosmidis, Julie; and Templeton, Alexis S.: Self-Assembly of Biomorphic Carbon/Sulfur Microstructures in Sulfidic Environments. Nat. Commun., vol. 7, no. 12812, 2016.
49. Dartnell, Lewis R.: Ionizing Radiation and Life. Astrobiology, vol. 11, no. 6, 2011, pp. 551–582.
50. Ciesla, Fred J.; and Sandford, Scott A.: Organic Synthesis via Irradiation and Warming of Ice Grains in the Solar Nebula. Science, vol. 336, no. 6080, 2012, pp. 452–454.
51. Sinanoglu, Vassilia J., et al.: Microbial Population, Physiochemical Quality, and Allergenicity of Molluscs and Shrimp Treated With Cobalt-60 Gamma Radiation. J. Food Protect., vol. 70, no. 4, 2007, pp. 958–966.
52. Abomohra, Abo El-Fatah, et al.: Effect of Gamma Radiation on Growth and Metabolic Activities of Arthrospira Platensis. Braz. Arch. Biol. Technol., vol. 59, 2016.
53. DiRuggiero, Jocelyne, et al.: Repair of Extensive Ionizing-Radiation DNA Damage at 95°C in the Hyperthermophilic Archaeon Pyrococcus Furiosus. J. Bacteriol., vol. 179, no. 14, 1997, pp. 4643–4645.
54. Kottemann, Molly, et al.: Physiological Responses of the Halophilic Archaeon Halobacterium sp. Strain NRC1 to Desiccation and Gamma Irradiation. Extremophiles, vol. 9, no. 3, 2005, pp. 219–227.
55. Le Postollec, A., et al.: Investigation of Neutron Radiation Effects on Polyclonal Antibodies (IgG) and Fluorescein Dye for Astrobiological Applications. Astrobiology, vol. 9, no. 7, 2009, pp. 637–645.

56. de Diego-Castilla, Graciela, et al.: Assessing Antibody Microarrays for Space Missions: Effect of Long-Term Storage, Gamma Radiation, and Temperature Shifts on Printed and Fluorescently Labeled Antibodies. Astrobiology, vol. 11, no. 8, 2011, pp. 759–773.
57. Derveni, Mariliza, et al.: Effects of Simulated Space Radiation on Immunoassay Components for Life-Detection Experiments in Planetary Exploration Missions. Astrobiology, vol. 12, no. 8, 2012, pp. 718–729.
58. Kminek, G.; and Bada, J.L.: The Effect of Ionizing Radiation on the Preservation of Amino Acids on Mars. Earth Planet. Sci. Lett., vol. 245, 2006, pp. 1–5.
59. Dartnell, Lewis R., et al.: Degradation of Cyanobacterial Biosignatures by Ionizing Radiation. Astrobiology, vol. 11, no. 10, 2011, pp. 997–1016.
60. Parnell, John, et al.: Searching for Life on Mars: Selection of Molecular Targets for ESA's Aurora ExoMars Mission. Astrobiology, vol. 7, no. 4, 2007, pp. 578–604.
61. Daly, Michael J.: A New Perspective on Radiation Resistance Based on Deinococcus Radiodurans. Nat. Rev. Microbiol., vol. 7, no. 3, 2009, pp. 237–245.
62. Pitonzo, Beth J.; Amy, Penny S.; and Rudin, Mark: Effect of Gamma Radiation on Native Endolithic Microorganisms From a Radioactive Waste Deposit Site. Radiat. Res., vol. 152, no. 1, 1999, pp. 64–70.
63. Buchan, David, et al.: Selective Sterilisation of Undisturbed Soil Cores by Gamma Irradiation: Effects of Free-Living Nematodes, Microbial Community and Nitrogen Dynamics. Soil Biol. Biochem., vol. 47, 2012, pp. 10–13.
64. Krisko, Anita; and Radman, Miroslav: Protein Damage and Death by Radiation in Escherichia Coli and Deinococcus Radiodurans. PNAS, vol. 107, no. 32, 2010, pp. 14373–14377.
65. Saeed, A., et al.: Effects of Very Low Dose Fast Neutrons on Cell Membrane and Secondary Protein Structure in Rat Erythrocytes. PLoS One, 2015.
66. Tate, R.E.: The Light Weight Radioisotope Heater Unit (LWRHU): A Technical Description of the Reference Design. LA–9078–MS, 1982.
67. Sanchez, Rene Gerardo, et al.: Kilowatt Reactor Using Stirling Technology (KRUSTY) Demonstration: CEDT Phase 1 Preliminary Design Documentation. LA–UR–15–26603, 2015.
68. McClure, Patrick; and Poston, David: Design and Testing of Small Nuclear Reactors for Defense and Space Application. LA–UR–13–27054, 2013.
69. X–5 Monte Carlo Team: MCNP—A General Monte Carlo N-Particle Transport Code, Version 5. LA–UR–03–1987, 2008.
70. Aamot, Haldor W.C.: Instrumented Probes for Deep Glacial Investigations. U.S. Army Materiel Command Technical Report 210, 1968.
71. Federal Aviation Administration: Metallic Materials Properties Development and Standardization (MMPDS). Battelle Memorial Institute MMPDS–11, 2016.
72. National Aeronautics and Space Administration: Structural Design and Test Factors of Safety for Spaceflight Hardware. NASA–STD–5001B, 2016.
73. Young, Warren Clarence; and Budynas, Richard G.: Roark's Formulas for Stress and Strain. Seventh ed., McGraw Hill, New York, NY, 2002.
74. Heineman, Willie, Jr.: Design Mass Properties II: Mass Estimating and Forecasting for Aerospace Vehicles Based on Historical Data. NASA JSC–26098, 1994.